Doctoral Dissertation
Doctoral Program in Civil and Environmental Engineering (33rd Cycle)

Electrokinetic delivery of reactants for groundwater remediation

Andrea Gallo
* * * * * *

Supervisors
Prof. Rajandrea Sethi, Supervisor
Prof. Tiziana Tosco, Co-Supervisor
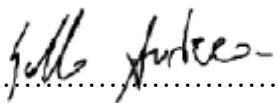
Correlator
Prof. Massimo Rolle

Doctoral Examination Committee:
Prof. Pietro Paolo Falciglia, Referee, University of Catania
Prof. Massimiliano Fabricino, Referee, University of Napoli
Prof. Daniele Di Trapani , Referee, University of Palermo
Prof. Raffaella Pomi, Referee, University of Roma "La Sapienza"
Prof. Alberto Tiraferri, Referee, Polytechnic of Torino

Politecnico di Torino
March 10, 2021

I hereby declare that, the contents and organization of this dissertation constitute my own original work and does not compromise in any way the rights of third parties, including those relating to the security of personal data.

....

Andrea Gallo

Turin, February 13, 2021

Summary

The promising results obtain from laboratory and pilot-scale application of electrokinetic transport to the delivery of amendments for groundwater remediation are leading to an increasing interest for the techniques as a valid alternative to hydraulic injection in porous media. The different transport mechanism for EK leads to a better mixing with the pore solution, and thus the contaminant, and allow to overcome the limitation posed by low-permeability areas, simultaneously addressing the issue of back diffusion from the latter. A deeper understanding of electrokinetic phenomena in complex geometries (higher than 1D) and scenarios (heterogenous porous medium) is therefore pivotal for its efficient and effective implementation in full-scale implementations. The present work aims to investigate some of the complex mechanism involved in the EK transport of solutes, increasing the current knowledge-base and providing tools and information for a more efficient use of EK in groundwater remediation application.

Two-dimensional experiments were performed to investigate the influence of charge interactions phenomena in homogenous permeable porous media. The use of a full 2D geometry allowed to enable multidimensional transport components and investigating their mechanism and impact on extent on mixing and reaction kinetics toward a model pollutant. It was possible to show that the pore solution composition controls the delivery, spatial distribution and mixing of the injected amendments; reactivity experiments allowed to elucidate the impact on the reaction rates and amendment efficiency. Important implications are drawn, of both scientific and practical relevance; the gained knowledge on the mechanism and effect of charge interactions opens to the possibility of employing such effect to control and maximize the delivery efficiency. The process-based mathematical model developed will provide an important tool to support the design of EK implementation to improve the distribution of reactants and nutrients.

Experimental tests on the delivery and reactivity of amendments in low permeability inclusion were performed in 1D geometry, to determine the impact of charge interactions, determine the optimal parameter for the delivery and assess the ability of the reactants to remove a model pollutant. The use of a buffer in the electrode chamber allowed to prevent the plume stalling commonly associated to EK delivery in low permeability porous medium; it was also possible to determine an influence of the buffer ionic concentration on the migration velocity without any modification in the potential gradient applied. Lastly, electrokinetic transport was applied to the delivery of amendments in clay inclusions in a 2D geometry for which hydraulic delivery proved unable to penetrate the low-permeability inclusion as expected. For electrokinetic transport, the results of the previous experiments played a fundamental role in defining the optimal conditions for the delivery. Exploiting the multidimensional effect arising from charge interactions it was possible to reduce the plume displacement and maximize its penetration in the clay layer, whereas a non-optimized protocol showed significantly lower efficiency (although still higher than advection-dispersion). The results obtained are very promising in the application of EK for the remediation of groundwater in heterogeneous aquifers, as it would be possible to improve the decontamination of low-permeability area reducing the secondary contamination arising from back diffusion.

Acknowledgment

"Bear in mind that the wonderful things you learn in your schools are the work of many generations. All this is put in your hands as your inheritance in order that you may receive it, honor it, add to it, and one day faithfully hand it on to your children."

Albert Einstein

Contents

List of Tables

List of Figures

List of Symbols

K_H	*Hydraulic conductivity*	m s^{-1}
η	*Dynamic viscosity*	kg m^{-1} s^{-1}
g	*Gravitational acceleration*	m s^{-2}
k_H	*Hydraulic permeability*	m^2
v_A	*Amendment advective velocity*	m s^{-1}
v_C	*Contaminant advective velocity*	m s^{-1}
R_A, R_C	*Retardation factor for amendment and contaminant*	
v_e	*Effective fluid velocity*	m s^{-1}
Q_A, Q_C	*Ionic charge of amendment and contaminant*	
$J_m^{EM}{}_i$	*Electromigration mass flux for the i-th component*	mol m^{-2} s^{-1}
$k^{EM}{}_i^*$	*Effective ionic mobility for the i-th component*	m^2 s^{-1} V^{-1}
c_i	*Concentration of the i-th component*	mol m^{-3}
$\nabla\Phi$	*Potential gradient in the porous medium*	V m^{-1}
D_i^*	*Effective diffusion coefficient for the i-th specie*	m^2 s^{-1}
z_i	*Valence and polarity of the i-th specie*	
F	*Faraday's constant*	96485 C mol^{-1}
R	*Ideal gas constant*	8.314 J K^{-1} mol^{-1}
T	*Absolute temperature*	K
τ	*Tortuosity*	

$\acute{L}$	*Average path in the porous medium*	m
L	*Shortest path in the porous medium*	m
n	*Porosity*	
τ_g	*Geometrical tortuosity*	
$\mathbb{T}_g$	*Geometrical tortuosity coefficient*	
$\mathbb{T}$	*Tortuosity coefficient (generic)*	
D_i	*Diffusion coefficient for the i-th specie in free solution*	$m^2\,s^{-1}$
v_i^{EM}	*Electromigration velocity for the i-th specie*	$m\,s^{-1}$
v_i^{EO}	*Electroosmotic velocity*	$m\,s^{-1}$
ε	*Electrical permittivity*	$C\,V^{-1}\,m^{-1}$
ζ	*Zeta potential of the bulk porous medium*	V
α	*Particle size constant for the Helmholtz-Smoluchowski equation*	
l_D	*Capillary cross section / pore throat size*	m
k^{EO}	*Electroosmotic permeability for the i-th specie*	$m^2\,s^{-1}\,V^{-1}$
q^{EO}	*Volumetric electroosmotic flow for the i-th specie*	$m^3\,s^{-1}$
A_i	*Cross sectional area for a single pore*	m^2
A_T	*Cross sectional area for the porous medium*	m^2
k^{EP}_i	*Electrophoretic mobility for the i-th specie*	$m^2\,s^{-1}\,V^{-1}$
ζ_{NPs}	*Zeta potential of colloidal particles*	V
r	*Colloidal particle radius*	m
$k^{EK}_{obs}\vert^{\pm}_i$	*Total electrokinetic mobility for the i-th ionic specie*	$m^2\,s^{-1}\,V^{-1}$
$k^{EP}\vert^{\pm}_i$	*Electrophoretic mobility for a generic colloid*	$m^2\,s^{-1}\,V^{-1}$
$k^{EM}\vert^{\pm}_i$	*Electromigration mobility for a generic solute*	$m^2\,s^{-1}\,V^{-1}$
ρ	*Resistivity*	$\Omega\,m$
ρ^{eff}	*Effective resistivity in the porous medium*	$\Omega\,m$
m	*Cementation coefficient*	

σ^{eff}	*Effective conductivity in the porous medium*	S m^{-1}
σ_r	*Conductivity arising for the porous medium CEC*	S m^{-1}
σ_w	*Conductivity of the bulk solution*	S m^{-1}
X, Y	*Wyllie and Southwick [1] geometrical coefficient*	
$\sigma_{\pm}$	*Conductivity of anion and cation*	S m^{-1}
$t_{(\pm)}^{f}$	*Hittorf number for the bulk solution*	
$t_{(\pm)}^{S}$	*Surface Hittorf number*	
n_C	*Interconnected porosity*	
φ	*Geometric coefficient for surface conductivity*	
σ_f	*Fluid conductivity*	S m^{-1}
σ_S	*Surface conductivity*	
Σ	*Specific conductance*	S m^{-2}
r_g	*Grain radius*	m
E^{app}	*Applied potential at the working electrodes*	V
E^{eff}	*Potential drop in the capillary (or porous medium)*	V
E^*	*Potential losses in the system*	V
J_i	*Mass flux for the i-th specie*	mol m^{-2} s^{-1}
J^{ADV}_{i}	*Advective mass flux for the i-th specie*	mol m^{-2} s^{-1}
c_i	*Concentration for the i-th specie*	mol m^{-3}
u	*Advective velocity*	m s^{-1}
J^{TOT}_{i}	*Total mass flux for the i-th specie*	mol m^{-2} s^{-1}
J'_i	*Generic mass flux for the i-th specie*	mol m^{-2} s^{-1}
v'_i	*Drift velocity for the i-th specie*	m s^{-1}
v	*Bulk velocity*	m s^{-1}
J^{DIFF}_{i}	*Diffusion mass flux*	mol m^{-2} s^{-1}
∇c_i	*Concentration gradient for the i-th specie*	mol m^{-4}
ω_i	*Generic mobility for the i-th specie*	m^2 s^{-1} V^{-1}

F^{act}	*Generic force responsible for the mass flux*	
e	*Elementary charge*	$1.602 \cdot 10^{-19}$ C
k_b	*Boltzman constant*	$1.38 \cdot 10^{-23}$ J K^{-1}
i	*Current density*	A
∇i	*Current density gradient*	A
$z_{\pm}$	*Generic charge (anion or cation)*	
$v_{\pm}$	*Generic velocity (anion or cation)*	m s^{-1}
$c_{\pm}$	*Generic concentration (anion or cation)*	mol m^{-3}
n_+	*Cationic stoichiometry in a generic salt $[A^{m+}]_n[B^n]_m$*	
m_-	*Anionic stoichiometry in a generic salt $[A^{m+}]_n[B^{n-}]_m$*	
C	*Scaled concentration*	mol m^{-3}
$D_{\pm}$	*Generic diffusion coefficient for a ionic specie*	m^2 s^{-1}
D'	*Complex diffusion coefficient*	m^2 s^{-1}
R_i	*Reaction term*	mol m^{-3} s^{-1}
θ	*Water content of the solid matrix*	
μ_i	*Electrochemical potential for the i-th specie*	J mol^{-1}
μ_i^0	*Standard electrochemical potential for the i-th specie*	J mol^{-1}
a_i	*Activity coefficient for the i-th specie*	
E_p	*Electrostatic potential*	V
v^*	*Effective advective flow velocity*	m s^{-1}
v_D	*Darcy velocity for the advective flow*	m s^{-1}
CR	*Circularity*	
Ro	*Roundness*	
$M_{i,0}(t)$	*Zeroth order spatial moment*	mol m^{-3}
$c_i(x,t)$	*Concentration for the i-th specie in a spatiotemporal domain*	mol m^{-3}
$M_{i,1}(t)$	*First-order spatial moment*	m
$M_{i,2}(t)$	*Second-order central moment*	m^2

$x_{i,m}(t)$	*Plume centroid position*	m
Dil	*Dilution index*	m^2
$p_i(x,t)$	*Point concentration for the i-th specie*	$mol\ m^3$
A_{mix}	*Mixing area*	m^2
σ_T	*Free solution conductivity*	$S\ m^{-1}$
D_i^L	*Longitudinal dispersion coefficient for the i-th specie*	$m^2\ s^{-1}$
D_i^T	*Transversal dispersion coefficient for the i-th specie*	$m^2\ s^{-1}$
Pe_i	*Peclet number for the i-th specie*	
$\delta,\ \beta$	*Empirical constants*	
r_i	*Reaction term (sink/source)*	$mol\ m^{-3}\ s^{-1}$
r_{MnO4}	*Reaction term for permanganate*	$mol\ m^{-3}\ s^{-1}$
$k_{r,\ MnO4}$	*Kinetic constant for the reaction glucose/permanganate*	$m^3\ s^{-1}\ mol^{-1}$

Chapter 1

Introduction

1.1 Motivations and thesis outline

Groundwater constitutes an important resource for human society, thanks to its extensive distribution across the globe. It plays a pivotal role in hydrogeochemical cycles and supports human activities, such as agriculture, by recharging the surface streaming water bodies and providing a supply of water through extraction wells [2]. Its dynamic connection with surface water and with the soil allows groundwater exploitation [2, 3], but on the other hand leads to the contamination of the aquifer determining the transport and spreading of the contaminant from its source, which can be either above- or underground [3-5]. As a result of the lack of control on human activities and groundwater exploitation in the past, we are currently facing the need of groundwater remediation to preserve the exploitability of such resource [2, 4]. A recent inventory estimates 20000 European sites and up to 355,000 sites in the United States which requires remediation from contamination [6, 7]. Such numbers do not include the whole world, and those sites classify as 'potentially polluted', which means no sufficient data are available yet. It is therefore clear how remediation technologies must be made affordable and versatile, to allow a rapid deployment and decontamination so that the quality standard for human consumption are met, also in the case of emergency implementation [7]. The approaches to face a groundwater and subsoil contamination are many and evolved during the years. A first distinction can be made between *ex-situ* and *in-situ* techniques, the former requires the extraction of the groundwater from the aquifer and an off-site treatment plant for the actual decontamination [8, 9], while the latter

allows the contaminant removal on the polluted site or even directly in the aquifer [10-13]. From the literature comparing *in-situ* and *ex-situ* techniques it is evident that both approaches present strengths and weaknesses, which are defined by the specific characteristic of the polluted site and the pollution itself [9, 12]. At present time, *in-situ* techniques are preferred over *ex-situ* treatment [5, 9] (e.g., soil washing, soil flushing, vitrification, thermal desorption) for many reasons, for example they avoid the physical removal and transport of the pollutant, hence the risk of exposing other environmental compartments to contamination (e.g., due to spilling, volatilization, etc.) [5, 14]. Other advantages are related to an easier implementation on sites which does not presents the topographic features required by *ex-situ* methods, for example location in urban areas would require traffic, local activities, and infrastructure disruption with significant impacts beyond the health risk posed by pollutant handling in a populated area [5, 9, 14]. Such aspects far outweigh the greater control over the process and faster decontamination of *ex-situ* methods [8, 9, 12, 14], considering that the latter also requires a noticeable technological effort for the installation of the treatment plant [9] or a disposal site [14]. Among the different *in-situ* approaches, great attention has been devoted to reactant delivery in the subsoil to target the contaminated area or, alternatively, to create a reactive area on the pollution flow path to obtain a chemical (dechlorination, reduction oxidation) or a physical (precipitation, adsorption) removal of the contaminant [4, 5, 8, 9]. These techniques are based on the injection of reactive solutes (e.g., reductants, oxidants) or reactive and sorptive nanomaterials (e.g., nanometallic particles, graphene, nano-sized activated carbon) through wells or boreholes which are then transported to the target zone by means of pressure driven flow or the basal aquifer flow [4, 5, 9, 15]. It follows that, beside the material reactivity towards the target pollutant, the success of the remediation depends on an optimal injection and delivery to ensure good contact between reactant and pollutant, maximization of the area of delivery and reactant efficiency. This is one of the greatest issues that must be addressed in the design steps, since highly heterogenous subsoil or the presence of low permeability layers can negatively and significantly affect the remediation outcome when the hydraulic delivery (by advection-dispersion) is employed [5, 7, 9, 16].

Relatively to *in-situ* remediation, the direct delivery of amendments is usually obtained by exploiting wells and a combination of pressure driven flow and aquifer basal flow to obtain a uniform distribution over the entire polluted area [5, 16, 17]. It follows, hydraulic conductivity of the subsoil plays a fundamental role in determining the effectiveness and efficacy of the delivery, and therefore the choice

of the most suitable injection technology is pivotal in determining the remediation outcome [7, 17]. The hydraulic conductivity of natural porous medium spans over 10 orders of magnitude and depends on the medium lithology and grain size [5, 18, 19]:
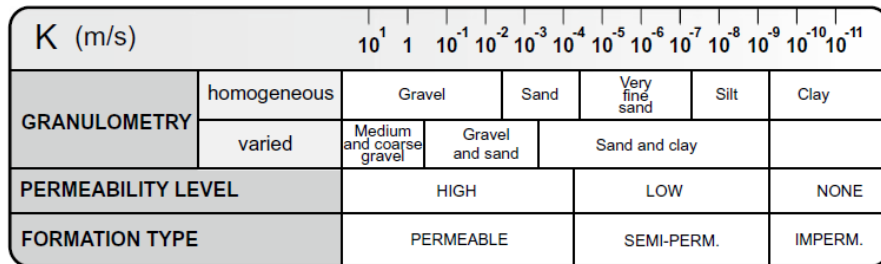
Figure 1) Typical hydraulic conductivity for natural porous media with different lithology and grain size, adapted from Sethi and Di Molfetta [5]

It must be pointed out that hydraulic conductivity (K_H) is a function of both porous media properties (defining hydraulic permeability, k_H) and fluid properties (density ρ, dynamic viscosity η and gravitational acceleration g) [5, 18]:

$$K_H = \frac{\rho g}{\eta} \cdot k_H \ .$$

Equation 1

The injection techniques can be classified based on the strategy to access the aquifer and the pressure applied for the delivery of the reactant, as reported in [5, 9, 13, 17, 20].

Table 1) Most common application conditions for Well and Direct Push injection

PRESSURE	Well Injection	Direct Push Injection
Low	Yes	Never
Medium	Yes	Yes
High	Rare [21]	Yes
GRANULOMETRY		
Fine	No	Yes
Medium	Yes	Yes
Coarse	Yes	No

3

Low pressure injection (gravity-fed only if the hydraulic head created by the remediating solution is applied) allows a uniform distribution of the amendments but is suitable for homogenous subsoils with high hydraulic permeability only. The presence of low permeability inclusions can lead to reduced delivery or even null delivery in such areas, with a significant reduction of the remediation efficacy. Moreover, due to the low flow (high residence time) and the high reactant concentration in proximity of the well walls, clogging and fouling resulting from geochemical or bacterial interactions can further reduce the injectability [13, 17, 20]. Lastly, the area affected by a single well (Area of Delivery, AoD) in low-pressure injection is low, it follows that a high number of injection wells is required with higher costs for the application [5, 13, 17]. Medium pressure injection from wells aims at reducing some of these shortcomings; the higher pressure allows for implementation in a wider range of subsoils and heterogeneous conditions but also introduces additional costs and a careful design of the injection [9, 13, 20]. The use of pumps and packers (inflatable seals) is implemented to seal a section of wells and allow their pressurization; during the injection, the packers can be moved to extend the injection height [5, 9, 13]. Lastly, Direct Push (DP) injection does not use wells or boreholes, but hollow rods placed in the subsoil using an oleodynamic mallet (e.g., GeoProbe®) [13, 17, 20]. Although DP injection is easier and cheaper to implement (it does not require well excavation) it is unsuitable for very coarse (cobble), very fine soil (silts) and for consolidate media. When medium or high pressures are applied, either from wells or by DP, a careful design tailored to the site characteristic (soil density, hydraulic conductivity, amendment fluid viscosity) is required in order not to exceed the fracturing pressure of the porous matrix [5, 13, 20]. If fracturing occurs, new preferential flow paths are created in the porous matrix with very high hydraulic permeability. As a consequence, the amendments distribution is not uniform and unreactive zones are formed reducing the remediation efficacy. In extreme cases the fracturing can extend to the surface leading to daylighting of the injected substance and a loss of amendments [13, 17, 22]. Both effects nullify the greater Area of Delivery achievable by fracturing, therefore for most *in-situ* remediation a careful design of the injection, specifically tailored to the site, is required to define the optimal number and distribution of injection points and the pressure applied to balance application costs and remediation efficiency [5, 9, 13, 17, 20]. The low or null accessibility of low-permeability formations in the aquifer represents a significant limitation for the remediation process, as discussed in details by Kueper, et al. [23]. Considering a contamination source, either above- or underground, the pollutant is initially transported and distributed by the aquifer flow in the permeable portion of the

porous medium. With time, in the process of aging, the contaminant diffuses in the low-permeability layers, creating secondary sources which operate by *back diffusion* (Figure 2). It follows that the amendment delivery in the low-permeability layers is of paramount importance for a successful remediation, otherwise other approaches (e.g., multiple treatment trains, hydraulic barriers, PRBs) are required to address the secondary sources, especially if short-lived reactants are used for the remediation of the permeable zones.
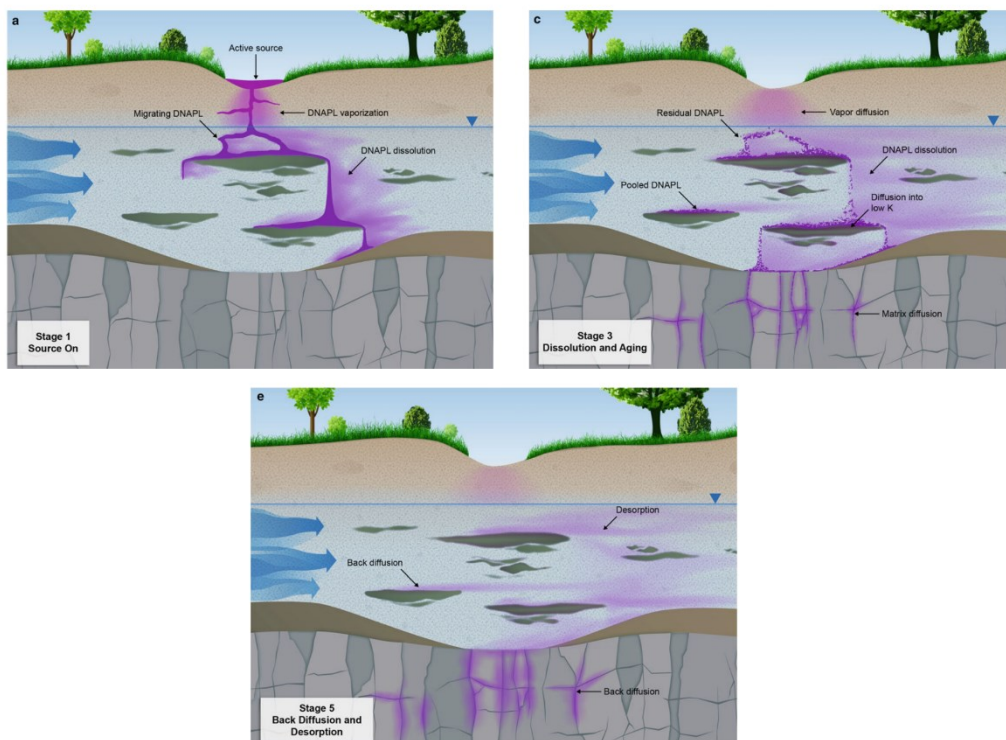
Figure 2) Evolution of a dense non-aqueous contaminant (DNAPL) in the presence of low-permeability layers showing the formation of secondary sources and contaminant backdiffusion; adapted from Kueper, et al. [23]

As the sole increase of injection pressure to overcome advective delivery limits is very likely to lead to fracturing or a flow bypass, in both cases the reactants are not delivered efficiently or at all in the low permeability zones [10, 20, 22, 24]. The principle of electrokinetics (now at the core of electrophoretic analytical techniques) were brought to the attention of the scientific community by F. F. Reuss [25, 26]; electrokinetic is now applied in many fields [27-30] including to soil matrices so that the transport of species could be operated by an electric field [31, 32]. The initial studies and the formulation of the fundamental equation describing the transport mechanisms were carried out in a single glass capillary; later authors

extended electrokinetics to sandy soil as it can be defined as a system of interconnected capillaries [25, 26]. The first application of electrokinetics (EK) to subsoil relates to their consolidation by electroosmotic dewatering [33-35], but soon the potential of the technique was understood and studies on contaminant mobilization and removal was approached in both permeable and low-permeable soils [13, 36, 37]. In such studies, the objective was to achieve the extraction of the contaminant from low-permeability areas and its transport to the electrodes, where it can be removed by pumping or electrochemical reaction. The techniques, based on coupling electroosmotic flow and electromigration, proved very efficient and additives (surfactants, ligands) were used in combination with EK to improve the contaminant extraction [36, 38-40] for both heavy metals [40, 41] and organic pollutants [42]. In recent years, an increasing number of studies started to explore the possibility to use EK transport to deliver amendments in substitution to advective delivery [11, 43-45] since EK transport is independent from hydraulic permeability [37, 46-48]. It was observed that EK delivery allows direct amendments delivery (or contaminant extraction) in low permeability media in short times, whereas in advective regime the delivery occurs by diffusion, and longer times are required [5, 13]. Promising results were obtained in biological remediation applications, where EK was used as a mean to improve the delivery of nutrients and/or electron donors (e.g., lactate) [49, 50] or specialized bacteria strain [50, 51] in low-permeability media.

To offer a comparison of hydraulic- and electrokinetic-driven delivery, three factors should be considered:

- delivery itself, which is the ability to transport the amendment in the desired portion of the aquifer.
- Mixing, which is used to identify the contact achieved between the amendment and an ideal pollutant dispersed in the aquifer during the delivery.
- Spreading, which is intended as the result of the transport and dispersion of the amendment on the longitudinal and transversal direction.

Despite the complex relation of electrical conductivity with soil granulometry and physical properties [52, 53] it is possible to estimate the transport rate for clayey and sandy medium, representative of low and high hydraulic permeability respectively [37, 54], reported in Figure 3. It is possible to notice that the hydraulic gradient allows faster transport rates in permeable porous medium, but both

electroosmosis and electromigration are more performing in low-permeability materials such as clays.
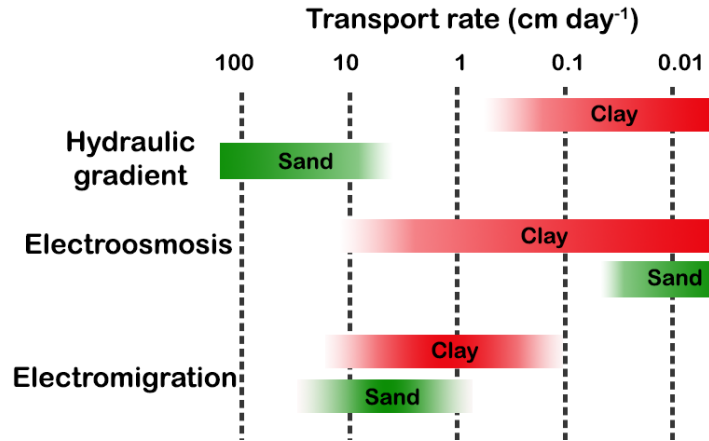
Figure 3) Transport rates ranges estimated for hydraulic gradient and electrokinetic phenomena in clay and sand porous media, adapted from Alshawabkeh [54]

When mixing is considered, the contact of amendments and contaminants is pivotal for a successful remediation; in hydraulic-driven delivery the transport rate for each chemical specie is determined by the effective fluid velocity (v_e) and the retardation factor [5, 18]. It follows that the mixing will occur only if the retardation factor of the contaminant (R_C) is greater than the one of the amendments (R_A) (thus the transport rate is higher for the amendment):

$$\begin{cases} v_A = \dfrac{v_e}{R_A} \\ v_c = \dfrac{v_e}{R_C} \end{cases}.$$

<div align="right">

Equation 2

</div>

In addition, due to the transport of the amendment as a bulk volume and the injection hydraulic displacement mixing is limited to the plume fringes and thus the amount of amendment which enters in contact with the contaminant is significantly lower that the injected quantity. For electrokinetic-driven delivery the charge of the single specie contributes to both the transport rate and direction; three different main scenarios can be identified and are reported in Table 2 for a simplified case of a permeable porous medium (electroosmosis is neglectable):

Table 2) Mixing probability for different scenarios in electrokinetic delivery.

SPECIES CHARGE	MIGRATION DIRECTION	MIXING
Opposed $(Q_A^+/Q_C^-\ ;\ Q_A^-/Q_C^+)$	Opposite	Assured, high mixing
Neutral contaminant	Contaminant only subject to basal flow	Assured, good mixing
Equal charge	Same	To be verified, function of charges and diffusivities

Q_A: charge of the amendment ion responsible for the reaction
Q_C: charge of the contaminant

In the case of an opposed charge sign between the amendment and the contaminant the two migrates in opposite direction, therefore as long as the amendment injection is performed correctly the contact between the two is assured; neutral contaminants (e.g., NAPL) are only subject to the basal flow, it follows the transport rate for the amendment is orders of magnitude greater and the mixing is assured. Lastly, in the case amendment and contaminants carry the same charge sign their mixing depends on the specific charge magnitude and diffusivities, which contributes to determining the migration velocities of the single species. In the case of low-permeability medium the effect of electroosmosis must be considered, generally the mixing is assured in the case of opposed charge while a specific evaluation is required for the other two cases. When electromigration dominates the delivery the entirety of the injected amendment enters in contact with the contaminant, as no fluid flow is involved, and thus a more efficient use of the reactant is achieved.

The fundamental equation describing the electrokinetic transport are nowadays well-established, and the fate of solutes and colloids in a porous matrix under an external electric field can be easily predicted [46-48, 55, 56]. However, the equations were obtained for simple geometries, generally a single cylindric glass capillary [46, 57] or a homogeneous gel matrix [58] and controlled conditions. Although these mathematical theories maintain their validity in a soil porous matrix and have proved to correctly describe the electrokinetic phenomena [31, 36, 59, 60], most laboratory scale application studies focus on a narrow range of conditions and oversimplified geometries [38, 61-64]. The complexity of the system coupled with the multiple transport phenomena at play and controlling variables calls for a more structured approach to explore the effect of boundary conditions on the amendments or contaminant transport. The data obtained can then be used to develop

mathematical tools or add to the wealth of knowledge on example cases, to support the design of full-scale application of electrokinetic transport applied to groundwater and/or subsoil remediation. The aim of this work is to increase the delivery efficiency of amendments in both homogenous and heterogeneous porous media, the latter addressing the problem of delivery in low-permeability inclusions. To achieve an advancement towards an easier implementation of EK delivery, both non-reactive and reactive scenarios were investigated in both one- and two-dimensional geometry. Different scenarios were explored in lab-scale scenarios simulating the delivery of oxidants and reducing agents commonly employed for In-Situ Chemical Oxidation and In-Situ Chemical Reduction. Moreover, thanks to a collaboration with the Denmark Technical University (DTU Environment, Professor Massimo Rolle and PhD fellow Riccardo Sprocati) a mathematical model (NP-Phreeqc-EK) was developed using COMSOL® to predict the fate of the injected permanganate.

This thesis is divided in three sections, besides this Introduction; Chapter 2 discusses the theoretical background of electrokinetic transport in porous media, the main phenomena, the relevant system variables, and the basis of the modelling approach. Chapter 3 is dedicated to the investigation of the permanganate delivery and distribution in a homogenous porous medium under different background conditions, in order to explore the influence on the delivery area and efficiency. In the second part of the chapter the experiments were repeated in a reactive regime on a model pollutant to evidence the implications for a remediation application, providing important evidence on mixing mechanisms during EK. The NP-Phreeqc-EK mathematical model was applied to all the experimental results. Chapter 4 presents an investigation dedicated to the delivery of amendments in low-permeability inclusions, for the optimization of the delivery process and to demonstrate the ability of the amendment to effectively promote the degradation of an immobilized model pollutant. A first set of experiments was performed in 1D geometry to optimize and validate the potential of EK delivery for the degradation of pollutants immobilized in the low-permeability layer, while in the second part of the chapter the study is extended to a 2D geometry. Finally, the last chapter is dedicated to summarizing all experimental findings and presents the implications for full scale applications of EK delivery.

2.2 Aims of the study

The present study aims at increasing the knowledge-base on electrokinetic transport of reactants for groundwater remediation, investigating some of the unresolved and less explored aspects of the technique. Specifically:

• The effect of charge interactions on the transport, mixing and reactivity of amendments in homogeneous porous media. The study is the first performed in a full 2D geometry to explore the multidimensional transport (namely, longitudinal and transversal), whereas previous studies were performed either in columns or 2D experimental set-ups with an amendment injection on the entire cross-section (thus masking multidimensional transport components). Important mechanism acting on plume dispersion, migration velocity and mixing with the soil solution will be examined in both conservative and reactive regime, drawing important conclusions and implications for groundwater remediation applications. A mathematical model was also developed and validated on the experimental data, proving an important tool for the understanding of EK mechanisms [65].

• The mechanism of amendments delivery in low-permeability porous media, normally inaccessible by hydraulic delivery. The study was performed in a one-dimensional geometry to explore:

1) The ability of buffer recirculation in the electrode chambers to prevent the stalling in the amendment delivery previously observed [66-68] and its effect on the migration velocity and delivery in a clay inclusion within a sandy medium.
2) The ability of EK-delivered amendment to maintain and explicit their reactive properties in the low-permeability inclusion. This study was performed on a dye (as model contaminant) to allow for a direct visualization of the reaction development, hence avoiding complex sample procedure from the clay layer that might alter the process. Both oxidative and reductive amendments were delivered, identifying differences in the process with relevant consequences for a full-scale application in groundwater remediation.

• Based on the results of the previous experiments, a protocol was devised to obtain the delivery of permanganate in a fully 2D set-up. Both the clay inclusion

10

and the permanganate did not extend over the entire set-up cross section, allowing for multidimensional transport effect, arising from both charge interactions and flux balance (namely, electromigration and electroosmosis) to manifest. The electrokinetic-assisted delivery was compared to a traditional hydraulic delivery in a similar set-up geometry and experimental conditions. The evidence previously collected proved fundamental in developing the optimal delivery strategy.

Chapter 2

Electrokinetic phenomena in porous media

Electrokinetic (EK) processes occurring in a porous medium are affected by manifold variables, depending on chemical-physical properties of the porous media itself, the chemistry of the soil solution and the substance target for the transport. Such complex system is strictly interconnected and also highly affected by the electric field applied, and the subsequent modifications strongly affect the electrokinetic transport. The detailed knowledge of such interactions and mechanisms are essential to predict the fate of the amendment, specifically its ability to be delivered and its capacity to mix and react with the contaminant, in the design of an EK-assisted delivery.

In this chapter, the physical phenomena driven by the application of an electric field to a saturated soil will be addressed, with focus on their governing variables (e.g. Zeta Potential, electrical mobility, and surface charge) and their interconnection. The theory developed for electrokinetic analytical technique will be discussed and adapted to natural porous media, in order to obtain the fundamental equations to describe the single components of EK transport. Following, the chemical processes at play, their effect on the EK advection and the means to control them will be discussed. Finally, the theory of electrical-driven advection will be presented, with the equation used to model the electrokinetic transport.

2.1 Overview on electrokinetic systems

Electrokinetic (EK) processes result from applying an electric direct current (DC) to an electrolyte, hence creating a current density over the cross-sectional area comprised between the electrodes. The mathematical theory for electrokinetic transport has been initially developed mostly referred to electro-chromatographic analytical techniques, where the electrodes are placed at the two ends of a single capillary filled with an electrolyte solution [46, 55, 57]. In the case of electrokinetic remediation, the porous matrix can be seen as a 'bundle' of capillaries, each of them consisting in a pore channel that is saturated with the soil solution [36, 37]. Four different phenomena will take place once a DC electric field is applied to the system: a) electromigration b) electroosmosis c) electrophoresis c) electrolysis, where the latter is a chemical phenomenon while the rest are physical phenomena. All EK phenomena are affected by manifold variables, depending on chemical-physical properties of the porous media itself, the chemistry of the soil solution, the substance target for the transport and the electric field applied, along with the subsequent modifications it causes. A detailed knowledge of the aquifer properties then required to properly understand and predict EK transport, as these properties determine whether a compound is effectively subject to an EK-induced transport, the resulting mass flow, and its direction (namely, towards which electrode the transport occurs). In order to proceed further in the discussion, a common terminology must be defined, especially regarding the two electrode polarities. This need arises from the different nomenclature criteria for cathode and anode, as well as to define a common terminology for the relevant system variables [34, 69, 70]. From a chemical standpoint the definition of cathode and anode is univocal: "reductions occur at the anode, consuming electrons; oxidations occur at the cathode producing electrons" [71]. From an electrical standpoint, which is more appropriate when describing a physic-based phenomenon, cathode and anode are defined according to their polarity. Since cathode and anode hold a respective polarity rather than absolute polarity the cathode can be either the positive or the negative electrode, depending on the occurring process [34, 69, 70]. If the system work as a galvanic cell, hence current is produced by spontaneous reduction-oxidations (e.g. fuel cells), the cathode is the positive electrode [69]. In systems where current is consumed to do a work, as is the case for EK, the cathode is the negative electrode [34]. Therefore, in the case of electrokinetic transport, which requires current consumption, the cathode is always the negative electrode [31, 37] and current flows from the anode to the cathode as cationic flux, as by convention [72].

The simplest system is comprised of a conductive liquid medium, referred as background electrolyte contained in a micro- or nano-channel and the sample to be transported across the capillary. The power supply allows to set a potential difference between cathode and anode; the resulting current obeys Ohm's law, where the resistivity is determined by the electrolyte conductivity. [36, 46, 48, 57, 73].
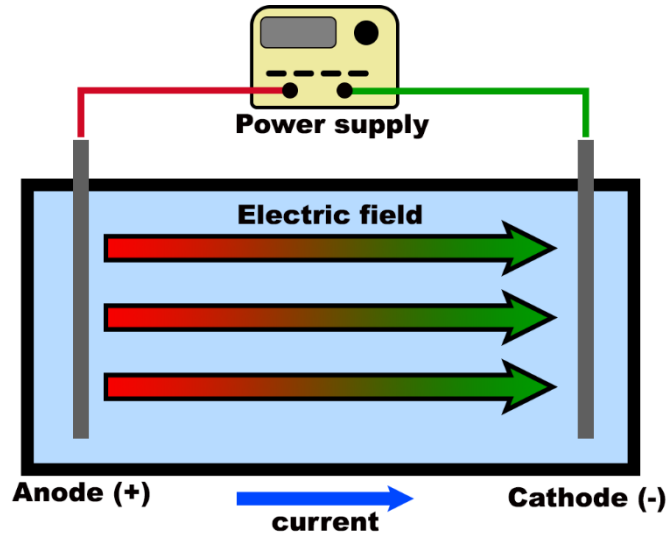
Figure 4) Generic schematics for an electrokinetic system depicting the principal components of an experimental set-up and the main electrical parameters.

In most soils the solid matrix is a poor conductor, therefore applying the most generic definition of current, a charge flux, it follows that in a liquid electrolyte conduction is carried by ions. [39, 74-77]. The electric field thus generated will affect i) the soil solution ii) the colloidal suspension in the soil solution iii) the soil particles [37, 48, 73]. Three different physical phenomena arise from such interactions: electromigration, electroosmosis, and electrophoresis which will determine the transport fate of the sample. The net contribution of each of these components is determined by soil mineralogy, porosity, tortuosity and soil solution, composition and conductivity, [37]. Simultaneously, the soil solution and the porous matrix are also affected by reduction-oxidation (redox) reactions [57, 78], which occurs only at the electrode surface [64, 79, 80].

2.2 Electric-driven physical phenomena in porous media

From a general standpoint, every physical phenomenon enabled by an electric field occurring in a porous media is a response of a net charge in the media itself to the polarity of the electric field [46-48, 57]. In a saturated porous media, two types of charge can be identified:

- Ionic charge: due to the presence of the electrolyte the soil solution contains dissolved ions, characterized by a point-charge proportional to the elementary charge e and the ion valence z [46, 47, 57].
- Surface charge: solid particles hold a charge due to unbalanced bonds in their edges structure, which is distributed on the solid surface [81-84]. For a proper approach to EK, a distinction must be made among colloids dispersed in the soil solution and the porous matrix. The former, being able to move within the pore channels (although with size constraints) are defined mobile charge [85, 86]. The soil matrix, unaffected by either hydraulic or electrokinetic flow, is defined immobilized charge. This difference will result in a significantly different EK behavior [57, 78, 82, 84, 87]

The ionic charge results in *electromigration* (EM), the direction of the migration flux depends on the ionic charge, cations (positive ions) will move towards the cathode while anions (negative ions) will move towards the anode [36, 37, 88]. The surface charge of the solid matrix results in *electroosmosis* (EO), often defined as "the relative motion of a liquid to a spatially fixed charged surface"[57]. In other words, EO results in an advective flow towards the electrode with the same polarity of the solid surface. The electrostatic driving force does not act directly on the solid matrix, but to the ion gradient which is formed by the interactions with the electrolyte [36, 46, 48, 73]. The surface charge of the colloids is responsible for *electrophoresis* (EP); such phenomenon is similar to EM, as it acts directly on the particle which bears the charge, but it is described by the same theory which applies to EO [36, 46, 47, 89, 90]. Hydraulic flow and chemical diffusion can coexist with EK transport; Darcy and Fick law can be used to accurately describe the respective transport but a careful evaluation in the definition of the driving gradient is required.

In the following sections, the different phenomena will be discussed in detail separately extending the electrophoretic theory to porous media. Once the constitutive equation will be defined, we will proceed to a comprehensive approach in order to define a general equation for a complex system where all the above-mentioned processes occur.

2.2.1 Electromigration

Electromigration (EM) refers to the motion of ions in the soil solution to the electrode of opposed charge, due to electrostatic attraction created when a direct current is applied [36, 37, 63, 91]. The mathematical approach considers ions as point-charges (hence, with zero mass and not subject to frictional forces) immersed in a homogeneous electrolyte [37, 92, 93]:
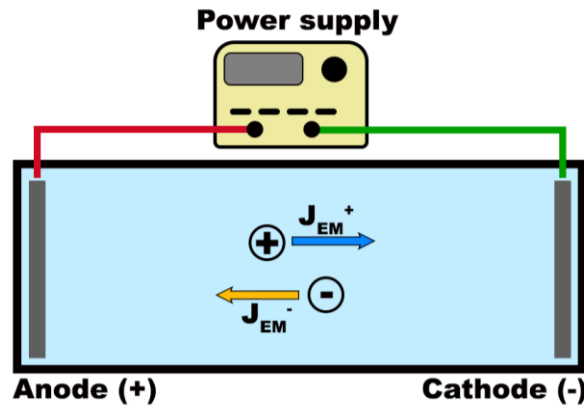
Figure 5) Schematic representation of electromigration of ions immersed in an electric field. The principal components of an experimental set-up are shown, with the migration behavior of anions and cations.

The EM flux is a response to a potential gradient, therefore a Fickian approach is applied to describe the electromigration flux for the *i-th* component over the system cross-sectional area [36, 37, 91, 94]:

$$J_m^{EM}{}_i = -k_i^{EM^*} \cdot c_i \cdot \nabla\Phi \; ;$$

<div align="right">Equation 3</div>

where J_m^{EM} (mol m^{-2} s^{-1}) is the EM mass flux, k_i^{EM*} indicates the effective ionic mobility (m^2 s^{-1} V^{-1}), c_i the concentration of the j-th species (mol m^{-3}) and $\nabla\Phi$ the potential gradient (V m^{-1}). When compared with a classic formulation of Fick's law of diffusion, the concentration gradient is replaced by the electric gradient and the dependency from the diffusion coefficient persists, scaled by electrostatic parameters as the ion valence. The migrational ionic mobility still lacks a defined and unanimously accepted mathematical definition, its most used formulation follows Nernst-Townsend-Einstein relation [37, 91]:

$$k_i^{EM*} = \frac{D_i^* \cdot z_i \cdot F}{R \cdot T} \; ,$$

where D_i^* is the effective diffusion coefficient (m^2 s^{-1}), z_i is the valence of the ion including the charge polarity, F is Faraday constant (96485 C mol^{-1}), R is the ideal gas constant (8.314 J K^{-1} mol^{-1}) and T is the absolute temperature (K) [37, 63, 84, 91]. Except at the nanoscale or considering a single linear capillary, the porous matrix affects the migrational mobility. Differently from a free fluid, where diffusion occurs along the shortest path, the porous medium introduces severe limitations to particle trajectories [31, 37, 94]. Firstly, ions cannot move through soil grains, but must travel around particles following the soil tortuosity; also, dead-end pores will be mostly excluded from electromigration. As a consequence, diffusion is expected to be slower than in free fluids, with direct effects on ionic mobilities [84, 88]. For this reason, the effective diffusion coefficient is introduced; many formulations are available with different levels of complexity. Some includes viscosity and adsorption but the most relevant variables affecting diffusion in porous media are geometrical parameters, specifically: *tortuosity* (τ) [84, 94]. Tortuosity is a parameter used to account for the complexity of the channel matrix in a porous material, in specific the fact that pathways can be significantly longer than the straight path between two points in the media [95-97].
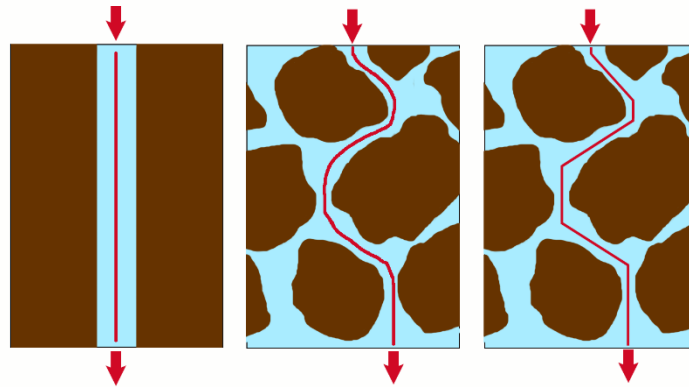
Figure 6) on the left, straight (shortest) pathway in a capillary channel with negligible Brownian dispersion; in the middle pathway lengthening introduced by the porous matrix, on the right schematic representation of geometric tortuosity.

The general mathematical definition of tortuosity is straightforward: it can be computed as the average pathway length (Ĺ) over the straight-line length (namely, the shortest path) [96, 98]:

$$\tau = \frac{Ĺ}{L} \; ;$$

$$\begin{cases} \lim_{n \to 1} \tau = 1 \\ \lim_{n \to 0} \tau = \infty \end{cases} .$$

Equation 6 implies that tortuosity increases with the reduction in porosity, however the extent of the reduction in the available pathways strongly depends on the considered phenomena different tortuosities are defined accordingly as geometrical τ_g, hydraulic τ_h, electrical τ_e and diffusive τ_d tortuosity [95, 96]. Usually, the values slightly differ to each other, and it is found as a general rule that τ_g has the lower values as its path can cut through the streamlines of hydraulic, electrical, or diffusive flow (Figure 6). Despite the presence of such variety of parameters, the problem of using tortuosity lies in the confusion among tortuosity and tortuosity coefficient or factor [95-98]. Focusing on geometrical tortuosity only, from its mathematical definition the value of τ_g is always expected higher than one, since the soil grain obstructs the most direct path. The geometrical tortuosity coefficient is defined as [96]:

$$\mathbb{T}_g = \frac{1}{\tau} ,$$

hence $\mathbb{T}_g$ is always lower than one. When it comes to use tortuosity to define the effective diffusion coefficient, we expect D^* to be lower than D, as a longer path will slow diffusion down. Therefore, two expression can be written, for tortuosity and tortuosity coefficient [94, 99]:

$$D_i^* = D_i \cdot \frac{1}{\tau} \qquad or \qquad D_i^* = D_i \cdot \mathbb{T} .$$

With this aspect in mind, we can proceed further expanding the mathematical definition of the electromigration flux and velocity [31, 37]. In the first work on the relationship between tortuosity and diffusion, the correct symbology is applied, and the leftmost formulation of Equation 8 is used [95, 97]. With this aspect in mind, we can proceed further expanding the mathematical definition of the electromigration flux and velocity [36, 37, 91, 93]:

$$J_m^{EM}{}_i = \frac{(D_i \cdot \mathrm{T}) \cdot z_i \cdot F}{R \cdot T} \cdot c_i \cdot \nabla\Phi \; .$$

<div align="right"></div>

$$v_i^{EM} = \frac{F}{R \cdot T} D_i^* \cdot z_i \cdot \nabla\Phi$$

<div align="right"></div>

From Equation 8 we can see how the electrolyte type and concentration plays an important role, but also how the soil texture influences the system. Literature data shows a greater significance of EM in coarse porous media (sand, gravel) than in fine porous media (clays, silt - see also Figure 3) [36, 54]. However, a more accurate approach must be taken regarding the migrational flux, since the potential distribution may also be affected by the porous matrix [77, 100] in a way which may compensate the reduction in the diffusion coefficient.

Mechanism of electromigration flow

As electromigration affects only the dissolved ions, the resulting transport is significantly different from advection [36, 37] with relevant implication for amendment reactivity in the field of remediation. In the advective scenario, the entire injected volume is subject to transport, namely the dissolved ions and the solution water; they move as a unit volume under the basal flow or an external pressure (e.g. injection well) [5, 18]. During advective transport, only the plume fringes interact with the surrounding pore solution and consequently are subject to dilution, while the bulk of the injected volume maintains its initial concentration, but it is not affected by mixing with the pore solution [5, 18, 19]. Electrokinetic transport affects the single ionic species, which can be equivalated to point charges (namely, with no mass): no frictional or viscous forces act on the transport and all the ions are subject to the same electric gradient [92, 101]. Not accounting for chemical diffusion and mechanical dispersion implies that the plume is not affected by dilution at all and is completely mixed with the pore solution. This difference from advective transport is remarkable, and leads to important implications for remediation applications, where amendment concentration plays a fundamental role in the reaction kinetics and efficiency. Firstly, the porous media permeability does not affect the delivery of solute amendments, allowing the remediation of low permeability layer such as clays and silts, otherwise inaccessible by advective transport [45, 66]. Secondly, EM also affects the mixing dynamics of the

amendment: since the transport involves only the ionic species, complete mixing of the entire injected concentration is rapidly achieved instead of a progressive mixing by diffusion and dispersion. It follows, the reaction kinetics are significantly increased, thanks to a higher reactant concentration; a careful evaluation is required in this regard as sometimes higher kinetics can result in a too fast consumption of the reactant. Nonetheless, electromigration delivery presents interesting aspects and potential in the field of environmental remediation of groundwater and subsoil for which it can be preferred over hydraulic advection.

2.2.2 Electroosmosis

Electroosmosis (EO) is often defined as "the relative motion of a liquid to a spatially fixed charged surface" [57] and plays a pivotal role in the electrokinetic transport of solute and colloids. Following its definition, electroosmosis phenomena always occur when an electric field is applied to an electrolyte in contact with a fixed charged surface. The surface charge of the solid matrix induces a rearrangement in the soil solution ion distribution, which leads to the formation of an Electrical Double Layer (EDL) and a bulk electroneutral solution [57, 102]. Specifically, the conservation of electroneutrality leads to an accumulation of counterions on the solid matrix to balance its surface charge. These ions are normally subject to electromigration; due to the strong coulombic forces and viscous effect [103], a drag force extends to the soil solution resulting in and advective electroosmotic flow (EOF) [46, 48, 57]. The EOF direction depends on the polarity of the charged surface, in more details EOF advection occurs towards the electrode of same polarity as the soil matrix, or in other words the opposite polarity of the EDL. It is very important to notice that given its nature EOF has a direction which acts indiscriminately on both cations and anions in the bulk soil solution, hence it will counteract electromigration and electrophoretic flux with the same charge sign than the surface charge [46, 57]. EOF magnitude depends on multiple parameters of both the solid surface, the pore solution, and the electric field strength [36, 48, 57, 91], which will be discussed in detail later in this section.

To better understand the EDL and to simplify the approach to the problem we need to address the nature of the surface charge, which arises from unbalanced charge in a material; two different type of causes are identified [36, 48, 73, 84]:

- Atomic substitution in the crystal lattice, involving atoms with same ionic size but different valence. It usually applies to silicates, where silicon atoms are substituted with aluminum given the difference in valence Si^{4+} and Al^{3+}, while isomorphic substitution is rare in oxides and non-silicate mineral in

general [36, 84]. Since isomorphic substitution does not modify the crystal lattice, a reduction of the cationic charge results in a net negative charge, carried by an oxygen atom. Such charge is defined *permanent*, as it is unreactive to pH equilibria.

- Non-bonded groups on the surface, which are always present in material with finite dimensions. In most cases such groups are hydroxyl groups, leading to a pH-sensitive charge, which can be positive, neutral, or negative [83-86].

$$\begin{cases} bulk - Si - OH + H_2O \leftrightharpoons bulk - Si - O^- + H_3O^+ \\ bulk - Si - OH + HO^- \leftrightharpoons bulk - Si - O^- + H_2O \end{cases} ;$$
$$bulk - Si - OH + H_3O^+ \leftrightharpoons bulk - Si - HO_2^+ + H_2O \ ;$$
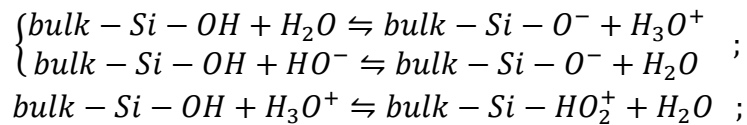
- Adsorbed species, such as organic matter, can create a layer with a pH-dependent surface charge. Such condition is common in real soils, but can be neglected in laboratory experiments performed with clean sands [19, 84].

The surface charge is therefore strongly dependent on the material history, its ratio of isomorphic substitution and its grain size which also affects the number of hydroxyls effectively available for dissociation and their dissociation constant. We then expect a different electrophoretic behavior for different type of sands and for clay minerals [85, 104, 105].
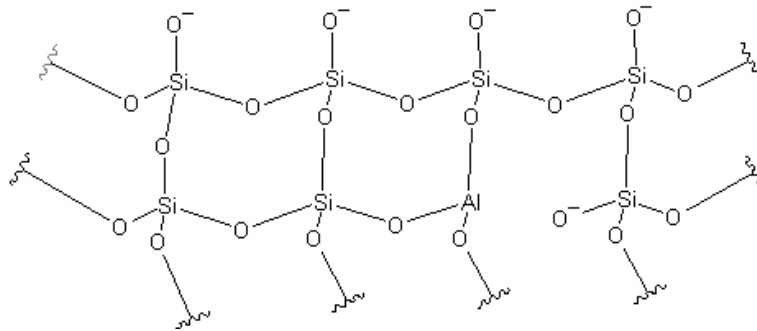
Figure 7) Effect of surface non-bonded hydroxyl groups and isomorphic substitution on the porous matrix surface charge. A generic flat representation of the clay crystalline lattice is used.

The magnitude of the electroosmotic flow (EOF) is strongly dependent on the EDL properties, which determine the charge distribution in the pore channels and therefore the strength of the coulombic interactions [46, 48, 57]. The determination of the charge distribution depends on the geometry of the double layer, which in turns is affected by the surface charge and electrolyte properties. Two different

mathematical theories have been developed to describe EOF in pore channels to account for the EDL thickness. Specifically, whether the EDL thickness is smaller or greater than the pore radius [48, 57, 106, 107]. In the former case, EOF is unrelated to the pore radii and depends only on Zeta Potential and electrolyte properties, in the latter EOF depends on pore radius and a different parameter must be used for the EDL potential. The Electric Double Layer theory must be then discussed in further details before introducing the constitutive equations for EOF evaluation [36, 46, 57, 73].

Electric Double Layer theory and electroosmotic flow

Considering a solid matrix with a surface potential Ψ^- (Volts) the formation of the EDL is independent from the application of a direct current. Such surface charge exerts an electrostatic force on the ionic electrolyte forcing an accumulation of countercharge in the fluid close to the surface [55, 57, 104, 106]. In an ideal system Helmholtz theory applies, which considers ions as point-charges. In this approximation, a cationic monolayer is adsorbed on the solid surface with charge $\Psi^+_{MONO}=\Psi^-$, hence the surface charge is completely balanced. Steric and coulombic interactions of real systems lead to a defect in the monolayer charge, namely $\Psi^+_{MONO}<\Psi^-$. The most accepted theory to address this defect, which represents a good compromise between complexity and accuracy, is the Stern model, which unifies Helmholtz and Gouy-Chapman theories [19, 57, 92]. According to the model three different layers are formed in the process [57, 106]: a) the Stern layer b) the Gouy-Chapman layer c) the solution bulk [57, 108, 109]. The Stern layer, or rigid layer, is formed at the solid-liquid interface by strong electrostatic attractions acting on the dissolved ions of opposite charge with respect to the surface [46, 57, 73]. Such electrostatic force extends also to the hydration water and coupling with frictional forces creates a stagnant layer impervious to advection [57, 106, 110]. The nature of the Stern layer can be addressed as a physical adsorption of an ionic monolayer, it follows that the thickness of the Stern layer is usually within units of Angstroms [55, 57, 106] and the surface charge cannot be fully balanced. The Stern layer boundary with the Gouy-Chapman layer is called *shear plane*; within the Stern layer the potential decrease linearly with distance [19, 55, 70, 110]. The Gouy-Chapman layer, or outer diffusive layer is formed to balance the residual surface charge; its potential decreases exponentially with distance from the surface to eventually reach electroneutrality in the bulk solution [55, 70, 106, 109, 111, 112].

Two scenarios can be identified, the first is defined 'thin EDL' and implies that electroneutrality is reached in the bulk solution, the other is defined 'thick EDL' and refers to those cases where the solution ionic composition is unable to balance the surface charge in the pore volume [19, 57, 82, 92]. The flow velocity depends on the diffuse double layer potential, however coulombic, viscous, and frictional forces within the EDL have also relevant effects [57, 113-115]. A detailed analysis of such phenomena is beyond the scope of the present work, but it is an important concept in understanding the velocity flow profile is the viscoelectric effect, namely an increase in viscosity with increase in the potential ψ [115, 116].
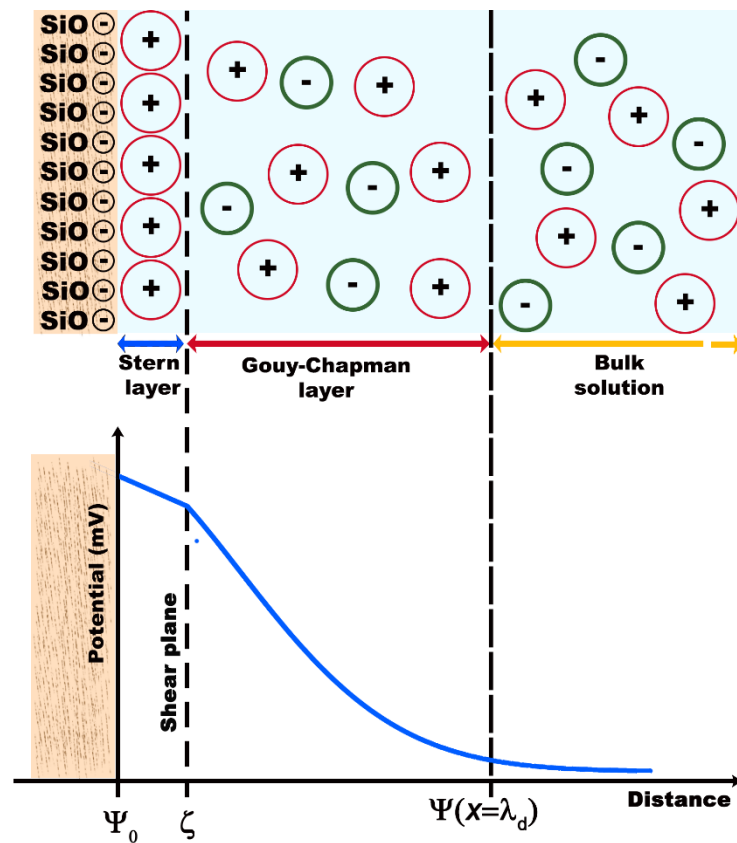
Figure 8) Schematic representation of the charge distribution and potential variation in the pore solution for an electrolyte in contact with a charged surface according to the EDL theory

The EDL theory defines a null velocity in the Stern layer and at the shear plane, whereas in the Guy-Chapman layer velocity increases with distance to the surface as ψ decreases according to the LPB equation. In the case of the "thin EDL" the bulk solution is electroneutral, such coulombic and viscous forces reduces and a velocity $v=v_{max}$ is reached. The resulting flat flow profile, in contrast with the

parabolic profile for hydraulic flow, reduces the dispersion during the electrokinetic transport. Such effect is of great relevance in case of reactive transport of amendments, as a reduced dispersion will result in higher local concentration and in higher kinetics rates [48, 57, 113, 115, 116]. In the "thick EDL" case, the viscoelectric effect extends in the whole pore radius and no bulk electroneutral solution can be identified. Consequently, the curvature in the velocity profile also extends over the pore diameter and the velocity at the center of the capillary is usually smaller than v_{max}. The resulting flow profile is parabolic, as for hydraulic flow, and the transport is subject to a higher dispersion and diffusion affecting reaction kinetics as mentioned above [46, 48, 57].
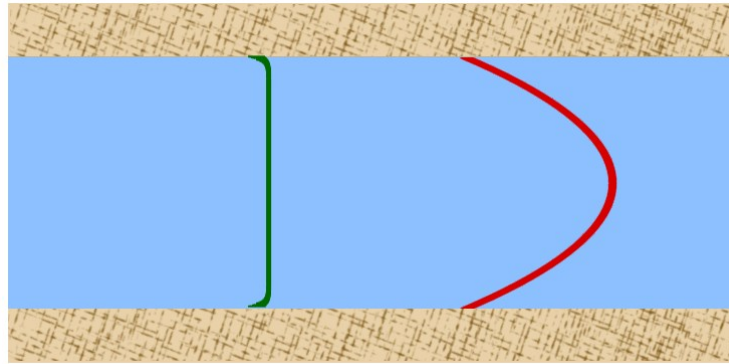
Figure 9) Flow profiles for a "thin EDL" scenario (green line), resulting in a flat flow profile, and for a "thick EDL" or hydraulic flow scenario (red line), resulting in a parabolic flow profile.

Approaching the EDL formation in soils, the system allows some relevant approximations. Given the soil mineralogy, Zeta Potential varies with pH and ionic strength [82, 84, 85, 104, 117] but in most cases the silicate phase is predominant, and except for quartz all silicates exhibit a negative surface potential. There are many literature works comparing experimental and computed data which support such approximation, which allows to define a common phenomenology of EO [81, 82, 112, 117, 118]. In all cases the flow will occur, it will move from the anode to the cathode; the flow magnitude depends on pH and will reach a maximum value at alkaline pH, while it will be close to negligible for acidic pH. The exact extent will remain a function of both soil properties, in terms of response to pH and ionic strength shielding of the surface charge, and electrolyte properties such as ionic strength [48, 57, 73].

When the "thin EDL" assumption is valid, and pore size does not affect the velocity profile, the electroosmotic flow is then described by the Helmholtz–Smoluchowski equation, which defines an electroosmotic velocity (v^{EO}) resulting from the application of an electric field [46, 48, 57, 59, 111]:

$$v^{EO} = \frac{\varepsilon \cdot \zeta}{\alpha \cdot \pi \cdot \eta} \cdot \nabla\Phi \ ,$$

where ε represents the solution permittivity (C V^{-1} m^{-1}), ζ the Zeta Potential (V), η the fluid viscosity (kg m^{-1} s^{-1}), $\nabla\Phi$ the electric gradient (V m^{-1}) and the constant α is used to account for the particle size with respect to the channel size (l_D, pore throat in the case of porous medium). In the case of larger particles $\alpha=4$, while for small colloidal particles $\alpha=6$; in the case of a solid porous matrix a value of $\alpha=4$ is found to be more appropriate [46, 48, 57].
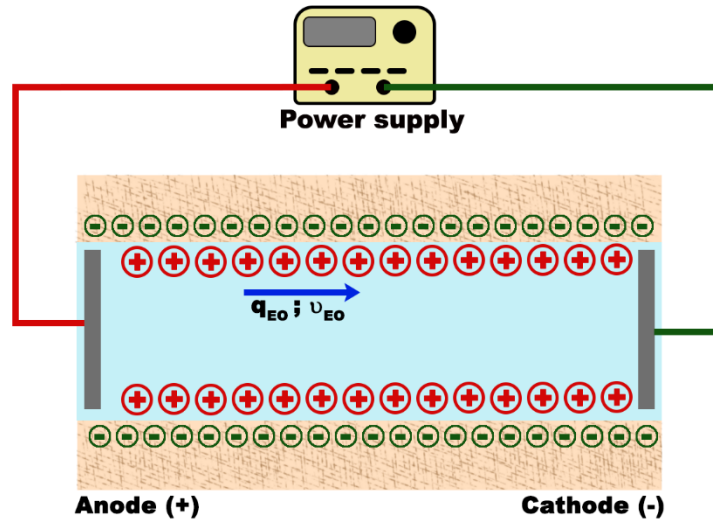
Figure 10) Electroosmotic flow dynamics in a negatively charged porous media, representative of a natural soil pore channel under application of a direct current.

From the electroosmotic velocity the electroosmotic permeability (k^{EO}) is derived [46, 48, 57, 73, 91]:

$$k^{EO} = \frac{\varepsilon \cdot \zeta}{4\pi \cdot \alpha \cdot \eta} \ ;$$

When the Helmholtz–Smoluchowski assumption fails for small pore radii, Schmid [119] introduced an alternative formulation for the electroosmotic permeability accounting for the pore radius and the volumetric charge distribution in the pore solution [19, 48, 119]. Although the model can be applied easily to homogeneous porous media, in the case of inclusions either an average value of R is used, or a set of N equations must be defined where N equals the number of solid phases in the system. Therefore, the most common approach is to apply the thin EDL approximation; such approach is supported by many literature works and allows an easier modeling approach maintaining good accuracy [35, 120, 121]. In both cases, the volumetric electroosmotic flow (q^{EO}) in a single capillary can be expressed as [19, 48, 57]:

$$q^{EO} = A_i \cdot k_{EO} \cdot \nabla\Phi \ ,$$

where A_i is the capillary cross-sectional area. To extend the equation to a porous medium, each pore channel can be assimilated to a single capillary, and therefore the total capillary cross-section (namely A=ΣA$_i$) can be approximated as the product of the cross-sectional area of the matrix A_T and the medium porosity [19, 48, 57]. The overall volumetric osmotic flow for a porous matrix is then defined as:

$$q^{EO} = n \cdot A_T \cdot k_{EO} \cdot \nabla\Phi \ .$$

Contrarily to EM, electroosmosis is predominant in fine porous media due to their higher surface charge compared to coarser materials [36, 37, 48]. It is also important to notice that EOF is associated with a hydraulic flow and a water displacement from the anodic to the catodic side of the system [34, 36, 121]. In time, if the hydraulic gradient is not counterbalanced by a pumping system, the Darcian flow will equal the electroosmotic flow and the system will reach a steady state. After such point, transport will be related to electromigration (and, eventually, electrophoresis) only [36, 122].

2.2.3 Electrophoresis

The phenomenon of electrophoresis (EP) consists in the transport of charged colloids or large molecules dispersed in the soil solution. The physic of the phenomenon contains elements of EM and EO, as the transport involves charged particles, which are no longer point-charges as ions, but their charge arises from their surrounding EDL [36, 46, 57, 123, 124].
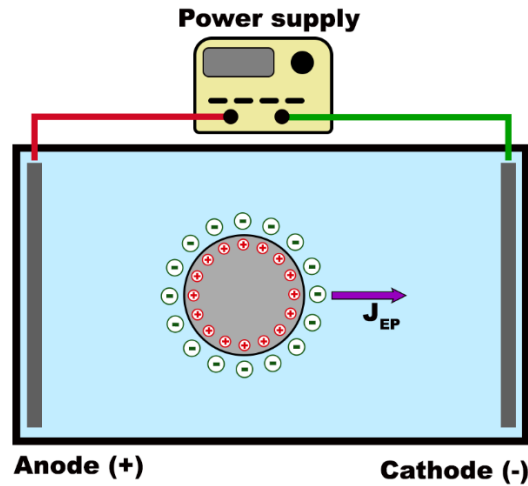
Figure 11) Representation of electrophoresis for a positively charged colloidal particle. Charge signs and electrophoretic flux direction are reversed for a negatively charged colloid. The electrophoretic flow is directed towards the cathode, as from the EDL theory the adsorbed charge can not balance the colloid surface charge.

The advection force is determined by the surface charge of the colloid particles (ζ_{NPs}), but since they are not point charges like ions (which means, a particle size r is defined), a frictional resistance is opposed by the fluid [46, 47, 57] As for EO, also in the case of electrophoresis the Helmholtz–Smoluchowski approximation allows a good and accurate description of the mobility in both ideal and real porous media [35, 36, 121] and the electrophoretic mobility is defined as follows:

$$k_i^{EP} = \frac{\zeta_{NPs_i}}{6\pi \cdot \eta \cdot r_i} \; ,$$

<div align="right">Equation 15</div>

Since the present works focuses on the transport of solutes, a further in-depth discussion would be excessive and without feedbacks from the experimental activity.

27

2.2.4 Total electrokinetic flow

In the most generic system containing a background electrolyte and a charged sample both electroosmosis and either electromigration (for soluble ions) or electrophoresis (for colloids) occur simultaneously [46]. Since the surface chemistry of most soils results in a negative surface charge, the electroosmotic flow will have cathodic direction. Contrarily, electromigration and electrophoresis depend on the charge of the ion, or the particle, constituting the injected sample. The overall effect depends on the reciprocal strength of EO and EM (or EP), and consequently from the species concentration and mobilities, as well as from geometrical and chemical parameter of the solid matrix [46, 57]. To consider the total flux two approaches are suggested. The first is preferred for analytical techniques (electro-chromatography) and consists in computing an effective electrokinetic mobility (k^{EK}_{obs}) for cations and anions respectively, as [46]:

$$k^{EK}_{obs}|_i{}^+ = k^{EO} + \begin{cases} k^{EP}|_i{}^+ \\ k^{EM}|_i{}^+ \end{cases},$$

$$k^{EK}_{obs}|_i{}^- = k_{EO} - \begin{cases} k^{EP}|_i{}^- \\ k^{EM}|_i{}^- \end{cases}.$$

<div align="right">Equation 16</div>

A different approach is suggested for electrokinetic transport in porous media [31, 125, 126], which considers the electroosmotic flow as an advective component of the total flux equation, namely the Nernst-Plank-Poisson equation that will be discussed in the last section of this chapter. Both approaches are equally valid, for a more general approach the latter is to be preferred as it allows a simultaneous evaluation of the water displacement and of the electroosmotic hydraulic gradient. Assuming the study case is referred to a negatively charged capillary wall, as in the case of most silicate-based materials [85, 112, 117] Figure 12 depicts the different flow components.
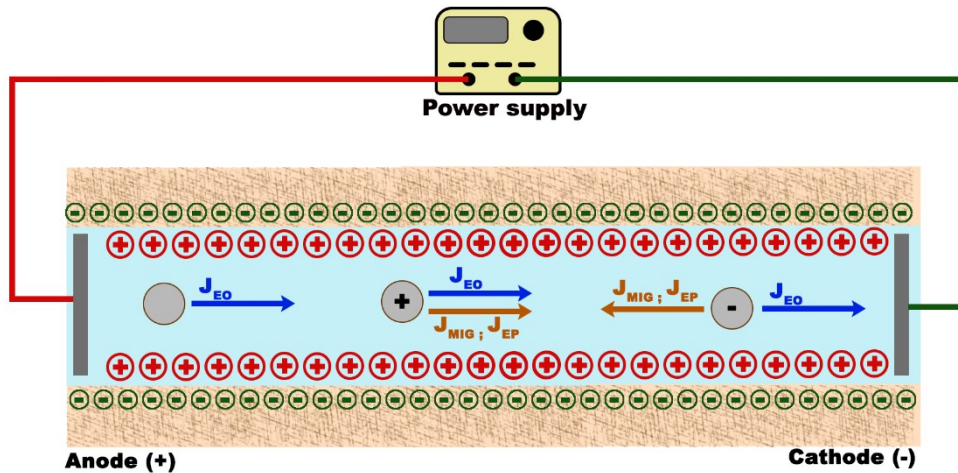
Figure 12) Schematic description of electroadvective forces acting (from left to right) on neutral, positively, and negatively charged species in a porous media subject to an electric gradient. The arrow length is not a measure of the single flux components magnitude.

Migration of cations will be sped up, while migration of anions will be slowed down, completely stopped or in extreme cases inverted in direction when electroosmosis prevails [46, 47, 57]; non-charged particles are usually transported by electroosmosis only, except when polarization effects occur [127, 128]. The system evolution also plays an important role: excluding variations in the EDL thickness and electromigration can result in local variation in ionic strength while pH variation can arise due to an unbalanced electrolysis. Both these parameters contribute to the definition of the Zeta Potential and thus to the magnitude of EOF, significant variations in solutes and colloids transport over time were observed in experimental works [66, 67, 80, 129].

2.2.5 Complex conductivity in porous media

For all the electrokinetic transport phenomena the driving force is the electric potential gradient, therefore its distribution in the porous media is of paramount importance in the prediction and modeling of EK applications. Since the soil porous matrix is non-conductive the electrical conductivity is ascribed to the soil solution only. However, in the same way we defined effective diffusion coefficient due to the presence of the porous matrix, an effective conductivity must be defined for an accurate description of the system [74, 100, 130]. The soil solutions affect ionic strength, hence conductivity, and ion composition, relevant for cationic/anionic exchange; the porous medium structure defines a) the fluid volumetric concentration (porosity) b) the conductive path, both in terms of length (tortuosity) and accessibility (cementation) since no conduction occurs in dead-end pores c)

surface chemistry (cation/anion exchange) [130]. These matrix properties are used to adjust the reference value for conductivity, provided by the electric conductivity for the free fluid. The most general equation, referred to clean sands, was developed by Archie [100] in terms of resistivity ρ:

$$\rho^{eff} = \rho_W \cdot n^{-m} \rightarrow \sigma^{eff} = \sigma_W \cdot n^{-m} \; ;$$

which implies the effective conductivity σ^{eff} is proportional to the solution conductivity σ_w scaled down by a form factor n^{-m}. The terms n is the soil porosity [74, 100, 130], while the terms *m* is defined *cementation* and increases when the fraction of disconnected pores increases. Such trend of the value of *m* is supported by the fact that all the water in dead-end pores do not participate in conducting the applied current [75]. Despite its simplicity, Archie's law has been developed considering a narrow range of soil types and fails to predict the conductivity for clayey soils [75, 131, 132]. To overcome such shorting of Archie's approach some empirical models have been suggested [75], but such approach is very limited for modeling purposes. Different theoretical models that approach the problem from an electrical standpoint have been presented [74, 75, 130]. The system is represented in terms of connected resistors, where the solid matrix, the exchange ions and the bulk solution are addressed separately [74]. The most widely accepted model was proposed by Waxman and Smits [77] and considers two resistors in parallel, one describing the bulk solution and one the exchanged ions on the clay surface [74, 77]. The formulation of the total conductivity derives from the work of Wyllie and Southwick [1] and states:

$$\sigma^{eff} = X \cdot \sigma_r + Y \cdot \sigma_w \; ,$$

where σ_r refers to the CEC, σ_w to the bulk solution, the geometrical factors X and Y cannot be defined independently from the specific porous medium, hence the model is of difficult implementation. A more advanced model based on the ionic distribution in the Stern and diffuse layer has been suggested by Revil et.al. [133, 134]. The model is developed as follows:

$$\sigma_{eff} = \sigma_+ + \sigma_- \quad ,$$

$$\sigma_\pm = t^f_{(\pm)} \cdot \sigma_f \cdot \varphi^m \cdot \left(1 - \frac{t^S_{(\pm)} \cdot \sigma_f}{t^f_{(\pm)} \cdot \sigma_f}\right)^m \cdot \left(1 - \frac{t^S_{(\pm)} \cdot \sigma_f}{\sigma_{(\pm)}}\right)^{-m} \quad ,$$

where the symbol $\pm$ in subscript indicates that the terms could refer to both a cation and an anion. In such model [133]:

- the current fraction transported by the electrolyte is defined by the "Hittorf transport numbers" $t_\pm^f$ proportional to the specific ionic mobilities.
- The parameter σ indicates the effective conductivity, divided in cationic σ_+ and anionic σ_- conductivity; σ_f refers to the pore fluid conductivity and σ_s to the surface conductivity. The latter is related to the surface specific conductance Σ_s and the grain size R:

$$\sigma_s = \frac{2\Sigma_s}{r_g} \quad ;$$

- The definitions of the geometrical factor φ and the cementation exponent m follow the previous models [74, 100, 130].

While a correct definition of effective conductivity is required for hydrogeophysics applications, such as determination of the formation factor or the study of microscale phenomena where the dependence from the porous matrix is more relevant, in the case of a macroscopic approach to electrokinetic delivery of solutes or colloids the need of a model depends on a case-by-case scenario. In homogenous sandy porous medium the use of the soil solution conductivity can suffice, allowing for a good mathematical description of the system. In the case of heterogeneous porous medium the differences between the porous media are more relevant, however a rigorous approach such as the one proposed by Revil, et al. [53] involves the experimental determination of the zeta potential in bulk conditions and of the Hittorf transference numbers. Dependency from soil solution composition, sandy porous medium, clay water content and compaction affect the relevant variables and would increase the complexity of the study. In the present work, a qualitative approach is applied to the study of electrokinetic delivery in

heterogeneous porous media to highlight the potential of electrokinetic delivery in the remediation of low-permeability layers.

2.3 Electric-driven chemical phenomena in porous media

The presence of a source of direct current in a liquid system during electroadvection leads to the occurrence of reduction-oxidation reactions (redox). Such reactions involve electrons transfer from a donor (reductant) to an acceptor (oxidant) and can be divided in half-reactions, where electrons are among the products and the reactants, respectively.

$$
\begin{array}{ll}
Red \rightarrow P_1 + ne^- & + \\
Ox + ne^- \rightarrow P_2 & = \\
\hline
Red + Ox \rightarrow P_1 + P_2 &
\end{array} \ .
$$
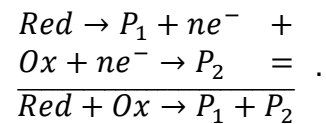
The product P_1 is the coupled oxidant specie for the reductant, while the product P_2 is the coupled reducing specie for the oxidant. In a natural system a reduction must be coupled with an oxidation to allow the electron transfer and the occurrence of half-reactions is regulated by their thermodynamic spontaneity, defined by their standard potentials E_0 [71]. In the case of galvanic or electrolysis cells, the electrodes participate to the process in Reaction 2 donating or sequestrating electrons, hence the two reactions occur spatially separated in the two electrode chambers and only at the electrode surface and most of the porous matrix is exempt from electric-driven redox reactions. An exception, of rare occurrence, is found when the porous media in contact with the electrode is comprised or coated with a high conductive material, such as metal nanoparticles. In such case a *diffuse electrode* is formed, extending the surface available for electrochemical reactions [37, 71, 135]. Although secondary reactions involving metal ions and chlorine can occur, electrolysis is the predominant redox process in the early stages (days) of EK applications [37, 64, 71, 135]. Electrolysis is a reaction system composed of two half reactions [37, 48, 64, 71, 135]:

$$anode \quad 2H_2O - 4e^- \rightarrow O_2^{\nearrow} + 4H^+ \quad E_0 = -1.229\,V \quad ,$$

$$cathode \; 2H_2O + 2e^- \rightarrow H_2^{\nearrow} + 2HO^- \quad E_0 = -0.828\,V \quad ,$$
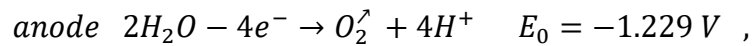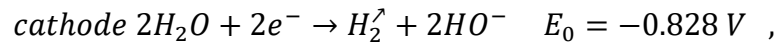
The two reactions occur with respective rates which lead to an equal molar production of H^+ and HO^-, so electroneutrality is maintained. This is evident, as although spatially separated the two half reactions are part of a single redox process which reduces to the water splitting reaction operated by a direct current I [71]:

$$2H_2O \xrightarrow{I} O_2^{\nearrow} + 2H_2^{\nearrow} \quad .$$
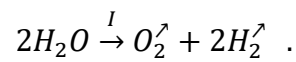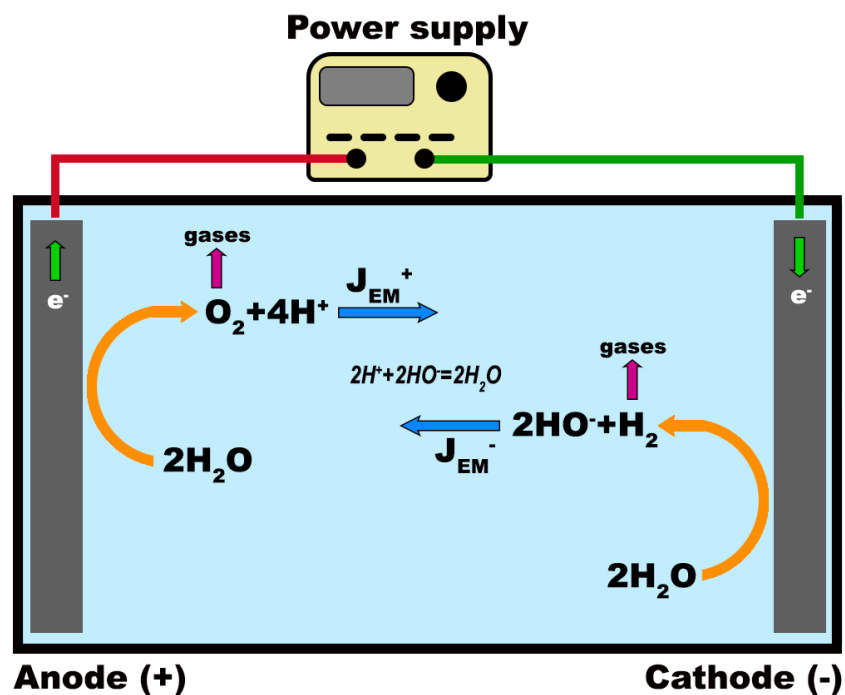
Figure 13) Schematic representation of electrolysis in water coupled with electromigration and neutralization of the acid and alkaline fronts.

During electrolysis global electroneutrality is maintained [101, 136], but as a result of the pH modification in the electrode chambers, two electromigration fluxes are generated. An alkaline and an acid advection flow fronts are formed, which move in opposite direction with a velocity proportional to the electrokinetic effective mobility, which must account for EOF when such process is relevant [37, 48, 64, 80, 135]. Two main consequences can be identified: a modification of the porous matrix and a modification of the soil solution. As the two fronts move in the porous matrix, their pH modifies the dissociation state of the silicate hydroxyls groups responsible for the surface charge [37, 48, 64]. Consequently, the Zeta Potential varies in the model: behind the alkaline front $Si\text{-}O^-$ groups will increase in number due to deprotonation of $Si\text{-}OH$; behind the acidic front $Si\text{-}O^-$ groups will decrease in number due to their protonation to $Si\text{-}OH$; very rarely $Si\text{-}OH_2^+$ groups are formed in natural soils or clays [85, 117, 137, 138]. The noticeable effect is a variation in the electroosmotic flow rate, in the acidic zone EO is suppressed while in the alkaline zone EO is magnified. Also, each advancing front represents a zone presenting an excess charge with different composition [37, 48, 71, 139]: all the electrokinetic mobilities (EM, EO, EP) will be affected by the two pH fronts, and different transport regimes will develop in the porous matrix, changing their zone of influence with time [48, 64, 80, 135]. The production of gaseous species – hydrogen and oxygen – does occur only on the electrode surface [37, 47, 57], hence if the electrodes are installed directly in the porous matrix, the gases will build up and progressively desaturate their surroundings. After a certain time, all EK phenomena will stop since the gas layer will insulate the electrode and open the circuit; if a hydraulic flow is present the gases bubbles will also be transported in the porous media, extending the desaturation with consequences not only on EK, but also on the partition and oxidation state of the porous matrix and the contaminants (e.g., NAPL volatilization, heavy metal oxidation or reduction). For these reasons it is common practice to place electrodes in wells or boreholes, which allow both gas venting and the control of pH by adding acid and/or base or recirculating a buffer solution [80, 140].

Lastly, secondary reactions are more likely to occur in complex systems (natural soils in field application of EK), where metal ions can be precipitated or transformed at the cathode, also if chloride salts (e.g., NaCl) are present, for example as electrolytes or tracers in experimental set-ups, chlorine gas is produced at the anode [37, 140]:

$$M^{n+} + ne^- \to M^{0\downarrow} \ ,$$

$$M(OH)_n + ne^- \to M^{0\downarrow} + nHO^- \ ,$$

$$2Cl^- - 2e^- \to Cl_2^{\nearrow} \ ,$$
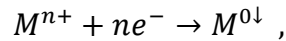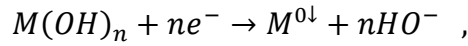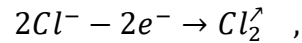
Such reactions will induce local changes in the soil solution, and a local variation in the conductivity of the porous matrix. In the most extreme case, a relevant iron precipitation on soil grains could create a conductive layer that leads to an *diffuse electrode*, modifying geometry, surface area, extending the area where electrochemical reactions can occur [141]. However, given the most common electrode geometry involves placing them in a well or piezometer conditioned with the buffer solution, such effect is expected to be negligible.

A second relevant consequence of electrical-driven redox involves the charge density flowing in the system. When a current is applied to an unaltered system, electrolysis consumes electrons with rate depending on:

- Mass transfer from the bulk solution to the electrodes.
- Gas venting, which reduces their partial pressures and shifts the electrolysis reaction equilibrium towards the products.

At the same time, the faradic reactions, electrode polarization and overpotential modifies the potential drop across the electrodes. In an oversimplified notation [29, 62, 142]:

$$E^{app} = E^{eff} + E^* \ ,$$

where E^{app} is the potential set by the power supply, E^* is the global term for the potential losses and E^{eff} is the actual potential drop across the capillary [29]. However, modern power supplies can operate by imposing a constraint on either current or voltage to maintain the other parameter at the desired value. Choosing the operative mode is subjective and depends on the specific application of EK. Working at constant current allows to reduce Joule heating and to define a constant rate for the electrochemical reaction, which simplifies an eventual neutralization of

the acid/alkaline species at the electrodes [62, 64, 136, 140]. However, a proper electrokinetic approach would require constant voltage conditions, since the potential drop across the system is the driving force for all EK transport phenomena [37, 43, 142, 143]. Undoubtedly, due to concentration gradients and soil inclusions, local variations in the current distribution will also determine local potential distortion. Nevertheless, using the potential as boundary condition instead of the current allows a more accurate and formally correct modeling. Introducing electrolytic reactions in the modeling of EK phenomena is very complex, since as opposed to chemical reactions in the porous matrix, they depend on multiple interconnected factors.

2.4 Modeling electrokinetic transport

The equations described in the previous sections for each electrokinetic phenomenon are referred to ideal systems and are in most cases referred to analytical techniques, where the system conditions are precisely controlled by the user and simplified approaches are applied. In the case of electrokinetic remediation and transport, the mass flux of the sample depends upon multiple factors and flux components [31, 92, 125, 126, 136]. As the system must abide Ohm's law, all migration mechanisms – advection-dispersion, EM, EP, EO – will alter the system, influencing the principal variables regulating electroadvection [31, 101, 125, 126, 136]; electrochemical reactions are also affecting the principal system variables.

A global approach to the different flow components (namely hydraulic advection, Fickian diffusion, electroosmosis, electromigration, and electrophoresis) [31, 125, 126] is then required to account for all contributions to the system evolution. The mathematical laws describing each phenomenon still holds, however other boundary conditions must be set to understand how each component affects the relevant variables and the other advective and diffusion phenomena [31, 101, 144]. Despite many models have been developed [31, 55, 144], most of them are based on heavy assumptions and neglect some components relevant for the overall phenomenon, resulting in a reduced ability to describe the system and helping in its understanding [31, 55, 126]. A more generic approach that allows a more accurate description is a *coupled modeling*, using the appropriate equations to describe separately all relevant processes and implementing a feedback system to exchange information between each block to output a global effect on the system [101, 125, 126, 136, 145]. The model complexity can be identified in two areas: number of chemical components and species concentration. The latter is responsible for higher degrees of interaction between the different chemical species, especially due to

coulombic forces, which are negligible in diluted systems. The former is responsible of an increased number of interactions, which requires a set of equations for each component [92, 101]. To obtain a model with good descriptive abilities, the first approach is relative to the simplest system, comprised of a diluted component; once the fundamental equations and boundaries conditions are set, the complexity will be increased to concentrated electrolytes [31, 92, 101].

2.4.1 General coupled approach

For a non-reactive single component system the basic boundary condition is the law of mass conservation, referred to a control volume [92, 101], however in a multicomponent system we must carefully define the concept of fluid velocity. The average fluid velocity is composed of the single species velocities [92], and chemical reactions cannot be neglected. However, if the mass balance is valid for the whole system, the sum of the chemical rates for all present species equals to zero (which means, no matter is created or destroyed).

For a fluid containing charged species, the transport of the single ionic species must be considered besides the bulk fluid. Hence, a detailed description of an electrokinetic system must comprise 1) fluid mechanics; 2) mass balance: 3) transport of charged species; 4) current flow description; 5) charge balance (electroneutrality) [92, 101, 125, 126]. From the system complexity we can derive that the i-*th* specie velocity may differ from the average fluid velocity, due to concentration gradient (diffusion effects), difference in fluid density and charge density. Each specie, due to its unique set of physicochemical properties will be subject to different forces and present different velocities [92]. However, in absence of external forces except from the bulk flow, each specie will be transported according to the advective flux:

$$J_i = J_i^{ADV} = c_i \cdot u \quad .$$

All other transport phenomena (generic flux J_i') occur with respect to the advective flux, therefore the single component velocity will add, as a vector quantity, to the bulk velocity. A generic *i-th* component with a velocity v_i will modify the total flux as follows [92]:

$$J_i^{Tot} = J_i^{ADV} + J_i' = c_i \cdot v + c_i \cdot (v_i' - v) \quad,$$

where v_i' indicates the *i-th* specie velocity with respect to the average bulk velocity v, and is usually defined *drift velocity* [92]. To proceed further in the model development, let us define a specific physical phenomenon instead of a generic J_i' and let us consider diffusion, which is generated by concentration gradients and for diluted system described by Fick's law [92, 101, 126]. Since we are considering porous media, we must remember to use the effective diffusion coefficient corrected by porosity and tortuosity [94, 95].

$$J_i^{DIFF} = -D_i^* \cdot \nabla c_i \quad.$$

Hence, for a hydraulic flow with diffusion Equation 24 becomes:

$$J_i^{TOT} = c_i \cdot v - D_i^* \cdot \nabla c_i \quad.$$

When system components are subject to an external force, F^{act}, which effects extent varies for each chemical specie composing the system, in the most general approach the velocity for the *i-th* specie is defined as [92]:

$$v_i' = \omega_i \cdot F^{act} \quad,$$

where ω indicates the mobility of the specie, namely the resulting velocity with respect to the applied force (N^{-1} s^{-1}). The mobility term ω is determined by the specific phenomenon that is being considered; in the case of electromigration we already discussed the Nernst-Einstein-Townsend equation; considering the definition of the electric force ($F^{act} = F^{el} = -z_i \cdot e \cdot \nabla \Phi$) which leads to [31, 92, 125, 126]:

$$J_i^{TOT} = c_i \cdot v - D_i^* \cdot \nabla c_i - \frac{z_i \cdot c_i \cdot e \cdot D_i^*}{k_b T} \cdot \nabla \Phi \quad.$$

Equation 28 with ionic mobility in its implicit notation, describes the total ionic flux and it is named *Nernst-Plank equation* [92, 125, 126, 144]:

$$J_i^{TOT} = c_i \cdot v - D_i^* \cdot \nabla c_i - k_i^{EM} \cdot c_i \cdot \nabla \Phi \quad .$$

We can now recall the law of mass conservation for a system at its steady state and in the absence of chemical reactions the mass conservation, and then combine the mass balance with the Nernst-Plank equation also including the reactivity term, obtaining [31, 92, 125, 126, 144]:

$$\nabla \cdot J_i^{TOT} = 0 \quad ,$$

2.4.2 Current density during transport

For a system subject to an external current, which is carried by an ionic flux, the current density is defined by the total ionic flow [31, 92, 101]:

$$i = F \cdot \sum z_i \cdot J_i^{TOT} \quad .$$

Combined with the total molar flux the current is defined by advection, diffusion and electromigration, and for an electroneutral solution the advective flow (bulk flow of an already electroneutral volume unit) does not contribute to the ion flux, since [92, 101]:

$$i = F \cdot (v\sum z_i c_i - \sum D_i^* z_i \nabla c_i - \frac{F^2}{RT}\sum z_i^2 D_i^* c_i) \quad .$$

$$\sum z_i \cdot c_i = 0 \quad .$$

If the electrolyte has homogeneous composition, hence there are no concentration gradients, the only contribute to current density is given by

electromigration (Equation 34), and the system abides Ohm's law (Equation 35) expressed in conductance terms [92, 101] :

$$i = -\frac{F^2}{RT}\left(\sum z_i^2 \cdot D_i^* \cdot c_i\right) \cdot \nabla\Phi \ ,$$

$$i = -\sigma \cdot \nabla\Phi \ .$$

Combining Equation 34 and Equation 35 we obtain the Nernst-Einstein definition of conductance for the bulk solution (not accounting for eventual modifications caused by the porous matrix) [92, 101]:

$$\sigma = \frac{F^2}{RT}\sum z_i^2 \cdot D_i \cdot c_i \ .$$

Due to the conservation of charge and mass, assuming homogeneous reactions we obtain, for the totality of species [92]:

$$F \cdot \frac{\partial}{\partial t}\sum z_i \cdot c_i = -\nabla i \ .$$

If no time-dependent electric field is applied to the system, no displacement current is observed, and all current density is carried by the ion flux. The steady-state definition of charge conservation ($\nabla i = 0$) can be used to draw important conclusions on the physics of an electrokinetic process [92]. If we examine Equation 34 expanding the ionic mobility term:

$$i = -\frac{F^2}{RT} \cdot \left[\sum z_i^2 \cdot D_i^* \cdot c_i\right] \cdot \nabla\Phi \ ;$$

in the ideal case, for a binary electrolyte A^+B^- assuming identical ionic diffusion coefficients for anion and cation, we can define the conductivity with respect to the bulk molar concentration c_∞:

$$\sigma = 2 \cdot \frac{F^2 \cdot z^2 \cdot D^* \cdot c_\infty}{RT}$$

In this situation, electromigration of cations and anions will proceed at the same rate, maintaining electroneutrality and without the formation of concentration gradients [92, 101]. In a real case scenario, however, the abovementioned case is very unlikely. In most situations ionic diffusion coefficient varies from anion to cation, in the range of $0.3\text{-}9.5*10^{-9}$ (m^2 s^{-1}) with the highest values for H^+ and HO^- [92, 94, 101]. In these circumstances the migration will proceed with different rates depending on the specific D_i^*; the same effect can be addressed considering the single contributes to the current flux. Each chemical specie is characterized with a transference number:

$$t_i = \frac{F \cdot z_i \cdot J_i}{i} \quad .$$

In the simplest system with no concentration gradients and no hydraulic advection J_i is due to electromigration only, hence it depends on the ionic mobility and therefore on the diffusion coefficients [92, 101, 136]. These differences would lead to different cationic and anionic fluxes, with a consequent concentration gradient. Therefore, the system reacts with a diffusive flux which opposes such gradients while they develop [92, 101]:

$$J_i^{MIG} = -J_i^{DIFF} \rightarrow -F \cdot z_\pm \cdot u_\pm \cdot c_\pm \cdot \nabla\Phi = D_\pm \cdot \nabla c_\pm \quad .$$

In a non-reactive system at steady state, diffusion counterbalance ionic migration, specifically it slows down ions with a high transference number and speed up ions with a low transference number, so electroneutrality and homogeneous concentration are maintained [101, 145]. For a binary electrolyte

composed of 'n' cations and 'm' anions the concentration to satisfy the charge balance is defined as scaled concentration 'C' [92, 101]:

$$C = \frac{c_+}{n_+} = \frac{c_-}{m_-} \quad .$$

The material balance for a generic specie (cation or anion) in a non-reactive system, abiding electroneutrality and subject to incompressible flow is defined by Equation 43 and leads to the definition of a zero balance for the electrolyte in its entirety (Equation 41):

$$\frac{\partial C}{\partial t} + u \cdot \nabla c = z_\pm \cdot \omega_\pm \cdot F\nabla \cdot (c\nabla\Phi) + D_\pm \cdot \nabla^2 c \quad ;$$

$$(z_+\omega_+ - z_{\omega_-})F\nabla \cdot (c\nabla E) + (D_+ - D_-)\nabla^2 c = 0 \quad ;$$

therefore we can write Equation 43 and define a complex diffusion coefficient (not to be confused with the effective coefficient arising from porosity and tortuosity) [92, 101]:

$$D' = \frac{z_+\omega_+ D_- - z_-\omega_- D_+}{z_+\omega_+ - z_-\omega_-} \quad .$$

If we expand the ionic mobility we obtain [92]:

$$D' = \frac{(z_+ - z_-)D_+ D_-}{z_+ D_+ - z_- D_-} \quad .$$

Also, in the absence of external current and advection we obtain a mathematical relationship which tells us that concentration gradients are associated with a current that does not depends on the applied electric field:

$$i = F \cdot \sum D_i^* \cdot z_i \cdot \nabla c_i \quad .$$

This evidence is of significant relevance in modeling the electrokinetic transport, as locally we may encounter deviation from Ohm's law when concentration gradients are present. A careful definition of the current density term is required, considering it is now composed of a migrational and diffusive term [101]. Besides the important information of local deviations from Ohm's law if concentration gradients are present, the charge conservation condition bears important significance in the electrokinetic delivery of amendments as in introduces significant limiting conditions.

2.4.3 Poisson-Nernst-Plank equation

Let us recall the Nernst-Plank equation from Equation 29 [101, 136]:

$$\frac{\partial c_i}{\partial t} = -\nabla(v \cdot c_i - D_i^* \cdot \nabla c_i - k_i^{EM} \cdot c_i \cdot \nabla\Phi) + R_i \quad .$$

To obtain the most general model for a porous medium, we must account for porosity (n) and water content (θ) of the solid matrix:

$$\frac{\partial (n\theta \cdot)c_i}{\partial t} = -\nabla(n\theta \cdot v \cdot c_i - n\theta \cdot D_i^* \cdot \nabla c_i - n\theta \cdot k_i^{EM} \cdot c_i \cdot \nabla\Phi) + n\theta \cdot R_i \quad ;$$

in the control volume to which the Nernst-Plank equation is referred, electroneutrality is maintained by coulombic forces as discussed above. The charge balance can be expressed in terms of charge density, and is well described by Poisson equation:

$$\varepsilon \cdot \nabla^2\Phi = -\rho \quad ,$$

where ε is the medium permittivity (C V^{-1} m^{-1}) and ρ is the charge density in the control volume [136]. Therefore, for a system comprised of N species the model is composed of a system of nonlinear partial equations (PDE) containing N Nernst-

Plank equations and one Poisson equation. In this way we are able to describe the strong interplay between electric potential and concentration in the soil solution; the model is defined *strongly coupled* [125, 126, 136]. Such system of equation is defined Poisson-Nernst-Plank, shortened in PNP equation. When the diluted electrolyte assumption fails, the mass balance, current flow and electroneutrality equations are still valid, but a modification of the PNP equation is required for the mass flux. The same need arise in ternary solutions, as two different concentration gradient may be present and each of them affects the flux of each specie. [101]. The first approach is to account for the different interactions between the species, which were negligible for diluted solutions, using the electrochemical potential as driving force for diffusion and migration. However, a simple substitution will result in an overcomplicated system since the electrochemical potential depends on both local composition and electric state. We can separate the contribute of concentration and electric field as [101, 125, 126]:

$$\mu_i = \mu_i^0 + RT \cdot \ln(a_i) + z_i \cdot F \cdot E \ ;$$

<div align="right">Equation 50</div>

where μ_i^0 is the standard electrochemical potential, a_i is the activity of the *i-th* specie and E is the electrostatic potential. When the electrochemical gradient is considered in the framework of the PNP equation it leads to a new term for activity, with the main structure unchanged from the diluted solution case [101, 125, 126]. For a porous medium the same modification applied in Equation 48 to account for porosity and water content is valid.

$$J_i^{TOT} = c_i \cdot v - D_i^* \cdot \nabla c_i - \frac{z_i \cdot c_i \cdot e \cdot D_i^*}{k_b T} \cdot \nabla \Phi - D_i^* \cdot c_i \cdot \ln(a_i) \ ;$$

<div align="right">Equation 51</div>

2.4.4 Numerical simulation of electrokinetic transport phenomena

Given the importance of Coulombic interactions, the effect of multicomponent transport [125, 126, 146] and the relevance of solution conductivity on the electrokinetic phenomena, a comprehensive approach is required to correctly describe and predict the evolution of an amendment delivery [65, 125, 126]. For this reason, a coupled approach is required, to describe the mass flow in all its

components, the Coulombic effects deriving for an applied electric potential and the eventual geochemical reactions, which determine the local ionic concentration and thus the conductivity [125, 126].

The modeling approach starts from the Nernst-Plank-Poisson equation (NPPE) which considers advection, diffusion (accounting for Fickian effects and activity coefficients), electrochemical effects (EM, EO, EP), soil properties (porosity). The resulting equation for the single specie total flux is the following [92, 125, 146]:

$$J_i^{TOT} = v^* c_i - n D_i^* \nabla c_i - n D_i^* c_i \nabla \ln(a_i) - n D_i^* \frac{z_i F}{RT} c_i \nabla \Phi \ ,$$

<div align="right">**Equation 52**</div>

where the terms represent, from left to right, advection, Fickian diffusion, activity coefficient gradients and electromigration. Electroosmosis contribution is introduced in the advection terms, applying the Helmholtz-Smoluchowski assumption, the EO velocity is computed from the EO mobility and adds to the specific discharge defined by Darcy's equation [5, 126]:

$$\begin{cases} v_D = \dfrac{K_h}{\eta} \nabla h \\ v_{EO} = -k_{EO} \nabla \Phi \end{cases} ; \\ v^* = v_D + v_{EO} \ ,$$

<div align="right">**Equation 53**</div>

The system must abide both material balance and electroneutrality (or charge balance), the latter is verified at both the macroscale and locally in every point of the system by the Poisson equation [92, 101, 126]. Since the current in electrolytes translates in ionic flux, the NPPE equation can be used to define the current density [92, 101, 126].

The co-existence of advective fluid flow, coulombic effects and ion flux requires a coupling of three different physical model: Navier-Stokes equation to describe the fluid flow, Nernst-Plank equation to describe the ionic flux, and Poisson equation to describe the coulombic interactions [126, 147]. The specific number of equations required to fully describe the system depend on the system complexity, each ionic component requires a NP equation, and each free coordinate direction requires a momentum conservation and a fluid continuity equation combining in a partial different equation (PDE) system. In addition to the physical

effects, the chemical composition also contributes significantly to the system evolution in the definition of the effective diffusion coefficient due to multicomponent transport. To account for these effects, the geochemistry of the system has to be considered and used as input to the PDE system for each time step.

The NP-Phreeqc-EK model [125, 126, 148] applies the PHREEQC code [149, 150] to the resolution of the coupled modeling of electrokinetic transport implementing a COMSOL-Phreeqc-RM coupling. Specifically, the initial solution composition is analyzed by the Phreeqc module, which returns a composition resulting from all the geochemical reactions and equilibria. These initial conditions are used by the COMSOL Multiphysics interface – composed of the Nernst-Plank PDE, the Poisson equation, the current balance and in case of fluid flow the Navier-Stokes equation – to compute the spatial species concentration distribution for a determined time step (desired as small as possible). The model output is used as a Phreeqc input for the calculation of species concentration, which is the passed to COMSOL for the transport computation; the iterative process is repeated for the desired transport duration, set by the operator [65, 125, 126, 148].

Chapter 3

Electrokinetic delivery of reactants: pore water chemistry controls transport, mixing and degradation

3.1   Literature background and motivations

The electrokinetic transport of soluble and colloidal species represents a valid alternative to hydraulic advection to achieve both extraction of contaminants [37, 38, 151] and the delivery of amendments for *in-situ* treatments (ISCO, ISCR, EK-Bio) [45, 49, 50, 152-154]. Specifically, in the case of solutes, the delivery mechanism is based on coulombic interactions between the dissolved ions and the applied electric field; therefore, parameters as pore size, solution viscosity, friction are in most cases negligible. More importantly, in its general application, EK delivery is independent from the porous medium hydraulic conductivity and thus can prove effective in those cases gravity feed, pressurized injection or Direct Push fail or present major shortcomings [7, 11, 13, 16, 17]. The principle of electrokinetics applied to soil and groundwater decontamination has been thoroughly explored by different authors [11, 37, 39, 63, 143] and the driving forces and mechanism are well known. Three principal transport phenomena are identified: i) electromigration (EM) acts on soluble species (namely, ions), ii) electrophoresis (EP) acts on mobile colloids iii) electroosmosis (EO) acts on the pore solution involved in the formation of the electric double layer. Each transport velocity depends on specific parameters of the target specie – valence and diffusion

coefficient for EM, solution properties, zeta potential and shape factors for EP and EO – and on the local electric potential in the porous medium; such variables are discussed in detail in the theoretical section. A great wealth of studies is dedicated to investigating how system variables affect the transport, and to defining strategies to maximize the reactant delivery. For example, Cherepy and Wildenschild [80] and Lee and Yang [140] discuss the effect of electrolysis and pH variation in the electrolyte and propose methods for maintaining stationary conditions; Gomes et. al. [43, 155-157] and Masi et.al. [63, 158] explored cases close to real applications investigating the effect of soil type, applied current, soil solution composition. However, most of the studies available in the current literature are limited to one-dimensional confined geometries, specifically circular columns [38, 61, 62, 159]. The few experiments carried out in two-dimensional systems involved an amendment delivery (or contaminant extraction) over the whole model cross-section [40, 45, 54, 63, 64], which leads to a one-dimensional behavior far from conditions relevant for a real application of EK delivery as discussed in Chapter 2. The literature works allowed to gather an insight of the processes and mechanism involved in the transport, particularly in those cases real soil samples were used [43, 63, 158] rather than ideal porous media; however, the mono-dimensional geometry eliminates the possibility for a spatial distribution of the current, dependent on the specific conductivity of the medium (namely, the porous medium and the soil solution). In an homogenous porous medium saturated with a single electrolyte, the applied electric field is equally distributed in the medium as it presents the same conductivity, hence the same resistivity, so that Ohm's law is upheld [92, 101]. When a second solution, or a second porous medium, fills a partial volume of the system, two resistance values can be identified affecting the current distribution and thus the electrokinetic transport. In a mono-dimensional system this effect is partially masked by the confinement of the model walls, which forces the current in flowing through all the model with the same intensity (Figure 14): the effect on the transport of a solute can be observed only on the longitudinal direction and results in a spreading of the injected volume [57, 78, 101]. In a two-dimensional system, the current distribution can vary depending on the local resistivity, hence on the ionic species and their concentration. The different current flow results in a focusing or defocusing of the electric field streamlines, which in turns affect the electromigration of the ions in solution introducing preferential pathways for the transport: both longitudinal and transversal distortion of the injected amendment occurs, causing relevant modifications on the portion of the aquifer interested by the delivery and reactivity towards contaminants. A correct injection strategy is therefore pivotal to reach the remediation objectives in terms of volume affected,

reaction kinetics and efficiency; a correct understanding of such phenomena can provide tools to support the design of the injection operation to maximize efficiency.
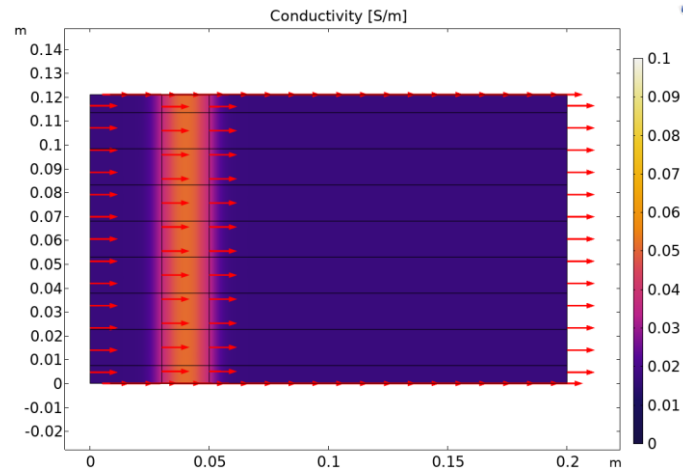
Figure 14) Current distribution and electromigration flow lines in a confined system with 1D geometry for the transport of a solute presenting a higher conductivity than the background. Color scale represents conductivity, lines represent the current distribution, while arrows the electromigration flux.
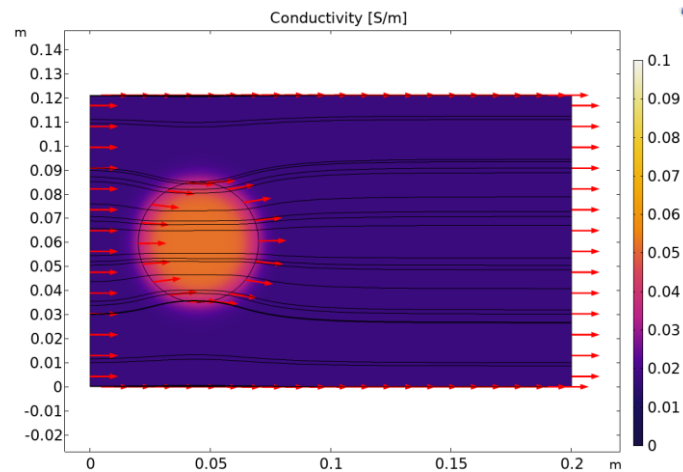
Figure 15) Current distribution and electromigration flow lines in a 2D system for the transport of a solute presenting a higher conductivity than the background. Color scale represents conductivity, lines represent the current distribution, while arrows the electromigration flux.

The objective of this work is to elucidate the multidimensional transport mechanism arising from charge interactions between the amendment and the background solution, with the purpose of optimizing the delivery, distribution, and

reactivity of amendments for groundwater remediation. This focus is aimed to add to the current literature on the mathematical modeling of electrokinetic assisted delivery, to account for multidimensional process so far only marginally investigated. This is of paramount importance in the design of filed-scale applications, specifically to optimize the injection well geometry and strategy (e.g., concentration of amendment, volume injected). The study was performed simulating a delivery of permanganate in a 2D model filled with an ideal homogenous porous medium and allowed to observe both longitudinal and transversal transport during electromigration. In the first part of the study the conservative transport of permanganate was explored to elucidate the plume distribution during migration, and the resulting Area of Delivery and local concentration; in the second part of the study a model pollutant was uniformly dispersed in the model to explicit the permanganate reactivity and investigate the influence of the multidimensional plume dynamics introduced by coulombic interactions. The experimental activity was coupled with the construction of a physical-based model using COMSOL and PhreeqC to describe and predict the system evolution in both conservative and reactive scenarios.

3.2   Materials and methods

The experiments to investigate both advective-dispersive and electrokinetic transport were conducted in a glass chamber built from two tempered glass panels mounted on an aluminum frame; the inner side of the frame is covered by polyethylene to ensure electrical insulation. The internal dimensions were 795x182x11 mm, for all the experiments the set-up was modified creating three chambers by placing two laser-cut bulkheads with a square-mesh, covered with a fabric filter. The inner chamber, measuring 300x180x11 mm, was filled with glass beads (Sigmund Lindner, Germany) having a grain size of 0.4-0.6 mm. The two side-sections are electrode chambers, no porous media is present to allow for solution recirculation to achieve an efficient neutralization of H^+ and HO^- and gas venting produced by electrolysis. Such configuration simulates the use of boreholes or wells to insert the electrodes in the subsoil during a real EK application; this allows the solution recirculation of a buffer solution for pH control, and also facilitates the insertion of the electrodes reducing the risk of wear or breaking when the electrode is driven directly into the ground. In the case of advective-dispersive transport the two chambers were used to establish the hydraulic gradient to obtain the desired seepage velocity in the porous medium. To prevent preferential flow patterns, the water level was set to 150 mm, while the porous media layer reached

180mm. The unsaturated layer is required to prevent a water table higher than the porous medium, which would cause daylighting in both advective and electrokinetic transport experiments. A scheme of the experimental set-up, including the recirculation system, power supply and electric parameter monitoring is presented in Figure 16.

Before each experiment, the glass beads, and the glass windows of the 2D set-up were cleaned using a 5% H_2O_2 solution to remove any residues from previous tests; hydrogen peroxide proved able to remove manganese precipitates (MnO_2), which would introduce a yellow-brown patina. The removal is required to have consistent colors for the photographic determination of permanganate and its quantification. After removing any washing solution residue with ultrapure water, the glass beads were conditioned with at least 5 pore volumes of the electrolyte buffer solution, one pore volume at a time, to obtain uniform conditions. A wet packing procedure was applied to fill the set-up, to eliminate the formation of unsaturated zones below the water table.

The electrodes used in the experiments to apply the electric field (Working Electrodes, WE) were graphite rods (ø6mm, L=300mm), specifically designed to be used as active electrodes and supplied by Elektrokul, Denmark. They were placed in the electrode chambers to obtain an electrode distance of 400 mm in al tests, to maintain the same applied voltage and achieve the identical input potential gradient. The electrodes were connected to a power supply (EA Elektro-Automatik, EA-PSI 5200-10A, Germany) operating in constant voltage mode providing 200 V, corresponding to a potential gradient of 0.5 V cm^{-1}. The corresponding current and the potential gradient in the porous medium were measured every hour by a multimeter (PeakTech 3315, Germany), the latter introducing two wire electrodes (Sensing Electrodes, SE) with a 2 mm exposed tip placed 10 mm deep and 10 mm from each bulkhead (distance 280mm). The monitoring of the current allows to investigate the ability of the recirculation to maintain constant conditions in the electrode chambers, specifically to counterbalance electrolysis. Monitoring the potential gradient in the porous medium is required by the presence of both the electrode chamber and the bulkhead, which create a complex interface bound to cause a potential drop from the theoretical applied value. The relevant electric parameters –potential gradient in the porous medium and applied current – were recorded every hour, while pH and temperature were measured at the beginning and end of each test in both cathodic and anodic reservoirs.

For advective-dispersive delivery, recirculation was operated between the two electrode chambers (which did not contain the electrodes, but only the buffering electrolyte) to create the hydraulic gradient necessary to obtain the desired seepage velocity. The value was set by the average velocity registered in the EK experiments (6.5 cm h^{-1} or 1.8E-5 m s^{-1}) and the required hydraulic head computed from the Darcy law and the definition of *effective porosity* (n_e or specific yield) [5]; the data relative to hydraulic permeability and effective porosity were obtained from available literature [160-162].

In the case of electrokinetic experiments, the recirculation was operated separately for each electrode chambers; specifically, the pump was used to extract the electrolyte solution from the electrode chamber to a reservoir with a two-channel tight seal, which resulted in an equal outlet flow directed to the electrode chamber regenerating the solution (schematics are provided in Figure 16). Using a flow rate of 40 mL m^{-1} in the entire volume of an electrode chamber is recirculated in little more than 10 minutes; both the fast recirculation time and the additional volume in the reservoirs allow to counterbalance the effect of electrolysis and obtain constant condition in the system for the whole test duration. The experiments were performed using a sodium carbonate/bicarbonate buffer at pH 9 (molar concentration ratio 1:10); the different conductivity scenarios were explored modifying the electrolyte concentration rather than the one of permanganate, hence the buffer capacity varies as well. In all cases, the concentrations were set so that pH remained in the neutral-alkaline range at the end of the experiment. Also, for this set of experiments, the same buffering solution was used to saturate the porous medium to reduce the system complexity and to facilitate the mathematical modeling, even though these conditions are far from a real groundwater composition.

The voltage applied to generate the electrokinetic transport was selected to provide a potential gradient of abt. 50 V m^{-1}, which was computed from the Nernst-Einstein-Townsend equation to provide a permanganate migration velocity equal to the one for the advection-dispersion delivery; the value also falls in the range usually applied for real-scale implementations [32, 66, 153, 163]. No hydraulic gradient is created by the recirculation system to avoid advection phenomena to interfere with EK; electroosmotic flow (EOF) is known to be minimal in coarse porous medium, such as the one used for the experiments; nonetheless, EOF is observed in the initial stages of the EK transport. Due to the separate recirculation for the anodic and cathodic chamber and the absence of an outlet weir, EOF is

rapidly balanced by the increased water level in the cathodic chamber. As the system comprises only dissolved ions, electrophoretic transport can be neglected for the conservative transport experiments. Given the time required to reach an equilibrium between EOF and the forming hydraulic gradient and the total test time it is safe to consider electroosmosis negligible for our purposes. It follows that the only active transport process in the system is electromigration.

Potassium permanganate was selected as substance object of the delivery since it is widely used as an ISCO amendment. In all experiments, permanganate concentration was equal to 3 mM, and the background electrolyte concentration adjusted to explore different conductivity scenarios for the electrokinetic delivery. Three experimental conditions were explored, in terms of ionic concentration of permanganate and background solution: the first scenario is defined "EK equal" and involves equal ionic concentration in the soil solution and permanganate; the second scenario is defined "EK low" and the third "EK high", referring to a background ionic concentration 3 times lower and 3 times greater than the one of permanganate, respectively. For the advective delivery, the background concentration matches the permanganate ionic concentration, falling in the "equal" conditions. For all the experiments 8 mL of solution were injected in the set-up; the injection was performed in a static system, which means a null hydraulic head for the advective-dispersive experiments and no applied electric field for the EK experiments. To obtain the maximum comparability of the experimental data, the syringe needle was modified to perform the injection centered in the set-up width and at the same depth in each experiment, also the injection was performed at the same distance from the cathodic bulkhead. No fracturing or preferential distribution of permanganate was observed in the experiments, every time the plume presented a circular shape and very little variation in its area, so that a unique value can be used as boundary condition for the construction of the mathematical model. As the injection was performed close to the cathodic bulkhead, an increase in the water table occurs, which is rapidly dissipated across the set-up with minimal effects on the permanganate transport given the type of porous media selected: this is accounted by a short waiting time between injection and the start of the experiment.
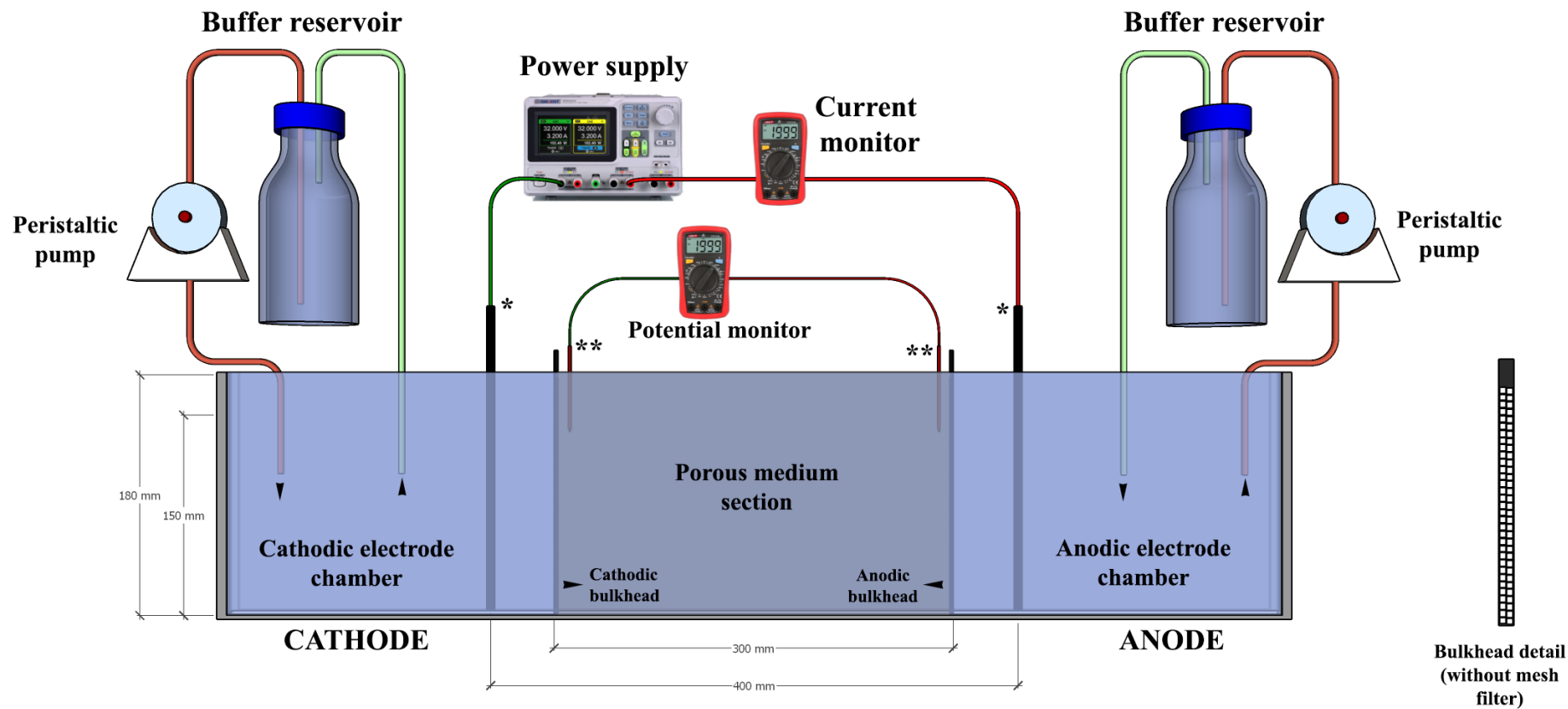
* Working electrodes - DC input
** Probing electrode - potential monitoring

Figure 16) Schematics of the experimental set-up for the electrokinetic experiments.

The reactive experiments were performed following the same protocol described above, with the difference of dissolving a non-charged organic compound in the electrolyte buffer solution. The choice of such compound was carefully evaluated: given the volumes at play a non-toxic chemical was found most suitable, but other requirements had to be taken in account: i) null or minimal electrochemical reactivity, so that the conditions in the electrode chambers can be maintained stable; ii) proved reactivity towards permanganate iii) limited system alteration of the system conditions with respect to the conservative transport experiments. The latter excludes all dyes, which would modify the background color and can prevent the quantification of permanganate from the photos. A compound which answers to all requirements is glucose, as different authors report the occurrence of glucose oxidation by permanganate, also in alkaline medium [164, 165]. Although there is no unanimous consent on the exact reaction pathway relative to the glucose products a general reaction can be defined for the process [166-168]:

$$C_6H_{12}O_6 + MnO_4^- \xrightarrow{H_2O, \ HO^-} Gluc^{OX} + MnO_2^{\downarrow} \ ,$$
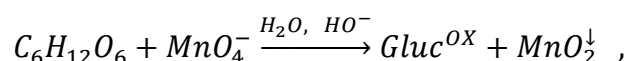
where 'Gluc^{OX}' indicates all the possible glucose byproducts (carboxylic acids, ketones, carbon dioxide). It is important to notice that the permanganate byproduct is a colloidal solid, of yellow-brown color which allows to visually follow the reaction and obtain qualitative information on its kinetics. All three scenarios – "EK equal", "EK low" and "EK high" – were explored, as well as the advective-dispersive transport. To fully describe the system in terms of charge conservation, the solution composition must be fully known to account for the reaction products; the concentration term in the charge continuity expression is substituted by a *reaction term* that accounts for the reaction kinetics: in the present case, the reaction terms refer to a bimolecular reaction. The system evolution was monitored by means of digital imaging performed by a Nikon D300 equipped with a Nikkor 50mm f/1.4g; the camera was placed to align the sensor parallel to the set-up and centered with respect to the porous medium section. The camera was set on manual exposure (f/16, ISO 200, 4 seconds exposure, White balance 5000 K) and the experiments were performed in a dark room to eliminate color and exposure variations by daylight. Back illumination was provided by an electroluminescent panel (1000x300 mm, EL-Technik, Germany) and front illumination, to eliminate shadow and reflexes, by a light bulb (Philips 4000 K, 806 lm, 100 mA, 9.5W). Images were acquired every minute at maximum resolution (4288x2848 pixels).

	Concentration (mM)			Driving force	
	KMnO$_4$	NaHCO$_3$	Na$_2$CO$_3$	Type	Magnitude
ADV	3	2.69	0.15	Advection	6.5 cm h^{-1}
EK Equal	3	2.69	0.15	Electromigration	50 V m^{-1}
EK Low	3	0.90	0.05	Electromigration	50 V m^{-1}
EK High	3	8.09	0.45	Electromigration	50 V m^{-1}

3.3   Experimental results
3.3.1 Conservative transport experiments

The result of the conservative transport experiments is firstly reported using the collected images showing the evolution of the permanganate plume (Figure 17-Figure 20).
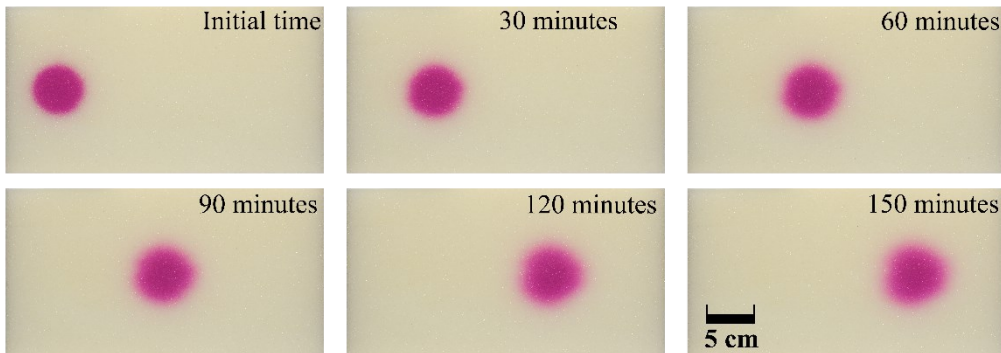
Figure 17) ADVECTION: permanganate plume evolution obtained from the collected photos, time step 30 minutes. Crop of the porous medium section only, excluding electrode chambers and tank frame.
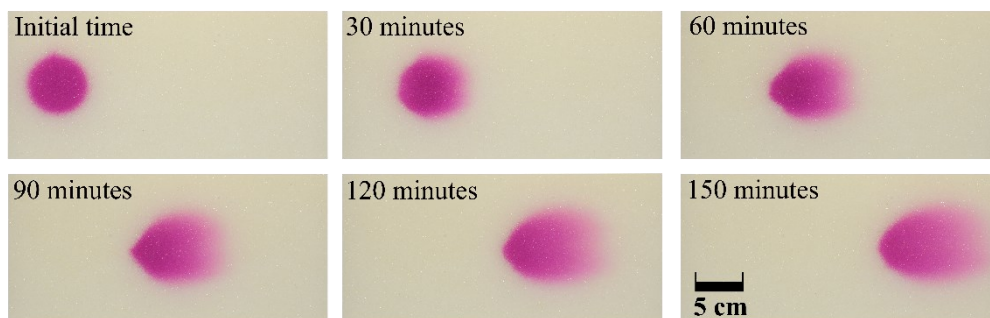
Figure 18) ELECTROMIGRATION – "EQUAL": permanganate plume evolution obtained from the collected photos, time step 30 minutes. Crop of the porous medium section only, excluding electrode chambers and tank frame.
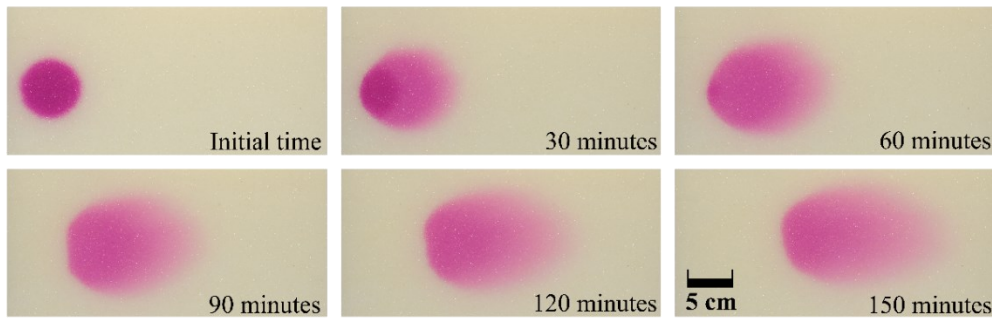
Figure 19) ELECTROMIGRATION – "LOW": permanganate plume evolution obtained from the collected photos, time step 30 minutes. Crop of the porous medium section only, excluding electrode chambers and tank frame.
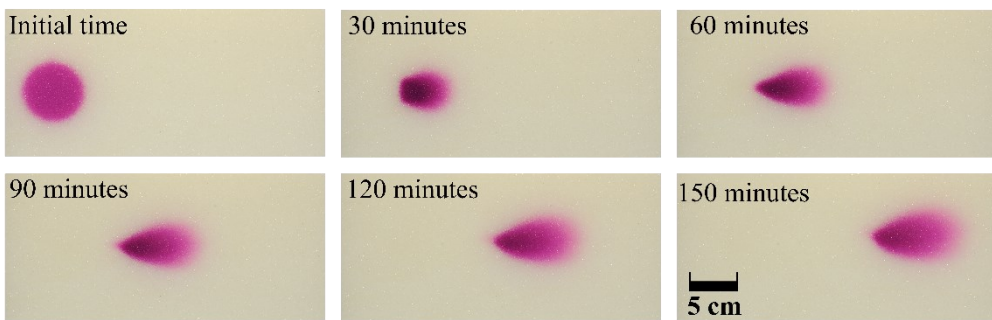
Figure 20) ELECTROMIGRATION – "HIGH": permanganate plume evolution obtained from the collected photos, time step 30 minutes. Crop of the porous medium section only, excluding electrode chambers and tank frame.

In the advection-dispersion experiments, the permanganate plume evolves following the theory of transport in porous media [18, 88] abiding Darcy's law and being subject to dispersion and chemical diffusion during the transport. For the three EK scenarios, the greater distortion along the electric field lines indicates that chemical diffusion is no longer the dominant driving force: electromigration and electrical dispersion regulate the plume deformation and transport. The effect on the plume dilution is much more significant than the advection-dispersion case and bears significant implications on the permanganate reactivity kinetics. The plume evolution in terms of migration velocity of the barycenter, area expansion, shape modification is summarized in Table 4 and reported in detail in Figure 21. Such evaluation was performed using the Particle Analyzer plugin for ImageJ [169], which uses the color contrast between permanganate and glass beads to identify the plume in each time frame (more details are provided in Appendix).

Table 4) Plume velocity, normalized area and roundness obtained from the collected images using ImageJ [169].

	Velocity (m s^{-1})			Normalized plume area		Roundness	
	Initial	*Final*	*Average*	*Initial*	*Final*	*Initial*	*Final*
ADV-DISP	1.78E-5	1.77E-5	1.79E-5	1	1.35	0.958	0.927
EK equal	1.93E-5	2E-5	1.85E-5	1	1.72	0.977	0.702
EK low	9.17E-6	1.38E-5	1.23E-5	1	3.42	0.967	0.638
EK high	1.13E-5	1.47E-5	1.29E-5	1	1.05	0.957	0.568

For the advection-dispersion transport (ADV) and "EK equal" the plume velocity results are comparable and coherent with a theoretical value of 6.5 cm h^{-1}. For the "EK low" and "EK high" scenarios the average velocity is about 2/3 of the advective and the "equal" case. From the original images (Figure 17) we can observe how in the advective case diffusion expands the plume fringes, consequently lowering the local permanganate concentration: the area (computed by the Particle Analyzer) increases by a factor 1.35 over the entire test duration. In both "EK equal" and "EK low" the area also increases, while in the "EK high" scenario the plume initially decreases its area and thus increase its concentration; then the area increases again to reach a final value close to 1 but with a significantly different shape (variation in roundness). This dilution effect and shape modification will play an important role in the understanding of reactive experiments and in the implications of EK transport for groundwater remediation.

As a shape descriptor, roundness was chosen over circularity to account for aspect ratio variations, rather than only perimeter and area [170]. The roundness value for the advective case is subject to little variations, in the $0.927 \div 0.957$ range; this indicates that diffusion dominates the plume expansion rather than dispersion, as the latter is an anisotropic process, whereas diffusion is isotropic. A limited dispersion can be explained with the regularity of the grain size, a perfectly round shape, and a well-packed medium; a scale factor might also be responsible as the plume travels for less than 30 cm [5, 171]. In all EK experiments the roundness decreases as the plume ovalizes; the lower final value is found for the "EK high" case as the longitudinal dispersion greatly surpasses the transversal one.
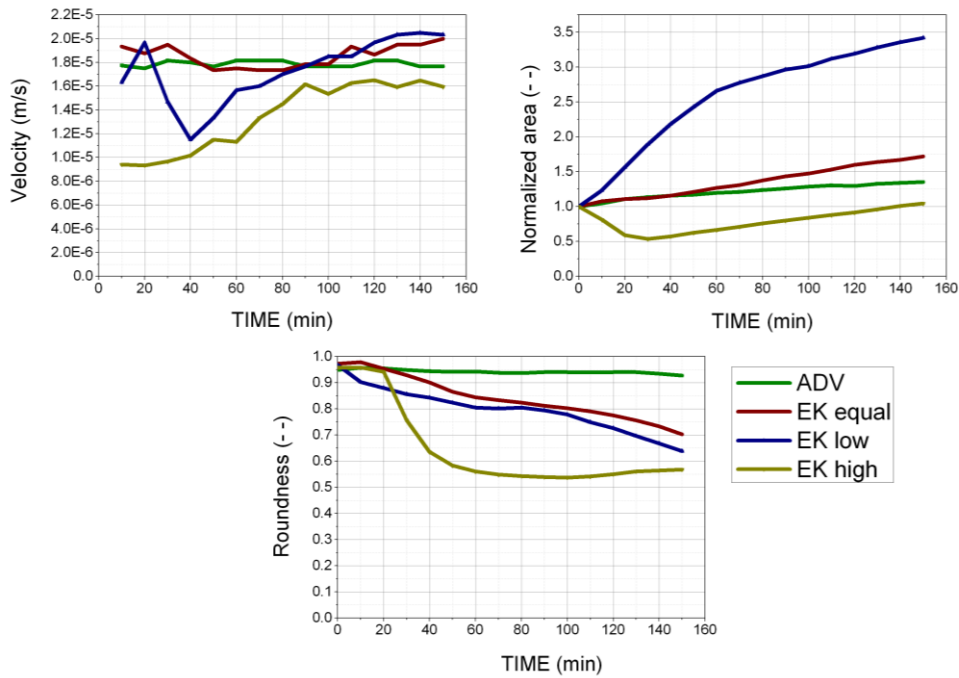
Figure 21) Comparison of velocity, normalized area, and roundness of the permanganate plume for the advective (ADV) and EK experiments; data time-step 10 minutes. Computed from collected images using ImageJ, see additional details in Appendix

A great degree of similarity is observed for velocity and normalized area between the advection-dispersion case and the "EK equal" experiment. The difference in the normalized area increment indicates that a different mechanism than chemical diffusion is responsible for the plume expansion, and such mechanism is characterized by an anisotropy between the longitudinal and transversal direction. The differences in the normalized area and roundness trends for "EK low" and "EK high" experiments support the indicates that the relative conductivity of permanganate with respect to the background solution strongly affects the electromigration dynamics. An indication that the same mechanism acts with the same extent, once defined conditions are reached in the system, is suggested by a similar slope in the increment of the normalized area for all the EK experiments starting from 60 minutes. It is also interesting to notice that in terms of migration velocity, in the "EK low" experiment the final velocity is comparable with the advection-dispersion and "EK equal" case, whereas in the "EK high" scenario the velocity is significantly lower. During the test, current and potential gradient were monitored every hour (values are summarized in Table 5); small

variations are observed in both parameters during the test, as the buffering solution limits concentration changes due to electrolysis. Although the pH variation at the anode is significant, especially for "equal" and "high" case, the pH does not reach acidic values and therefore limited modifications are introduced in the system.

Table 5) Experimental condition evolution during the electromigration experiments. pH and temperature were measured in the electrode chambers at the beginning and end of the experiment (3 hours), potential and current every hour.

	EK equal *equal background*				EK low *lower background*				EK high *higher background*			
∇Φ (V m⁻¹)	0 h	1 h	2h	3 h	0 h	1 h	2h	3 h	0 h	1 h	2h	3 h
	52.1	49.4	48.7	48.6	53.1	47.1	45.6	44.3	51.5	47.1	45.7	47.4
I (mA)	0 h	1 h	2h	3 h	0 h	1 h	2h	3 h	0 h	1 h	2h	3 h
	7.9	7.9	8.0	8.2	3.0	3.0	3.0	3.0	22.3	22.4	23.5	24.8
pH	0 h	3h ⊕	3h ⊖		0 h	3h ⊕	3h ⊖		0 h	3h ⊕	3h ⊖	
	9.10	6.67	9.96		8.88	7.70	9.18		9.15	6.61	10.01	
Temp. (°C)	0 h	3h ⊕	3h ⊖		0 h	3h ⊕	3h ⊖		0 h	3h ⊕	3h ⊖	
	21.3	21.6	22.2		21.9	22.2	22.5		21.7	22.0	22.1	

⊕: Anodic chamber   ⊖: Cathodic chamber

∇Φ: Potential gradient in the porous medium ; I: input current

All the gathered evidence are pointing to an electromigration-electrodispersion mechanism, where the former is responsible for the plume migration and the latter for its anisotropic expansion and shrinking. Our initial hypothesis of a strong effect by the background conductivity is then confirmed by the experimental data. A coupled effect of the different electrical conductivity, resulting in a local modification of the current density, and a mass limitation imposed by multicomponent coulombic interactions (effect of transference numbers for the dissolved species), contributes to the longitudinal and transversal transport components.

The experimental results were also analyzed using the images to quantify the local concentration of permanganate (see additional information in appendix for details on the calibration procedure), the data are presented in Figure 22 and compared with the computed plume profiles using a 2D forward model, describing both physical and electrostatic interactions in the set-up [125, 126]. The data confirms the results obtained from the Particle Tracking, specifically:

- In the advective scenario the plume shape is regular and is subject to little deformation, coherently with the classic flow theory in porous media; the experimental data and the computed values from the simulation (in advection-dispersion regime) are in good agreement.
- Significant plume shape alterations are registered in the EK experiments, which vary with the background concentration. In all three

cases it is possible to observe a fronting effect: the plume develops a smoother concentration profile on the front and a sharper one on its tail.
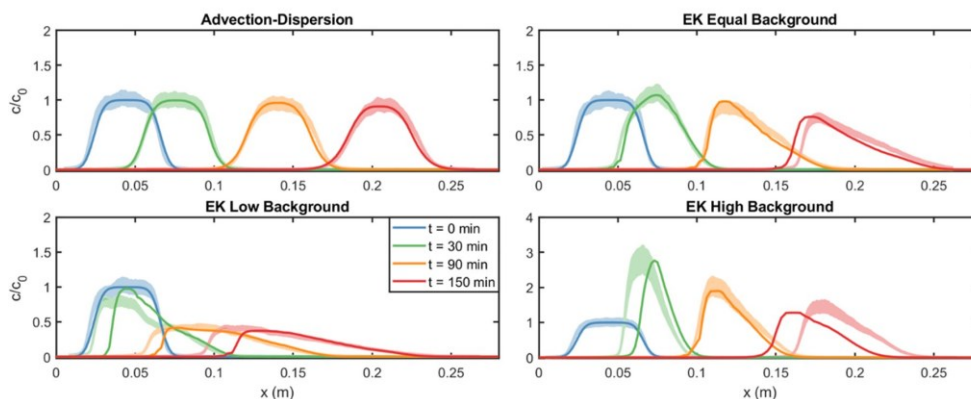
The latter evidence is well described and simulated considering the effect of charge interactions on the classic Nernst-Plank description of the mass fluxes of the present species. Similarly to the advective case, the results of the numerical simulations reproduce well the experimental observations, both in terms of plume profiles and local concentration values. For the "EK low" case (low background), the peak concentration progressively lowers until 1 mol m^{-3}, in the range of the background solution ionic concentration. The longitudinal transport which emerges from the profiles also shows the greater expansion and slower movement of the plume maxima. Contrarily, in the "EK high" test (high background) the permanganate concentration increases of almost three times in the first stages of EK transport, to then progress similarly to the "EK equal" scenario.

The different scenarios were analyzed using a modeling approach based on the Nernst-Plank-Poisson equation; using these data, it was possible to compute the major ions concentration in the pore water and the resulting electric conductivity; for the background solution Na^+ and HCO_3^- are considered, as $CO_3^=$ is a minor anion. For each ion, the concentration profile referred to the set-up length was obtained and compared to the total amount of ionic charge of the same sign in the system; the results are presented in Figure 23.
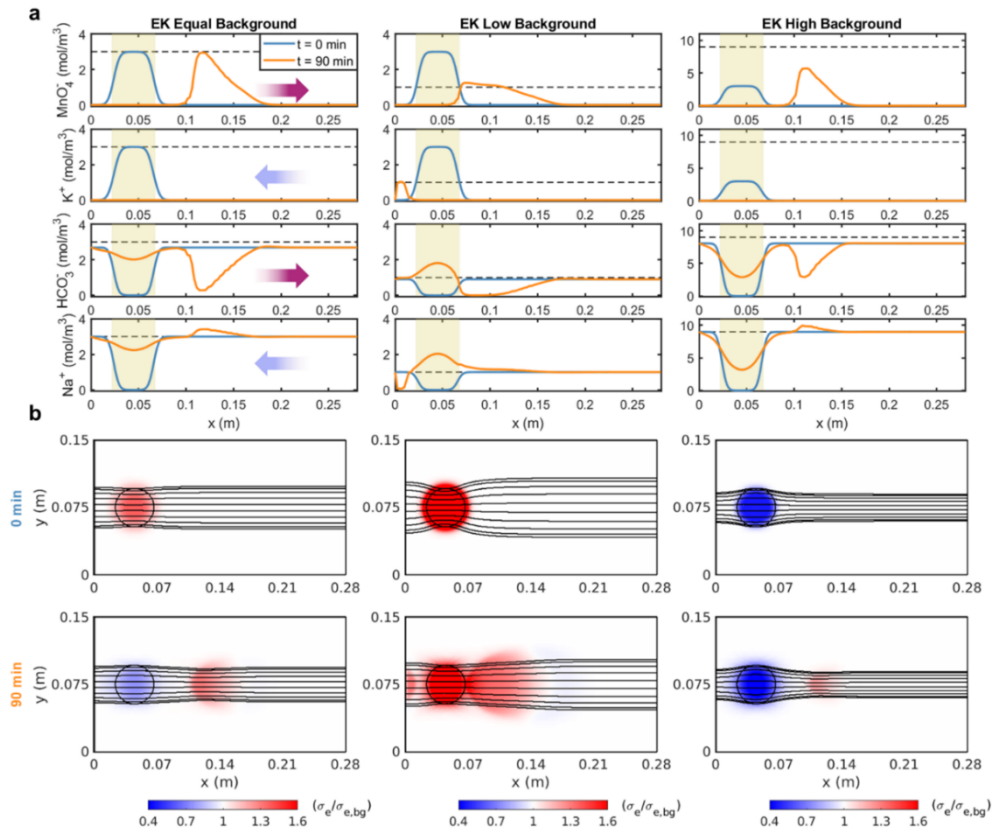
Figure 23) Simulated concentration of major ions present in the system at initial time and after 90 minutes: (a) shows a longitudinal cross section illustrating the plume dynamics at two different times during the test, the injection zone is highlighted in beige while the dashed line represents the total charge equivalents; (b) Normalized conductivity (on t=0 min) with respect to the background at initial time and after 90 minutes.

In the scenario with equal background, the MnO_4^- concentration corresponds to the equivalent ionic concentration and with the progressing of the migration the peak intensity does not vary significantly; the corresponding potassium injected in the system is completely extracted from the system boundaries in 90 minutes. The decreased concentration in the background ions (Na^+ and HCO_3^-) results from solution displacement caused by the injection and propagates in the system for the bicarbonate ion increasing its intensity. After 90 minutes, the concentration profiles of MnO_4^- and HCO_3^- are perfectly complementary, as it is required to maintain a neutral charge balance. The concentration profile for Na^+ closes the charge balance and accounts for differences in the diffusivity of the ions. The latter is responsible for the profile alteration of the plume front and tail, since while permanganate can move at his maximum theoretical speed in a permanganate background (which is, within the injection spot) to propagate in the background electrolyte a limiting factor is imposed by the bicarbonate lower diffusivity. This results in the more

pronounced front and in a sharp plume tail. As the ionic concentrations were equal for background electrolyte and permanganate the migration velocity is constant and very close to the theoretical value.

In the scenario with a lower background, the injected concentration of permanganate is significantly higher than the equivalent total charge, hence its migration in the system is limited by the soil solution. From the concentration profiles, after 90 minutes the concentration is equilibrated, and the permanganate plume has reached the "equal" condition; the profile evolution supports the lower velocity observed from the image analysis, both on the permanganate and potassium ions. The higher concentration of sodium and bicarbonate in the injection zone is required to maintain a null charge balance, or in other words is required to accept the ions displaced by the electromigration of MnO_4^-. In light of such data, it is also possible to explain the higher concentration in the plume tail in Figure 23 as the migration of the plume tail occurs in a system portion with "equal" conditions, namely the permanganate is migrating in permanganate. Even accounting for a dilution factor caused by the injection, the limiting effect from the lower background will be less than the one the plume front is subject to, causing a slight temporary accumulation of MnO_4^-.

In the last scenario, with a higher background ionic concentration, the limiting effect is acting differently, as due to the higher Na^+ concentration migrating towards the cathode a higher concentration of permanganate must migrate towards the ion for charge conservation. As for the previous cases the profiles of Na^+ and HCO_3^- after 90 minutes are complementary to the K^+ and MnO_4^- initial concentration profiles. As already discussed in the previous section, this result is of particular significance as electromigration of permanganate and multicomponent interactions are resulting in a concentration of the injected amendment that occurs opposing chemical diffusion and further increasing the concentration gradients.

The experimental evidence gathered clearly shows that the electrokinetic transport, shape, and local concentration of the amendment plume are strictly controlled by the background electrolyte concentration. It was also possible to show the cooperative effect of ionic concentration and diffusivities, as in the "EK equal" the higher diffusivity of MnO_4^- ang K^+ lead to higher conductivity for the amendment plume despite the same ionic concentration of permanganate and background electrolyte; this is clearly shown from the conductivity maps (Figure 23-b). It follows, the electrolyte conductivity is a spatially variable parameter in the

set-up, and significantly affects the electric streamlines, causing focusing and defocusing according to the medium conductivity: the electric filed streamlines focus in areas with higher conductivity and defocus in areas with lower conductivity. In the case "EK equal" and "EK low" background, the conductivity maps in Figure 23 shows a higher conductivity in the permanganate plume, and a focusing of the streamlines in the injection zone. After 90 minutes the "EK equal" scenario shows a higher conductivity for the permanganate plume, while the injection zone presents a lower conductivity due to the lower diffusivities of background ions that now occupy the injection pore space. In the "EK low" scenario the higher conductivity gradients between amendment and background results in a stronger focusing, while the slower migration results in the plume not leaving the injection area after 90 minutes. The stronger focusing in the plume tail also results in a strong defocusing in the plume front, which is the cause of a larger spreading of the amendment. Lastly, in the "EK high" case the pattern is opposite; the conductivity in the injection zone is lower for permanganate, hence the streamlines defocus in the plume tail and focus in the plume front, leading to a shrinking during its displacement towards the anode and an increase in its concentration, and thus in its conductivity.

The complex pore-scale flow and mass transfer processes regulate the macroscopic evolution of the injected plume, in terms of both shape and concentration, and requires metrics to allow the description of the amendments transport in the porous medium. Specifically:

- plume spreading is quantified by the second central spatial moments;
- the dilution index describes and quantifies the plume mixing.

Both descriptors were computed using the mathematical model and determined from the image analysis of the different experiments. A more detailed mathematical description of the spatial moments is reported in Appendix.

The images reported in Figure 17-Figure 21 and summarized in Figure 24 clearly show different plume shape, area, and solute concentration for the different explored scenarios. The longitudinal (x) and transverse (y) second central moment shows specific behaviors for the different scenarios. Referring to the advective-dispersive case, both longitudinal and transversal model shows a gradual increase consequence of hydrodynamic dispersion and diffusion of the plume fringes. In the "EK equal" scenario the plume spreading is larger in both directions, and it is even more pronounced in the "EK low" scenario; in the latter case the plume spreads over a large portion of the porous medium. The computed trends for the "EK low"

scenario show higher slope in the initial times of EK, which indicates a more effective spreading at earlier times. In the "EK high" scenario the spatial moments analysis shows the initial shrinking and the subsequent spreading of the plume; also, the rate of increase is more pronounced on the longitudinal direction resulting in higher moments at late times compared to the advection-dispersion case. For all cases, the computed moments (solid line in Figure 25) are in good accord with the experimental data obtained from the image analysis (shaded line in Figure 25).
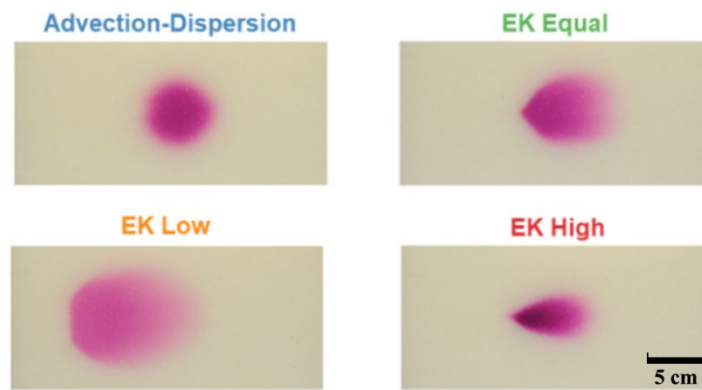
Figure 24) Plume shape after 90 minutes for the different transport experiments, images extracted from Figure 17-Figure 20
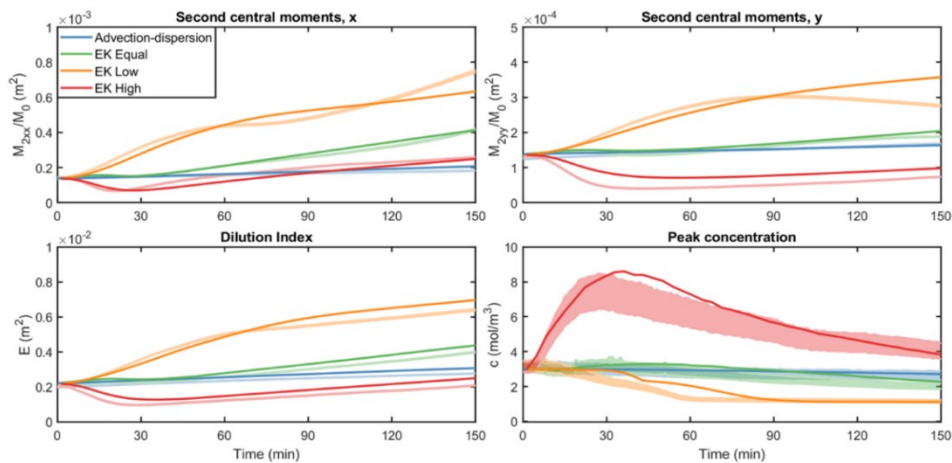
Figure 25) Second central spatial moment on the longitudinal (x) and transversal (y) directions, dilution index and peak concentration variation in time. Details on the mathematical data processing are reported in Appendix. Adapted from Sprocati, et al. [65]
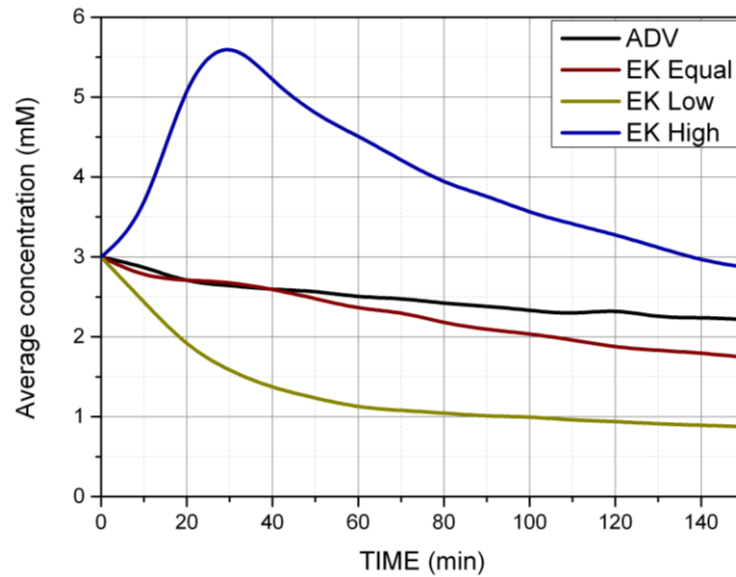
Figure 26) Average plume concentration computed from injected permanganate concentration and plume expansion/contraction (from ImageJ software)

The other metrics applied to describe the plume evolution – dilution index and peak concentration – are intrinsically related and are well suited to quantify the capability of the injected plume to mix with the background solution. In the advection-dispersion case the mild increase is coherent with hydraulic transport in a 2D system [172]. Dilution increases for the "EK equal" scenario while is more than double for the "EK low" case; these evidences show the capability of EK transport to effectively distribute the injected tracer or amendment in a larger volume than the advective-dispersive case. All the above-mentioned dilution indexes show monotonic increasing trends, a significant and interesting difference is found for the "EK high" scenario where the dilution index variation is non-monotonic. An initial decrease (to approximately half of the initial value in the first 30 minutes) followed by an increase is observed, with a final dilution index value similar to the one for the injected plume. The initial trend in the dilution index for the "EK high" case can appear counterintuitive if analyzed only in light of conventional mass transfer, since the plume dynamic acts decreasing its entropy and against the concentration gradient. However, as previously explained, in the EK regime charge interaction and conductivity gradients are strongly correlated with the primary driving force, thus prevailing and resulting in the plume shrinking and an almost three-fold concentration increase. It is also interesting to notice that the high degree of similarity is found with the normalized area obtained from the image analysis (Figure 21): i) in the index slope for later times; ii) in the final

relative values of the different scenarios. This evidence corroborates both the validity of the mathematical model and the calibration procedure since the normalized area was obtained by a simple plume tracing and geometrical computation. The same correlation can be found from the average plume concentration computed by multiplying the nominal initial concentration (3 mM) by the inverse of the normalized area. This is confirmed by the data presented in (Figure 26) and supports both the Particle Tracking analysis, the image calibration, and the modeling approach. As expected, differences in the peak concentration value are observed (e.g., for "EK high" maximum concentration abt. 8.6 mM for the moment analysis vs 5.8 mM from Particle Tracking) due to the different nature of the value; using the spatial moments (and the image calibration) a point concentration can be determined, while Figure 26 refers to an average plume concentration.

3.3.2 Reactive transport experiments

The results from the reactive transport experiments are presented in Figure 27 as time frames from the images collected during the experiments.
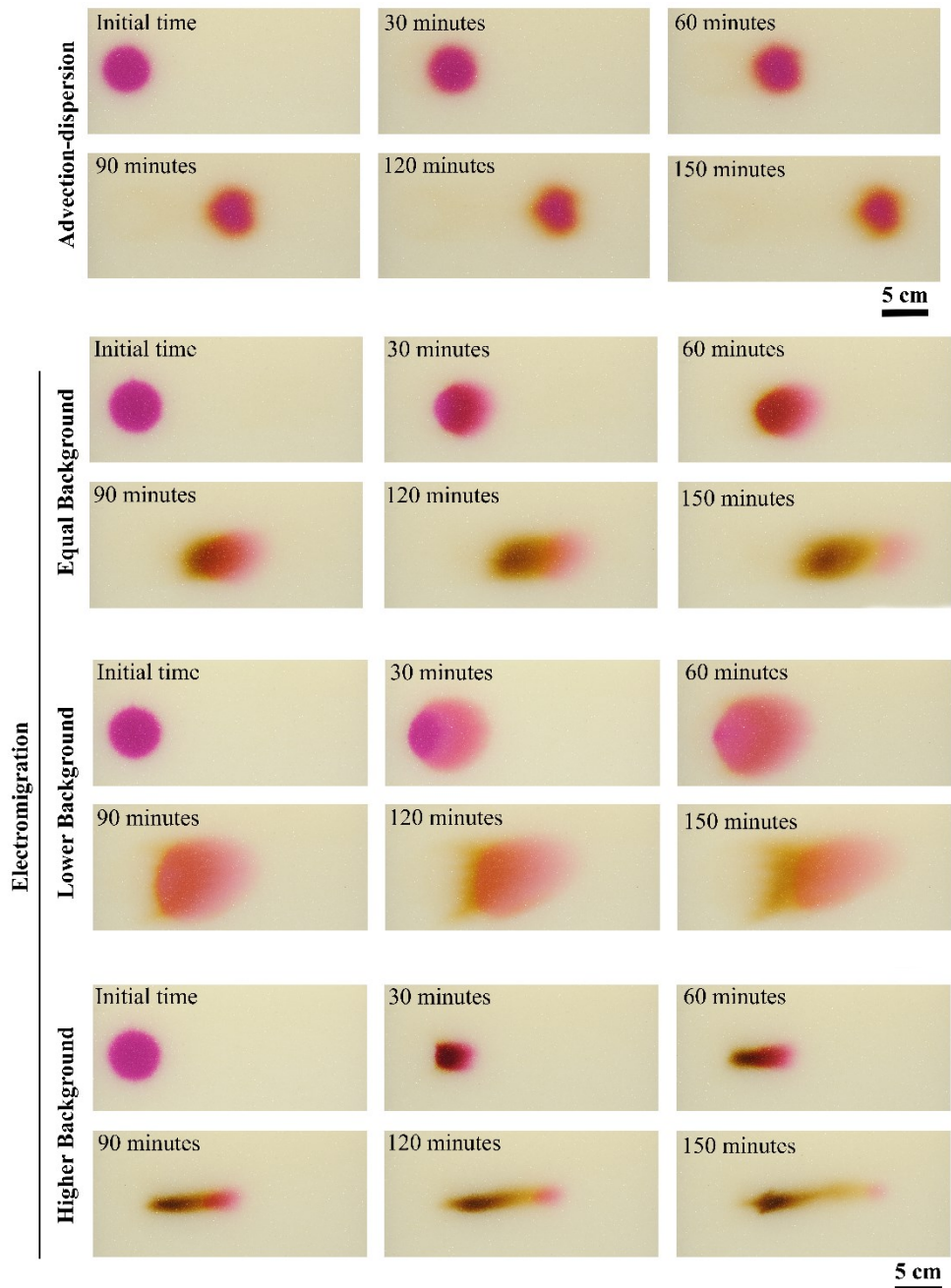
Figure 27) Plume evolution obtained from the photography acquisition during the reactive transport experiments; from top to bottom advection-dispersion, "EK equal", "EK low" and "EK high."

The impact on the permanganate reactivity during its electromigration (which is at the core of a ISCO application) caused by the different transport mechanism is evident. Focusing on migration only, in all explored cases, the residual permanganate plume migrates with a similar velocity to the conservative case (Figure 28) but significant differences are observed in reaction mechanism and kinetics.
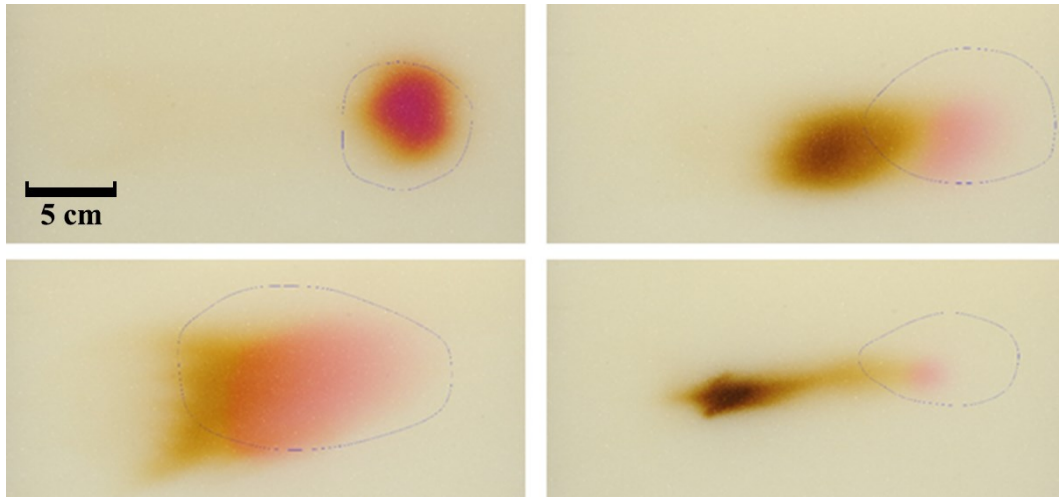
Figure 28) Comparison of the plume position at the end of the experiment (150 minutes) for the conservative test (blue line) and reactive test (color image); from top left proceeding clockwise: advective-dispersive, "EK equal", "EK low" and "EK high" scenario.

The advection-dispersion transport shows a reaction with glucose occurring on the plume fringes, as the entire solution volume injected is subject to the transport and thus the plume bulk is initially unaffected by mixing with the background solution. At the end of the experiment, most of the permanganate is still unreacted; although the formation the brown MnO_2 precipitate complicates the image analysis, it is possible to obtain a global velocity for the plume, which results equal to $1.83E-5 \pm 1.9E-7$ m s^{-1} (or 6.58 ± 0.7 cm h^{-1}) in good accordance with the velocity observed for the conservative advective transport. From a qualitative standpoint, also the plume shape at the end of the experiment is comparable.
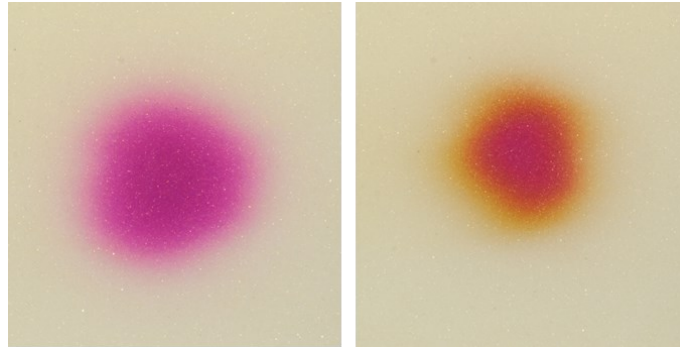
Figure 29) Plume shape after 150 minutes in the advective-dispersive transport experiment for the conservative case (left) and reactive case (right); the yellow color on the plume fringes is MnO_2 resulting from the permanganate reduction.

Analyzing the electrokinetic experiments, we can immediately notice a significant difference in the fact that the reaction does not occur on the plume fringes anymore, but it involves the plume bulk as a consequence of the different transport mechanism. The applied electric field causes the displacement of permanganate by electromigration but has no effect on the non-charged glucose or the pore water. The immediate consequence is that a higher permanganate mass participates to the reaction, hence higher reaction rates than the advective case are expected, but also that the three cases – equal, low, high – are bound to lead to a different degradation efficiency.

The similar color, in terms of RGB components, and the presence of a wide transition zone increase the image analysis complexity to a point where the data would no longer be of significance. No roundness and normalized area for the permanganate ion will be presented, and qualitative image analysis and numerical simulations will be used instead to discuss the phenomena at play. When permanganate and background solution present a similar conductivity (equal ionic concentration) the plume shape alteration is not extreme, the fronting effect results in a lower reaction kinetic than in the plume bulk. The plume evolution for the "equal" case also shows a significant consumption of permanganate, after 150 minutes a slight purple front is still visible in the set-up. The migration velocity appears not to be affected by the reaction, comparing the unreacted plume position (purple color) for the conservative and reactive case, the two centroids are close together (Figure 28). The evidence from the "EK low" scenario pictures a very different situation; immediately a much lower efficiency is observed in the permanganate reactivity as after 150 minutes the unreacted plume is still clearly visible; the same evidence results from a paler yellow-brown color of the reaction byproducts (MnO_2). Also, while the reactive area is narrower on the longitudinal

direction, the same extends more in the transversal direction than the "equal" case. Another relevant difference, directly depending on the electromigration in "EK low" conditions is the fact that the plume tail is initially less involved in the reaction, as 90 minutes are required for the plume tail to exit the injection area introducing a mixing limitation rather than a concentration limiting effect as in the "equal" case. Lastly, for the "EK high" case the reaction occurs with a faster kinetics caused by a higher permanganate concentration determined by the plume shrinking, which also results in a reduced area of the set-up which is affected by the reaction (Area of Delivery, AoD).

The mathematical model developed for the conservative transport can be modified with a reactive term that accounts for the permanganate consumption, the kinetic constant was determined empirically as no definite reaction pathway was found for the oxidation of glucose by permanganate. The ability of the model to correctly describe the concentration profile also allows the computation of the reaction rates: the results presented in Figure 31 support the previous discussion.

To provide metric for the different reaction kinetics, a mixing area A_{mix} can be obtained, and the permanganate mass in the domain computed (Figure 32). The mixing area is larger for the "EK low" and "EK equal" scenarios, for which the electromigration and the background solution composition leads to an extended mixing zone; the A_{mix} increases to a maximum, then decreases due to the permanganate consumption in the glucose oxidation. The mixing area is more limited for the ADV and "EK high" scenarios, although the two trends present similar values, it must be noted that the shape of the mixing zone is radically different: in the "EK high" the lower A_{mix} originates from the plume shrinking and is also associated with higher reaction rates, while in the advection-dispersion case the plume does not shrink and the low A_{mix} refers to a reaction limited to the plume fringes, hence associated with lower rates too. The mathematical model was applied to compute the permanganate consumption upon reaction with the glucose (Figure 32); non-linear trends are observed in the residual permanganate concentration, and a greater consumption is registered for the electrokinetic experiments. Specifically, "EK equal" and "EK high" show the highest efficiency as expected by the higher permanganate concentration and better mixing; the "EK low" scenario, despite a larger A_{mix} is also associated with a lower permanganate concentration, hence lower reaction rate. It is possible to quantify such differences in efficiency; the simulations show a 75% permanganate consumption over 150 minutes, whereas a 70%

consumption is registered for "EK low" and only a 35% for the advection-dispersion case.

An alternative estimate on the area of the set-up effectively interested by the amendment delivery (A_{mix}) can be provided by the plume path; the contour of the plume path for the conservative experiments is reported in Figure 30 with three still frames of the experiment (0; 60; 150 minutes). With advective transport the Area of Delivery (AoD) value is 114 cm^2, which increases for "EK equal" and "EK low" due to the plume expansion with AoD equals 129 and 133 cm^2, respectively. As in the "EK high" scenario the plume shrinks, the AoD is lower than both other EK and ADV scenarios, setting at a value of 83 cm^2. However, the plume dynamics also affects the local amendment concentration, which determines reaction rates and contaminant removal as previously discussed.
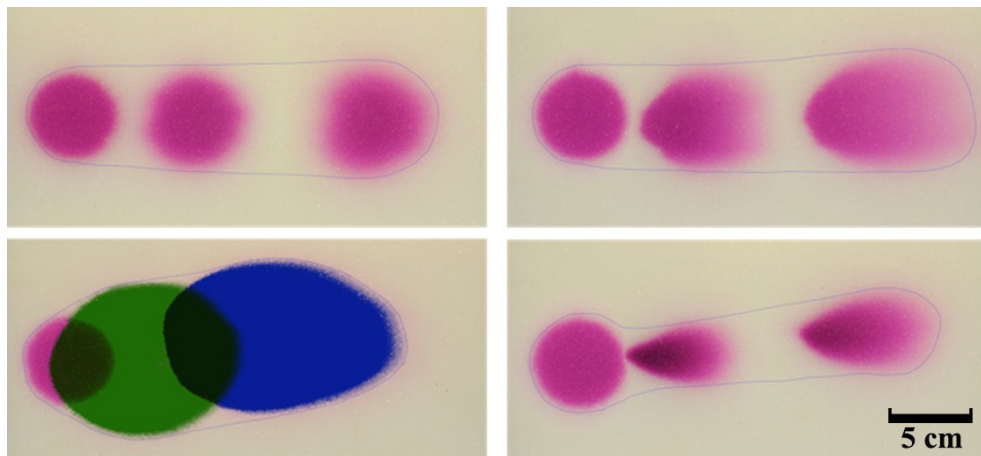
Figure 30) Cross-sectional area crossed by the permanganate plume, hence interested by the glucose oxidation. The blue line delimitates the entire glass beads area crossed by the plume, the spots refer to the initial, half, and final time of the experiments and are added to put the contour line in context. From top left clockwise: "EK Adv", "EK equal", "EK low" and "EK high" conservative experiments.
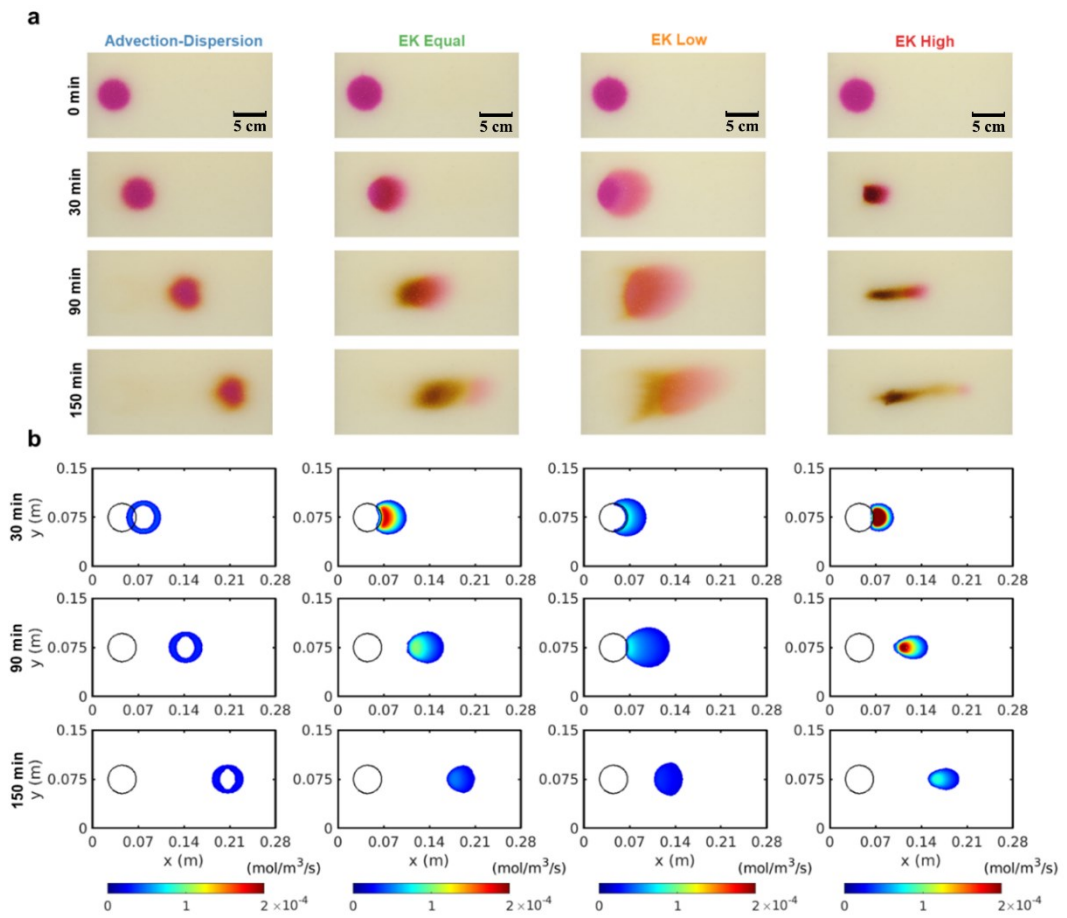
Figure 31) Plume evolution for the dynamic transport experiments and simulated reaction rates, adapted from Sprocati, et al. [65]. Part 'a' depicts the plume evolution using the collected photos, while part 'b' shows the reaction rates computed with the mathematical model, highlighting the differences between the different scenarios.
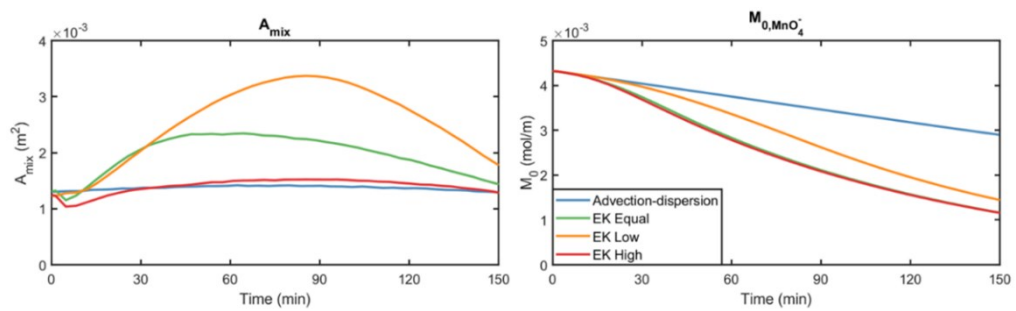
Figure 32) Mixing area referred to a threshold reaction rate of 2E-5 mol m^{-3} s^{-1} and permanganate consumption; adapted from Sprocati, et al. [65]. Data were obtained as computed quantities from the mathematical model, see Appendix for additional details

3.4 Conclusions and implication for groundwater remediation

The present study allowed to evidence that: i) electrokinetic delivery presents significant advantages for reactive amendments compared to advection-dispersion; ii) conductivity gradients must be considered in the design and optimization of an electrokinetic delivery aimed to groundwater remediation, as charge interactions introduce limitation to the amendment mass transfer, Area of Delivery, and reaction rates. The evidence gathered allowed to highlight important mechanisms of both scientific and practical relevance for the electrokinetic delivery of amendments. It was possible to demonstrate that the pore-water chemistry and the resulting microscopic Coulombic interactions can both limit and/or enhance the electrokinetic delivery of charged solutes. A mass transfer limitation is imposed by the background solution when the ionic concentration is lower than the injected amendment.

For homogenous and permeable porous medium advective delivery does not presents as many limitations as in low permeability layers, but the experiments clearly demonstrate the advantage in the EK delivery for the degradation of pollutants. For the advection-dispersion case the amendment reactivity is limited to the plume fringes, thus reducing removal efficiency, increasing remediation times, and possibly resulting in a waste of permanganate that exits the system boundaries unreacted. The electromigration technique allows to eliminate the fluid transport, thus achieving a complete mixing of the injected amendment which is evident from the reactivity of the plume bulk as well as fringes. Notwithstanding the conductivity gradient effects, in all cases the reaction rates and Area of Delivery are superior for EK than advection. For real case implementation, important implications can be found for contaminated sites in the vicinity of safeguard zones; the risk of permanganate escaping from the site boundaries are much higher for the advection case, and therefore additional measures are required (increased number of monitoring wells, push and pull technique, etc.).

From the different EK scenarios, it was possible to evidence the effect of electrodispersion, charge interaction and multicomponent transport on the permanganate longitudinal and transversal distribution during electromigration. In this perspective, the conservative experiments show:

- In light of a theoretical migration velocity equal to the seepage velocity, a slower migration (of about 33%) is achieved for the "low" and "high" scenarios, while the velocities match in the "EK equal" case.
- A significant variation in the Area of Delivery is obtained: "EK equal" 129 cm^2, "EK low" 133 cm^2, "EK high" 83 cm^2.
- An effect on the mass transfer of permanganate is determined by the electrical conductivity gradients between amendment and background in the "equal" and "high" cases; in the former the local concentration is homogenously reduced by plume expansion, while in the latter a local concentration in the plume center with more diluted fringes is observed. In all cases, the background concentration sets a limit to the mass transfer of the injected amendment: the amount of injected charge which can be effectively delivered is therefore determined by the background charge concentration.

These results present a significant importance by themselves, as the same focusing and defocusing effect is to be expected in heterogeneous porous media for soil types, which strongly influence the background solution conductivity (clays, silts, etc.). A characterization of the local soil conductivity appears pivotal for the correct design of an electrokinetic delivery procedure in such conditions to prevent, for example, the bypass of layers with lower electrical conductivity. When extended to the delivery of amendments in a contaminated porous medium, the plume dynamics observed play a fundamental role in reaction kinetics, reactant consumption and efficiency.

Firstly, the different mixing mechanism drastically modifies the limiting variable for the reaction, moving from a mixing limitation for the advective case, to a contact time in the EK delivery for which mixing is complete. It also follows, referred to the same system (or contaminated site, for a real application) extension, the EK delivery allows a more efficient use of the amendment, while the majority of permanganate results unreacted at the end of the hydraulic transport: using the mathematical simulation (color interferences prevents us from using the collected pictures) a 35% permanganate consumption is estimated in the advective case, a 75% for "EK equal" and "high" and a 70% for "EK low". Secondly, the delivery under the influence of electric fields allows to modulate the Area of Delivery by tuning the amendment conductivity with respect to the background solution, that is not possible in the conservative delivery in the reactive case:

- The greater AoD for the "low" case is associated with a lower local concentration, hence reduced reaction rates. At the end of the delivery experiment, a significant amount of permanganate is still unreacted.
- The lower AoI for the "high" case results in a higher local concentration and faster reaction rates, consuming almost all the injected permanganate.

Given the complexity of the process and the interdependence with the system variables and remediation goals, it is not possible to determined which scenario provides the greater efficiency, rather a case-by-case evaluation is required. In the present study the greater distance is traveled in the "EK equal" and "EK high" scenarios, with a similar permanganate consumption but given the greater plume extension in the "equal" case, a greater aquifer volume is remediated. It is true that a greater glucose oxidation is likely to be achieved in the "EK high" scenario, however in most cases a complete degradation in a small portion of the aquifer is not the remediation target, the objective is rather lowering the concentration below the legal limit. In this context the "EK high" case represents a highly effective use of the permanganate but entails a low efficacy, as the results may overachieve the remediation target, while an "EK equal" approach appears optimal. The "EK low" scenario, on the other hand, results in a wider Delivery area and a more uniform oxidation, which in some cases can prove the best delivery method to maximize the permanganate use and reduce, for example, the number of injection wells. However different scenarios can be pictured, for example when operating the remediation in a limited domain (e.g., if the contaminated site is contiguous to a water body), the "EK low" scenario is highly undesired as a greater amount of amendment would escape and possibly contaminates previously clean aquifers. In such conditions, a fast permanganate consumption is to be preferred, hence an "EK equal" or "EK high" delivery should be implemented.

Among the results, the mathematical model developed and validated with the experimental results can prove of strategic importance in devising the optimal injection and delivery strategy. The simulation of the conservative transport provides a very good description of the electromigration observed during the EK experiments, both in terms of velocity and plume dynamics. Using an empirical kinetic constant for the oxidation of glucose by permanganate and an unknown stoichiometry, the model predicts the system evolution with good accuracy in terms of permanganate consumption, plume dynamics and migration velocity. The gained mechanistic understanding of the coupled electrokinetic transport, the influence of the background solution conductivity and resulting plume dynamics can prove instrumental in increasing the performances, in terms of efficacy and efficiency, of

delivery strategies. These are not limited to ISCO and ISCR but can also be applied to deliver nutrients (lactate, ammonium, sulphate [163]), bacteria and microorganism in different remediation strategies. Thanks to the mathematical model ability to describe the delivery outcome, in both conservative and reactive regime, it can be used as a decisional support for the choice of the reactant concentration to operate in the "equal", "low" or "high" scenario and tune the Delivery area and reaction kinetics to the specifics of the site under remediation. The general mechanism of conductivity-limited delivery is not limited to permeable aquifers but can also be extended to heterogeneous porous media containing low permeability inclusions (clay, silts), where electromigration represents an effective strategy to overcome the low hydraulic permeability.

Chapter 4

Electrokinetic delivery of reactants in low permeability zones

4.1 Literature background and motivations

The delivery of soluble reactants is widely applied for the *in-situ* decontamination of groundwater and subsoils from different class of pollutants, for example organic compounds and heavy metals [20, 173, 174]. Based on the type of reactant used to promote the transformation of the pollutant in less toxic or non-toxic compounds two main techniques are identified: In-Situ Chemical Oxidation (ISCO) and In-Situ Chemical Reduction (ISCR). The former class uses an oxidant as reactant, and thus is highly effective on organic contaminants (VOC, NAPL, etc.) while it can cause a mobilization of heavy metals (and increase their toxicity, in the case of Cr^{III}/Cr^{VI}) [10, 17, 20, 24]; ISCR employs reducing agents and can effectively promote the decontamination from both organic pollutants [173, 175] and heavy metals [174, 176]. In both cases, the direct delivery and subsequent reaction of the amendment in the aquifer prevents the extraction of the contaminated phases (water, soil) and a reduces the risk of extending the contamination during their handling and transport to the landfill or purification facility required in *ex-situ* remediation [7, 9, 12]. Large scale applications of both ISCO and ISCR have been performed in different countries and succeeded in the site decontamination, proving the validity and potential of such approach [17, 20, 24]. The delivery of the reactant, them being oxidants or reductants, is usually performed by their injection from wells or boreholes and advective transport in the

78

porous medium [13, 17, 24]. Consequently, a careful characterization of the subsurface lithology and hydrogeological characteristics is paramount for a successful application and the attainment of the remediation goals. The advective delivery of solutes is strictly dependent from the medium hydraulic conductivity, and soil types as clays or silts are usually inaccessible to the advective flow and thus to the reactants [7, 10, 17, 20]. The presence of low permeability inclusions in a sandy aquifer will likely result in preferential flow paths and 'dead zones' where the reactant cannot be delivered, except via diffusion in extensive time, which are then excluded from the decontamination. Also, the contaminant diffusion in the low-permeability regions (especially in the case of DNAPL) creates long-lived secondary sources which lead to a slow release of the contaminants by back diffusion [23]. The possibility that the release from the secondary source zones determines a pollutant concentration exceeding the cleanup standards bears important implications in the remediation design and site management. Specifically, treatment trains (continued or repeated application of a remediation procedure) can be applied, but the use of short-lived amendments such as soluble oxidants and reductants may not be an effective solution [7, 10, 17, 20, 23, 24]. In this framework, the electrokinetic delivery of reactants can potentially represent a valid solution to overcome the delivery limitations in low-permeability regions, and to target the secondary sources preventing or limiting the contaminant back diffusion [11, 13, 23, 45, 177].

Electrokinetic delivery is a general term used to identify transport processes based on the application of a direct current to the aquifer system, the resulting coulombic interactions determine a driving force acting on solutes and colloids contained in the system that allows the electric conduction in the medium [36, 37, 56]. Three main transport mechanism are identified: electromigration, acting on the ionic charge in the solution bulk, electrophoresis, acting on the colloidal particles, and electroosmosis, acting on the ionic charge involved in the electric double layer at the grain surface [36, 37]. When referred to soluble reactants, as in many ISCO and ISCR applications, the electrokinetic transport is controlled by electromigration (EM) and electroosmosis (EO). The former consists in the coulombic attraction of point-charges; hence no frictional or viscous force is involved: ions are attracted to the electrode with opposite charge; electroosmosis consists in a fluid flow with a flat velocity profile, which in most cases is independent from the pore radii and is directed towards the electrode bearing the same polarity of the porous medium. Due to their nature, both processes are not affected by the soil hydraulic conductivity in

most natural conditions [11, 13, 66, 177] and thus low permeability layers become accessible to the injected amendments.

From a simplified simulation performed in COMSOL® it is possible to visualize the hydraulic and electric streamlines, directly comparable with the migration velocity field; for the hydraulic flow, the available data on medium porosity and permeability were used, while for the EK-driven simulation the complex conductivity (which means, considering the effect of the porous medium) was computed using the simplest formulation of Archie's law and average parameters found in the available literature. The images reported in Figure 33 clearly show that in the case of electrokinetic-drive transport the velocity field crosses the clay inclusion, while bypass occurs in the hydraulic scenario (refer to captions for more details).

Hydraulic delivery

Sand permeability : 2E-3 m/s
Clay permeability : 1E-9 m/s
Fluid velocity   : 0.85 m/day

EK-driven delivery

Solution conductivity: 1500 uS/cm
Sand conductivity: 450 uS/cm
Clay conductivity: 1160 uS/cm
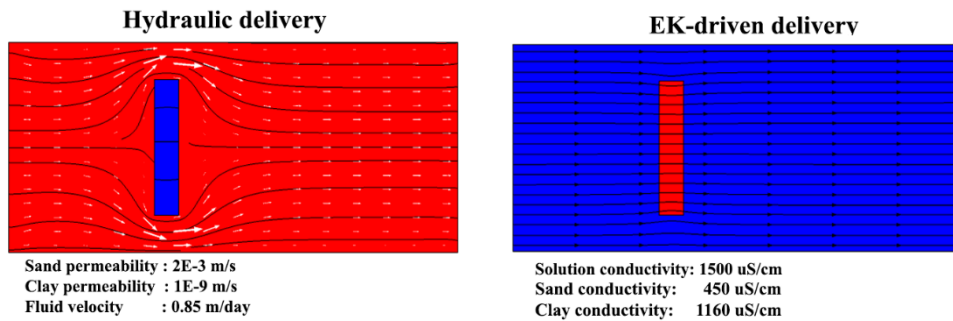
Figure 33) Simulation of velocity field for a heterogeneous porous medium in the presence of a hydraulic- (left) and electrokinetic-driven (right) transport. Values for hydraulic permeability of sand are obtained from previous experimentation [178, 179], whereas for sand an average value is used from literature; electrical conductivity values are obtained from experimental measures. The color scale is binary, used to better visualize the different properties of sand and clay. The reading is the following Red>Blue. The black lines represent the advective flow line in the first case and the electrical streamlines in the second.

However, it is important to correctly evaluate the extent of both EM and EO given their nature (see Figure 35). Most reactants for ISCO and ISCR are anionic species (Table 6), and thus EM causes their transport towards the anode. At the same time natural soils usually bear a negative surface charge, resulting in an electroosmotic flow (EOF) that opposes EM.

Table 6) Common reactants for ISCO and ISCR applications

ISCO amendments		ISCR amendments	
Permanganate	MnO_4^-	*Sulfur based reductants*	XS^{n-}
Persulfate	$S_2O_8^=$		
Sulfate radical	$SO_4^{-\bullet}$		
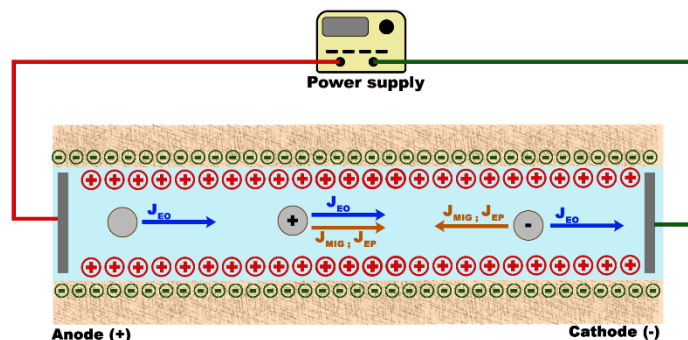
It is important to notice that the contaminant will also be subject to: i) the same EOF than the amendment, ii) an EM flux determined by its chemical properties; it follows that the mixing of the two species depends on the force balance but as a general approximation it can be assumed that: i) mixing always occurs with opposite charged reactant and contaminant, ii) mixing is likely to occur for a charged reactant and a neutral mobile contaminant, and iii) mixing must be evaluated for equally or neutral reactant and contaminant.

Different studies have focused on the electroosmotic flow in clay and other fine-grained soils, initially when EOF was used to promote soil dewatering as a consolidation method [34, 180, 181] and later when the applications were extended to contaminant extraction for groundwater and soil remediation [40, 61, 62, 122, 182, 183]. The extraction of both heavy metals [38, 61, 62] and organic compound [62, 122, 184] was achieved and sometimes coupled with electrolyte modifications (pH, surfactants, ligands) to improve contaminant mobility and extraction efficiency. Recently, more and more studies focused on the possibility to operate a direct delivery of amendments, in the form of both solutes [43, 45, 177] and nanoparticles [44, 143, 155], in soils with low hydraulic permeability. Most literature experimental works approach homogenous porous media that are composed solely by the clay or the generic low-permeability soil under study (e.g., marine sediments) [63, 153, 155, 185, 186]. The results show that electrokinetic transport is effective in allowing the delivery of amendments in soils otherwise seldom accessible to hydraulic flow, which would require delivery only by chemical diffusion [99]. These studies also brought to attention the high sensitivity to the system boundary conditions. Some literature works have focused on the delivery of soluble amendments, such as permanganate for ISCO remediation [66-

68], showing that pH plays a pivotal role and can radically modify the migration and delivery rates. A first study [66] approached permanganate transport in 1D systems, specifically cylindric columns, in homogenous and heterogeneous conditions; the latter were obtained packing the column with two layers of sand enclosing the clay (kaolinite) in the central column section. In both cases, pH-redox conditions in the electrode chambers proved to be detrimental to the migration, causing MnO_4^- reduction (to MnO_2) and precipitation: permanganate cannot be dissolved in the buffering electrolyte, but has to be injected by a well (or borehole) without a working electrode (which is, an electrode used to apply the electric field). In all the cases explored by the author under heterogeneous conditions permanganate was not delivered in the low permeability region of the column, and the results also point to a significant influence of EOF, which appears to trump electromigration. Further studies on the permanganate transport were conducted by Hodges et al. [67, 68] in an apparatus that allowed to eliminate pH effects and an effective and consistent delivery of permanganate in clays was achieved, by using a complex apparatus and suggesting complex operations for the pH control. Lastly, delivery experiments were performed in a 2D geometry with different low-permeability lenses configurations [45, 152] using ultra-fine glass beads in the first case and a fine silt (from ground silica) in the second study: in both cases delivery in the low permeability region was achieved, showing the potential of electrokinetic delivery for those soil conformations most challenging for the traditional advective delivery methods. However, the authors mention that in experiments on kaolin clay delivery proved difficult to achieve [152]. Moreover, both studies were performed coupling hydraulic electrokinetic delivery to achieve the transport of permanganate in the low-permeability regions, introducing the amendment on the entire set-up cross section thus eliminating the possibility of flow bypass, thus limiting the scalability to a real case scenario. Lastly, from a reactive approach, Chowdhury, et al. [45] address the issue of back diffusion from low permeability layers but do not address the reactivity within the layers themselves.

The aim of the present study is to improve and optimize the use of electrokinetics for the delivery of reactants in low permeability medium for groundwater and subsoil remediation, specifically: i) overcoming the permanganate stalling frequently observed [66-68]; ii) proving the ability of the delivered amendment to explicit its reactivity under the electric field in the low permeability layer; iii) performing and optimizing a delivery of an amendment in a low-permeability layer. The first part of the study, addressing points *i* and *ii*, was performed in 1D geometry, while to achieve the last objective, a 2D system

analogous to the one used in Chapter 3 was employed to create a sandy porous medium containing a low-permeability inclusion; the latter allowed to include in the study the effect of transversal dispersion (both hydraulic and electric).

4.2 Amendment delivery and reaction in 1D geometry
4.2.1 Materials and methods

Experimental apparatus

The experiments were performed in a self-constructed 1D system, comprised of a plastic (PVC) square pipe that was modified to create a tank similar to the one used in Chapter 3, only with a smaller size and reduced geometry (Figure 35).

* Working electrodes - DC input

** Recirculation in   *** Recirculation out
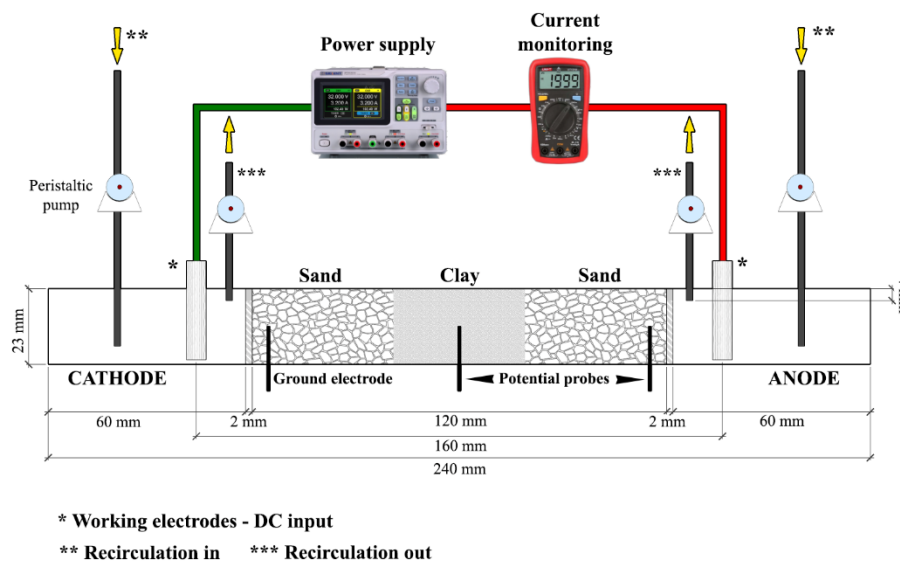
Figure 35) Schematic representation of the experimental set-up

The use of square over circular geometry was preferred, as a curved surface complicates the collection and interpretation of images during the experiment, introducing reflexes and increasing the required depth of field to obtain in-focus pictures. The set-up size was 240x25x25 mm, and it was divided in two electrode chambers (length 60mm) and a porous medium section (length 120 mm) separated by two bulkheads with a circular mesh covered by a HDPE mesh filter (pore size 105μm) to confine the sandy porous medium. The clay layer was placed at the center of the porous medium section and had a length of abt. 30 mm, while it extended over the entire set-up cross-section. Each electrode chamber was equipped with an electrode slot and two holes to insert the tubing for the recirculation system. The electric potential was applied using graphite rod electrodes ($\varnothing$ 6mm) connected to a DC power supply operating in *constant voltage* mode providing a potential

gradient equal to 3 V cm^{-1} across the entire system. The local electric potential in the porous media was monitored using wire electrodes (ø 0.8mm, exposed tip) across the entire medium (EL2) and the first half, specifically the first sand section and half the clay inclusion (EL2).
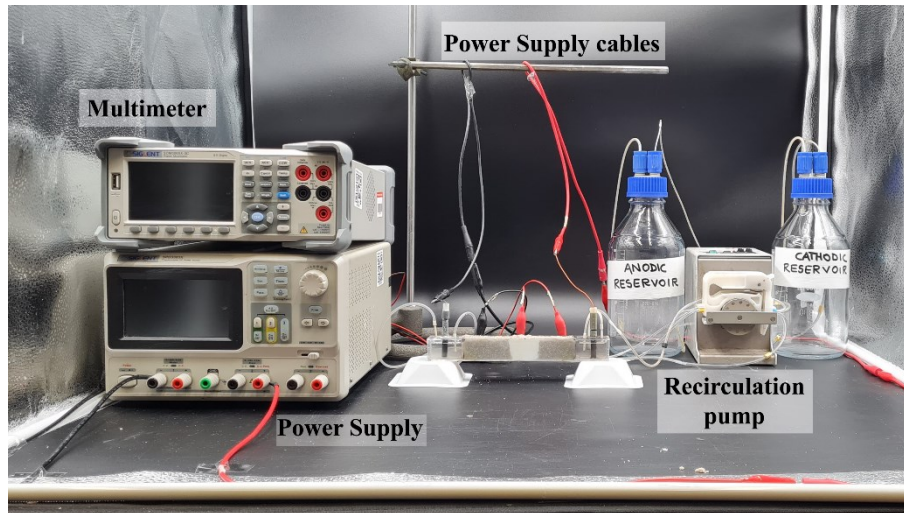
Figure 36) Photo of the experimental set-up for 1D tests
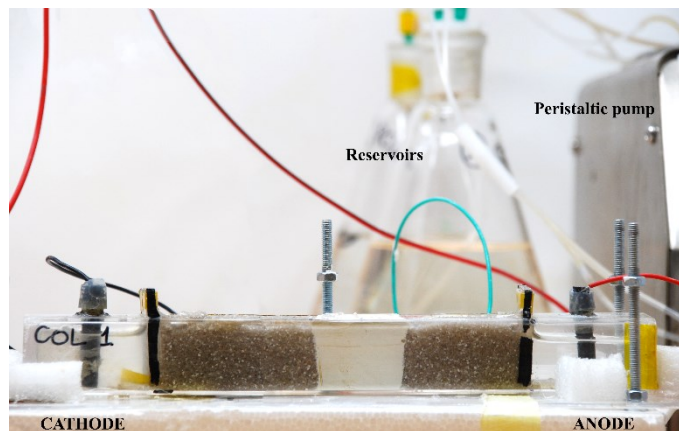
Figure 37) Detail of the 1D column prototype shot during the preliminary system testing, probe electrodes are installed on the rear side. The screws and polystyrene blocks were used for a consistent placing of the column in the set-up with respect to the DSLR camera.

Porous medium and solutions

The sandy porous medium used in the experiments was a quartz sand, while kaolin was used as low permeability inclusion; the principal porous media parameters are reported in Table 7. The background solution was prepared to simulate the complexity of a groundwater using different salts to obtain a TDS value of 0.82 g L^{-1}; the detailed composition of the solution is reported in

Table 8. To overcome the limitations in delivery observed by Roach [66], a buffer solution was recirculated in the electrode chamber to neutralize the electrolysis products and prevent pH fronts to significantly modify the electrokinetic properties of the porous medium. A phosphate buffer was selected, to maintain a neutral pH similar to the one of the background solutions; the monobasic/dibasic potassium phosphate ratio is defined by the final pH, while their absolute concentration was selected to provide the same conductivity of the background solution in order to reduce the system variables; the detailed composition and properties of the solution are reported in

Table 9. For the non-reactive delivery, the buffer concentration was respectively increased and reduced by a 2.5 factor to explore lower and higher conductivities.

The contaminant solution was prepared using methylene blue dye at a 0.1 g/L resulting in a conductivity of abt. 1400 μS cm^{-1}, comparable to the background and buffer properties. The use of a dye allows for a direct visualization of the contaminant and any variation occurring during the experiments, since sampling from the low-permeability layer is a complex operation that can radically alter the process. Lastly, potassium permanganate and a sulfur-based reducing agent were employed as representative amendments for the ISCO and ISCR remediation at a respective concentration of 11 mM and 8 mM to ensure the same electrical conductivity of the background solution, using the terminology of Chapter 3 this is an "equal" case; this means that the electrodispersion of the plume is minimized, limiting the variable affecting the plume dynamics.

Table 7) Technical data for silica sand and kaolin clay

		SILICA SAND	KAOLINE CLAY
Bulk density	(g cm^{-3})	1.4-1.5	0.35
d_{50}	(μm)	280	1.5
Porosity		0.45	

Hydraulic conductivity	(m s^{-1})	1.72E-3	<2E-8

Table 8) Synthetic water composition and properties

KH$_2$PO$_4$	(g L^{-1})	0.061
NaHCO$_3$	(g L^{-1})	0.042
NaCl	(g L^{-1})	0.538
NH$_4$Cl	(g L^{-1})	0.05
CaCl$_2$	(g L^{-1})	0.056
MgSO$_4$	(g L^{-1})	0.073
pH	(units)	6.8
Conductivity	(μS cm^{-1})	1470

Table 9) Composition and properties of the phosphate buffer for the reactive delivery

KH$_2$PO$_4$	(g L^{-1})	0.254
K$_2$HPO$_4$	(g L^{-1})	0.980
TDS	(g L^{-1})	1.234
pH	(units)	7.5
Conductivity	(μS cm^{-1})	1420

Experimental procedure

The 1D set-up was filled with a wet-packing procedure; prior to its use the sand was washed to remove colloids and other impurities and then rinsed with deionized water. Before packing the column, the appropriate volume of sand was washed with the at least 5 pore volumes of the background solution which will saturate the system. The clay layer was prepared from the clay powder, which was mixed with the contaminant solution to a 96%$_{V/W}$ using a spatula to obtain a homogeneous paste without lumps and introduced in the porous medium section using a large bore syringe. In the non-reactive experiment, the clay paste was prepared with the background solution instead. Table 10 reports the main parameters value for the different experiments.

Prior the reactive experiments, a batch degradation of Methylene Blue by the selected oxidant and reductant was performed in solution, collecting the UV-Vis

spectra of the reactants and byproducts of the reaction, to verify the effectiveness of the decolorization. The concentration employed were significantly different with respect to those for the delivery experiments due to elevated absorption and saturation of the detector.

The experiment procedure was the following: after the column was packed and the recirculation system at regime the background potential was recorded, in this time 1 mL of oxidant or reductant was injected in the column about 25 mm downstream the cathodic bulkhead. The power supply was then activated, providing the 3 V cm^{-1} potential gradient, and initiating the electrokinetic phenomena in the system. Photos were collected every 5 minutes using a Nikon D500 camera equipped with a Nikkor 17-55mm DX lens; to ensure consistent exposure, the camera was set manually, and the columns were placed in a photographic lightbox with controlled illumination. Input current and potential in the porous medium (EL1 and EL2) were measured using a digital multimeter equipped with a multichannel acquisition system (multiplexer) collecting data every 5 minutes.

Using the collected images it is possible to extract the plume velocity for the different experiments using ImageJ software [169]. The enhanced color images were obtained subtracting to the desired frame the photo of the column prior the reactant injection; the image in Figure 51 was obtained subtracting both the initial and final stage of the column for the first delivery cycle; in such way both permanganate and modification in the contaminated clay layer are greatly enhanced.

Table 10) Summary of experimental conditions (main parameters) for the non-reactive tests

		Electrolyte conductivity		$\nabla\Phi$	Clay pore solution	
		Background	Buffer	Input	Composition	Conductivity
Non-reactive	$\sigma_B < \sigma_S$	1470 μS cm^{-1}	570 μS cm^{-1}	310 V m^{-1}	Background	1420 μS cm
	$\sigma_B = \sigma_S$	1470 μS cm^{-1}	1420 μS cm^{-1}	310 V m^{-1}	Background	1420 μS cm
	$\sigma_B > \sigma_S$	1470 μS cm^{-1}	3650 μS cm^{-1}	310 V m^{-1}	Background	1420 μS cm
Reactive	$\sigma_B = \sigma_S$	1470 μS cm^{-1}	1420 μS cm^{-1}	310 V m^{-1}	Methylene Blue	1450 μS cm

$\nabla\Phi$ – Input: potential applied across the working electrodes.

Clay pore solution: solution used to prepare the 96%V/W paste to pack the column; conductivity refers to the free solution

4.2.2 Experimental results

Non-reactive delivery in the clay layer

The first tests focused on the simple delivery of permanganate in a non-contaminated clay inclusion to verify: i) the efficacy of the buffer recirculation in preventing permanganate stalling during transport [66], ii) determining the effective and homogenous delivery in the clay layer, and iii) optimizing the delivery procedure. In all three experimental conditions – with a buffer conductivity Lower ($\sigma_B < \sigma_S$), Equal ($\sigma_B = \sigma_S$) and Higher ($\sigma_B > \sigma_S$) than the one of the background solutions and the permanganate – an effective delivery can be observed. In Figure 38 a section of the column across the longitudinal axe is presented. The permanganate plume is homogeneously distributed in the core of the clay layer, thus preferential transport at the interface of the clay with the column walls can be excluded, and the ability of electromigration to access low permeability media is confirmed. Limited pH variations were detected in the electrode chambers; thus, the buffer recirculation is effective in preventing pH fronts to migrate in the set-up and cause permanganate stalling slowing of preventing its delivery in the porous medium.

Longitudinal cross section
exposing clay core
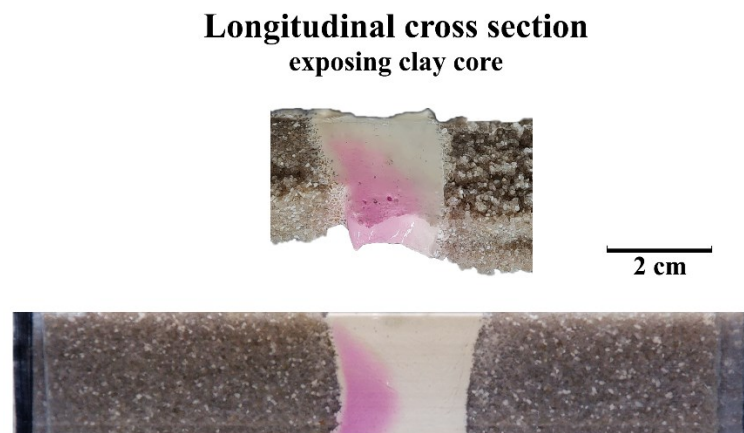
Figure 38) Longitudinal section of the porous medium exposing the clay core. After desaturation, the entire porous medium extracted flipping the column over (hence the top layer results flat, and the bottom layer irregular).

It was also observed that the conductivity of the buffer solution, contributing to the system total resistivity, significantly modifies the circulating current and consequently the potential in the porous medium. Referred to a buffer conductivity equal to the background, higher currents and potentials were observed in the case of a more conductive buffer, while lower currents and potentials for a less conductive buffer; results are summarized in Figure 39 and Table 11.

Table 11) Current, potential gradients, measured velocities, and travelled distance for the delivery experiments.

TEST	Current (A)	Gradient EL1 (V/m)	Gradient EL2 (V/m)	Initial velocity(m/s)	Distance traveled. (cm/6 hours)
$\sigma_B < \sigma_S$	4.3E-3	210	210	7.3E-6	6
$\sigma_B = \sigma_S$	6.3E-3	345	278	9.9E-6	3.1
$\sigma_B > \sigma_S$	6.9E-3	420	342	1.1e-5	8.2

A significant decrease in initial velocity (abt. 30%) is observed for a buffer less conductive than the background solution, while a slight increase is observed for a more conductive buffer (abt. 6%); it is also interesting to notice that the velocity general trend remains unaffected.

From the time lapses presented in Figure 41-Figure 43 it is possible to observe that the different velocities do not affect the ability to deliver the amendment in the clay layer. However, it is important to consider the time required to achieve the same penetration of permanganate; in the present set of experiments over a total time of 6 hours only the Equal ($\sigma_B = \sigma_S$) and High ($\sigma_B > \sigma_S$) case allowed the permanganate to reach the sand layer downstream the low permeability inclusion. An additional consideration can be made on the power consumption required for the delivery; in the present experiments higher currents were obtained by a modification of the system resistivity: it follows, the potential gradients in the porous medium are increased with a lower power consumption that would derive by increasing the input voltage.
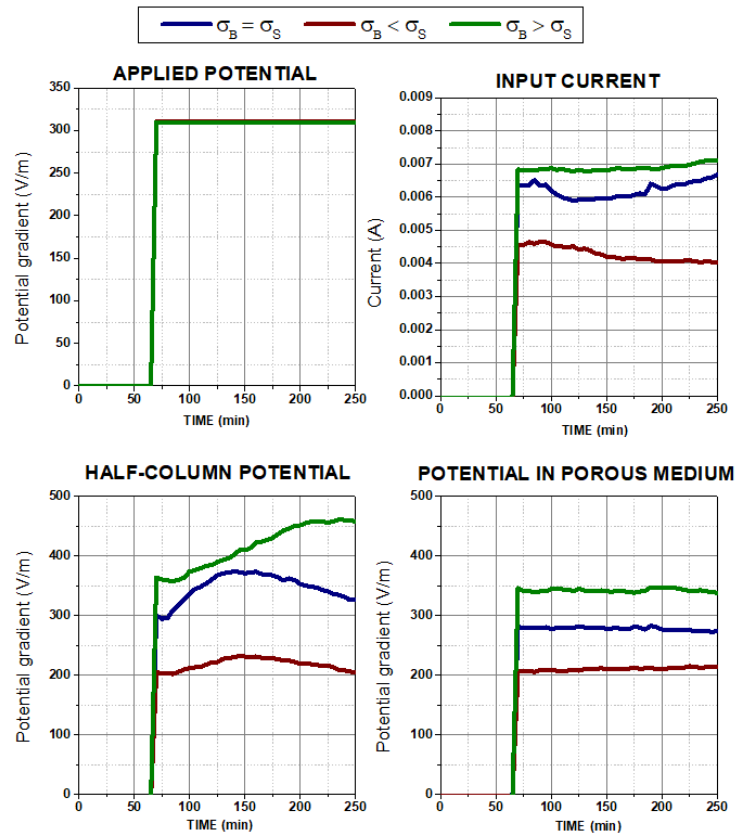
Figure 39) From top left clockwise: input potential gradient, input current, potential gradient in the porous medium for the different buffer concentrations. Half-column potential was measured between ground electrode (cathodic side) and the probe electrode in the clay inclusion; potential in porous medium was measured across the entire packed column.
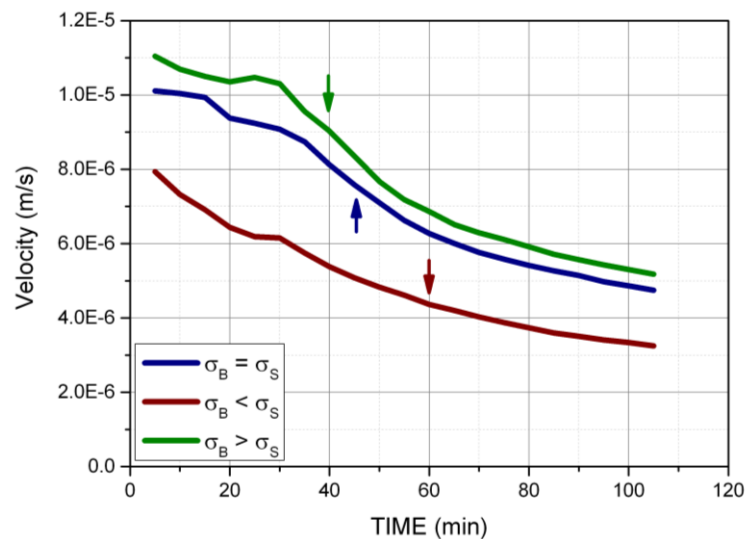
Figure 40) Migration velocity for the different buffer concentrations; the arrows indicate the time at which the plume reaches the clay layer.
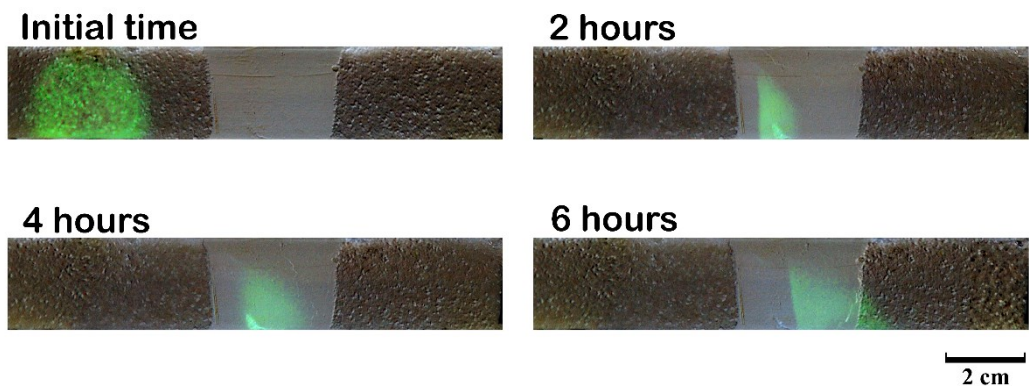
Figure 41) Plume evolution in the delivery of permanganate (enhanced colors) for equal conductivity - $\sigma_B = \sigma_S$
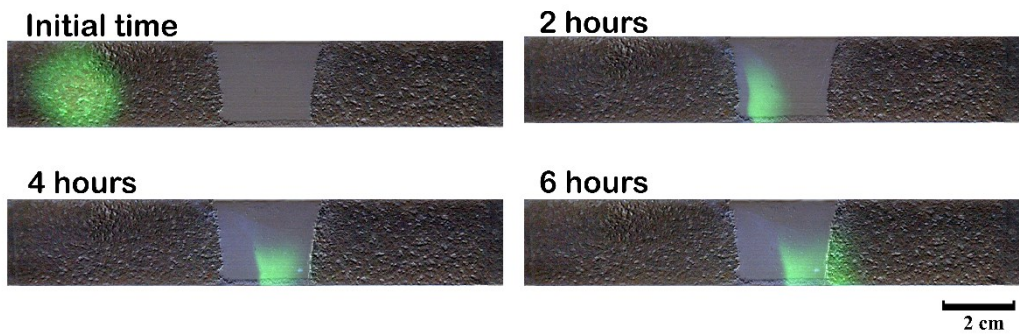
Figure 42) Plume evolution in the delivery of permanganate (enhanced colors) for higher buffer conductivity - $\sigma_B > \sigma_S$
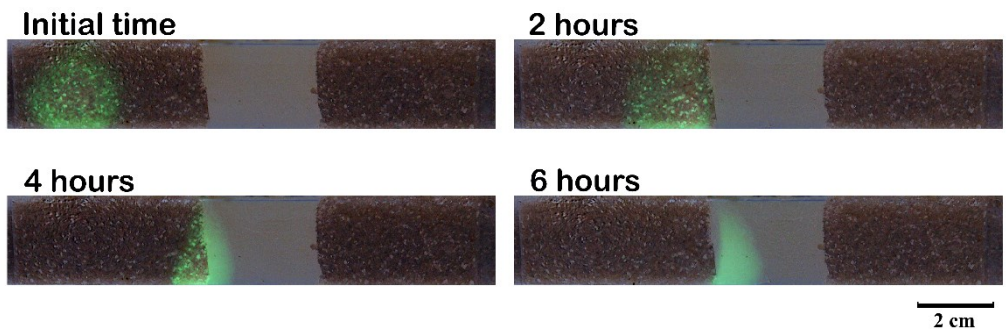
Figure 43) Plume evolution in the delivery of permanganate (enhanced colors) for lower buffer conductivity - $\sigma_B < \sigma_S$

Decolorization of methylene blue

The batch decolorization experiments (Figure 44) show that both oxidation and reduction are effective in transforming MB; it is also possible to notice that while the reductant does not lead to byproduct with a significant visible color, permanganate produces a strong background due to the formation of colloidal MnO_2. The test supports the ability of both reactants to transform completely MB and produce a change in color, thus providing visual evidence for the process.
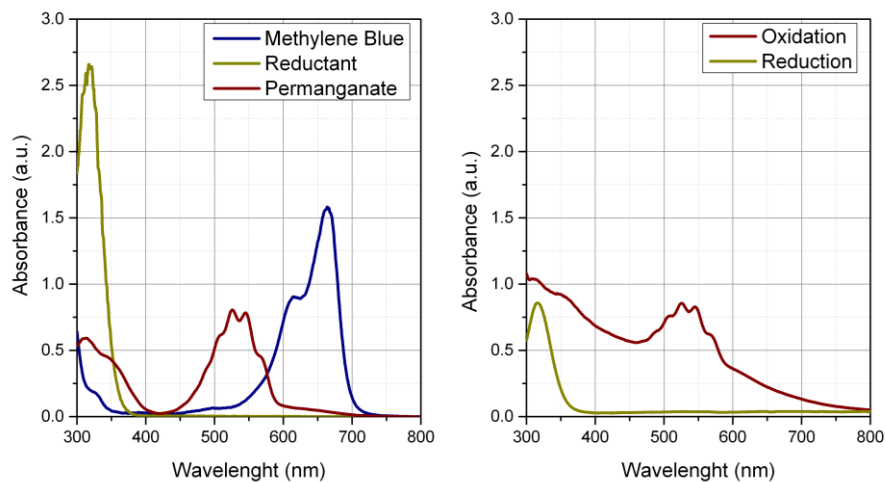
Figure 44) Left: UV-Visible spectra of the reactants (Methylene Blue dye, oxidant, and reductant); right: their mixture after a batch decolorization.

The results of the reactive experiments are presented using a collection of the pictures taken during the tests, reported in Figure 46 and Figure 50. At first glance, both the oxidant (permanganate) and the sulfur-based reductant are effective in promoting a decolorization of the methylene blue, which does not show mobilization from the clay layer in the 30-70 minutes required for the amendment to reach and penetrate the inclusion. However, when the two process are analyzed in detail, significant differences are detected between the two applications.

During the oxidative decolorization the permanganate migration in both the sand and the clay layers can be followed visually; a progressive compression of the plume is observed while approaching the inclusion with a resulting increase in concentration. When the permanganate has reached the clay layer, a sudden modification in the color is observed, the blue dye is consumed by the permanganate, which is reduced to the brown colloidal MnO_2. The first injection affects a clay area equal abt. 24% of the inclusion (1.3 cm^2), the plume shape presents a sloping profile, but it is homogenous on the entire inclusion height, no voids or blue spots are observed. When a second injection is performed, the

migration in the sand layer occurs normally but no effective delivery is observed in the clay. On the other hand, a bypass of the previously remediated layer is observed: in Figure 45 from 210 minutes it is possible to notice a slight purple color in the middle of the clay section but no evident change in the blue color.

The reductive decolorization application does not allow to follow the amendments migration, due to its lack of color; however, it is possible to observe the progressive decolorization of the clay layer. Compared to the oxidant, the first delivery of amendment affects and area equal to 16% of the inclusion with a slightly different profile shape but still homogeneous distribution along the vertical direction. Contrarily to the previous test, a second injection does result in an effective delivery of the remediated area in the clay, which reaches the 26% of the entire longitudinal area. The main experimental results are summarized in Table 12, they will be discussed in detail in the following sections.

Table 12) Main experimental results for the oxidative and reductive decolorization of methylene blue

DELIVERED AMENDMENT	VELOCITY IN SAND (m/s)		VELOCITY IN CLAY (m/s)		CLAY AREA AFFECTED		
	First Injection	*Second injection*	*First injection*	*Second injection*	*First injection*	*Second injection*	*Total*
Oxidant	9.93e-6	8.88e-6	4.05e-6	n.q.	24%	0%	24%
Reductant	n.q.	n.q.	1.02e-6	8.33e-7	16%	10%	26%

n.q.: not quantifiable due to lack of color or low color intensity

Initial time — **30 minutes** — **50 minutes** — **70 minutes** — **90 minutes** — **110 minutes** — **130 minutes** — **150 minutes** — **New permanganate injection** — **170 minutes** — **190 minutes** — **210 minutes** — **230 minutes** — **250 minutes** — 2 cm
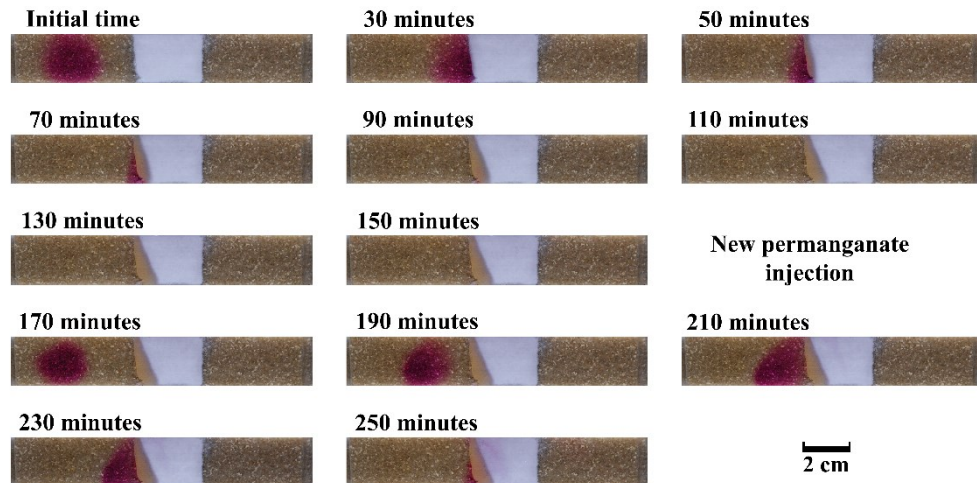
Figure 45) Oxidative decolorization of the contaminated low-permeability layer by permanganate

Initial time   70 minutes

130 minutes   190 minutes

240 minutes   300 minutes

2 cm
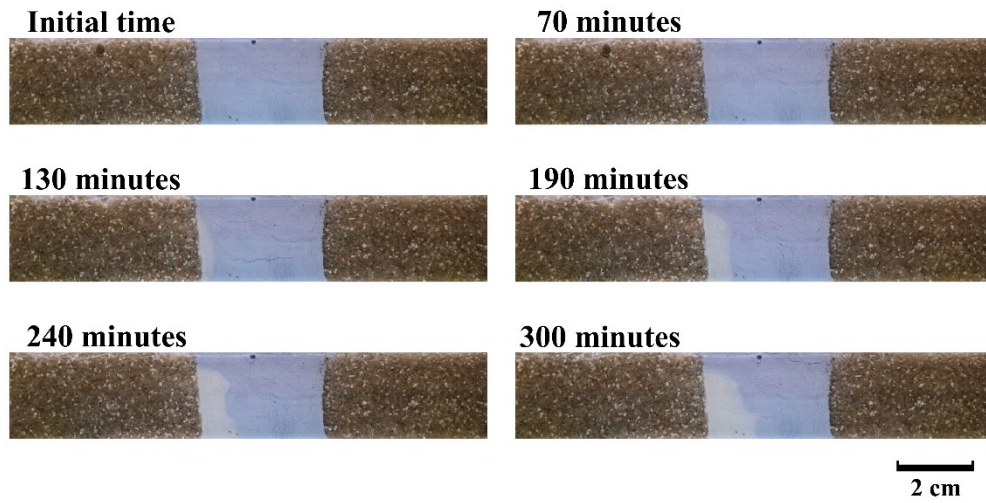
Figure 46) Reductive decolorization of the contaminated low-permeability layer using a sulphur-based reductant.

For the permanganate delivery, the plume front displacement was used to measure the migration velocity; it is possible to notice an initial constant value of abt. 0.063 cm min^{-1} which decreases closing to the low permeability inclusion likely due to the opposing electroosmotic flow. The medium modification resulting from the first remediation stage also reflects on the migration velocity: the second permanganate plume migrate at a lower velocity which does not decrease approaching the clay inclusion and does not penetrate the clay layer with a homogeneous front.
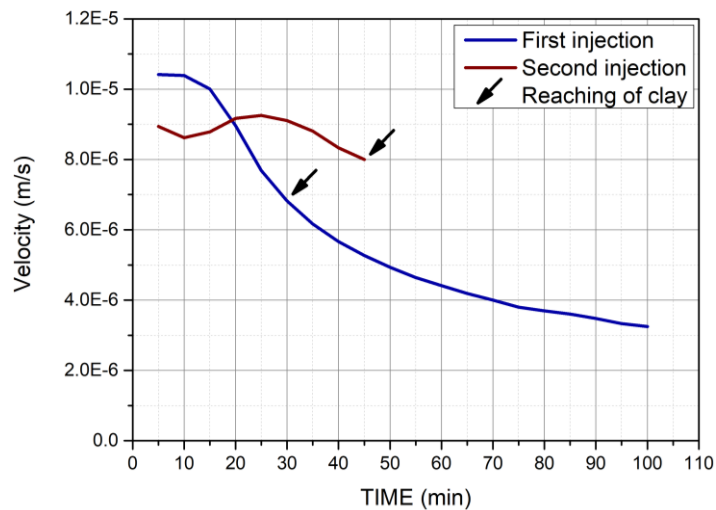
Figure 47) Migration velocity of the permanganate plume in the two stages of the oxidative remediation

94

Given the colorless nature of the reducing agent selected for the reductant delivery, the migration velocity in the sand layer cannot be determined by the photos collected. For transport in the clay layer, the expansion of the decolorized area can be used to quantify the migration velocity of the amendment. The average front velocity in the clay results equal to 0.00596 cm min^{-1} for the first injection and equal to 0.00612 cm min^{-1} for the second; the measured velocities are reported in Figure 48. Compared to the application of the oxidant, a reduced variation over time of the plume velocity is observed, the effect of the second injection of reductant can be observed starting from 200 min, which is the time required to migrate in the sand layer and the already decolorized clay. Using this point as starting reference for the second injection, which is, showing the expansion of the affected area in the clay, it is possible to observe the same trend of the first delivery only slowed down by the modification of the porous medium.
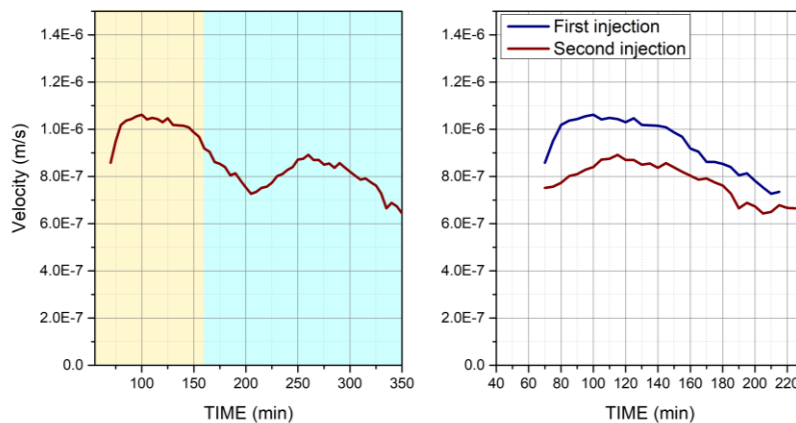
Figure 48) Velocity of the decolorization front in the clay layer (left) and comparison of the two injections delivery rates (right)

The current circulating in the circuit is reported in Figure 49 for both the experiments. It is possible to observe that the initial current value is similar for the two systems, as expected given the equal electrical conductivity of all the solutions, and the two systems present similar trends in the circulating current. The measure of the potential within the porous medium for the ISCO experiment showed a value across the entire porous medium equal to abt. 3.5 V cm^{-1}, while the potential in the first section (EL1) equals abt. 2.8 V cm^{-1}; both values show a limited variation over the entire experiment (standard error ± 2 mV). The potential in the reductant delivery experiment shows significant variations over time that prevents their use

for further comparison since the reducing agent could be interacting with the electrode material introducing a bias in the measure.
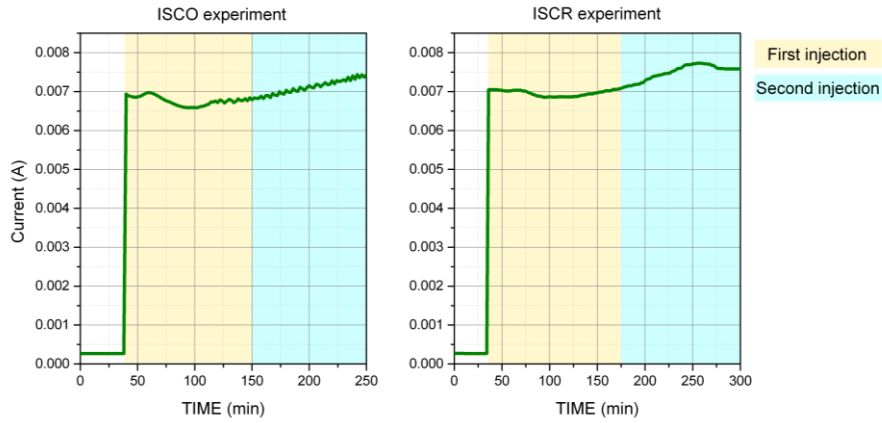
Figure 49) Current circulating in the system to grant the 3 V cm⁻¹ potential gradient.

To investigate further the permanganate stalling, from the results displayed in Figure 50 the bypass of the second permanganate injection becomes evident though no reaction is noticed (a green halo can be clearly seen downstream the clay layer). Applying the processing to the 80min frame in Figure 45, we obtain an image showing both the MnO_2 residues (blue) and the advancing permanganate plume (green) within the contaminated clay layer (yellow). Such evidence confirms that the decontamination reaction occurs as soon as permanganate enters the clay layer and the remaining plume crosses an area already containing MnO_2 nanoparticles, which however appears not to oppose the migration of the plume tail still in the upstream sand. Such evidence is suggesting that the modification responsible for the failure of the second delivery evolves over time and is likely caused by the formation of a colloidal solution in a medium highly responsive to surface modifications which reflect on the electroosmosis rates opposing the electromigration responsible for permanganate delivery.
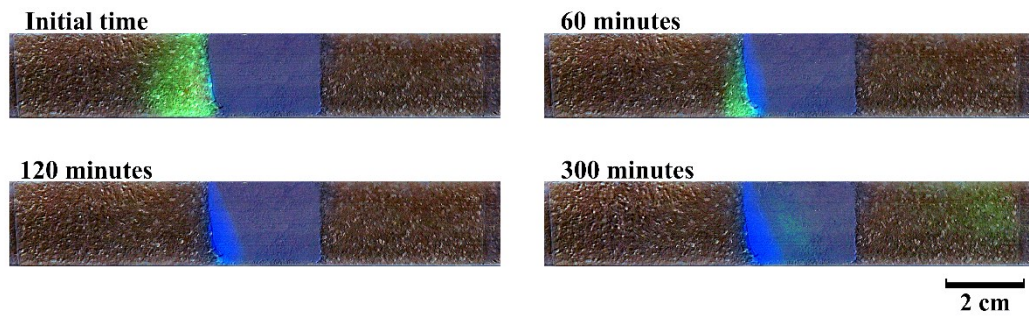
Figure 50) Enhanced color images showing the system evolution during the ISCO decolorization of the methylene blue dye in the clay layer.
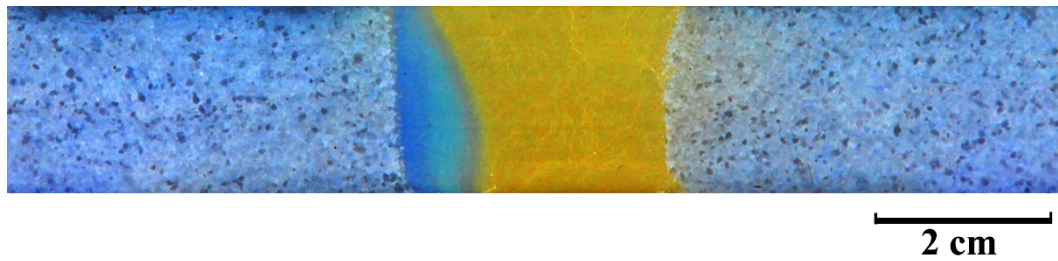
Figure 51) Enhanced color image showing the advancing MnO_4 plume in the clay layer and the methylene blue degradation.

4.3 Amendment delivery in low permeability regions in 2D geometry

4.3.1 Introduction

The previous experiments, in accordance with the available literature [11, 45, 67, 153], demonstrated the ability of electrokinetic transport to deliver amendments in low permeability layers surrounded by a sandy porous medium. It is widely known that amendments delivery in low permeability porous media still presents a technological challenge in groundwater remediation [7, 11, 16, 24] as hydraulic flow tends to bypass such areas, which are accessible almost exclusively via fracturing or chemical diffusion [177]. Both approaches present significant drawbacks: the former causes a non-homogenous distribution of the amendments while the latter requires extensive time and residence time of the amendments. However, while in 1D geometry the flow path for the permanganate plume during EK delivery is confined by the system boundaries, in 2D geometry transversal flow path are also present that can significantly affect the amount of reactant effectively delivered in the low permeability layer. The available literature exploring 2D geometry structured the experiments with an injection extending on the entire set-up cross section [45, 63, 152] thus eliminating the possibility to observe transversal transport mechanism. In homogenous porous media the eventual conductivity modification of the conductivity caused by the pore structure, due to tortuosity or charge interactions [53, 133, 134], affects the whole system equally. In the case of a low-permeability inclusion, especially for clayey soils, the dependency of the surface charge from pH and Ionic Strength significantly increases the complexity of the system, especially since other factors besides tortuosity and physico-chemical properties of the soil solution, for example Zeta Potential, Electric Double Layer thickness and solution salinity contribute to conductivity in porous media [74, 75, 100, 130, 131]. As the clay layer is non-mobile, except for an eventual colloidal mobilization, it results in a permanent conductivity discontinuity in the system causing a focusing or defocusing of the electric streamlines if its conductivity does not match the one of the sandy backgrounds. Also, an electroosmotic flow component of greater magnitude that the one in the sandy medium is added in the system, which interacts with the amendment plume and contributes to the total mass flux.
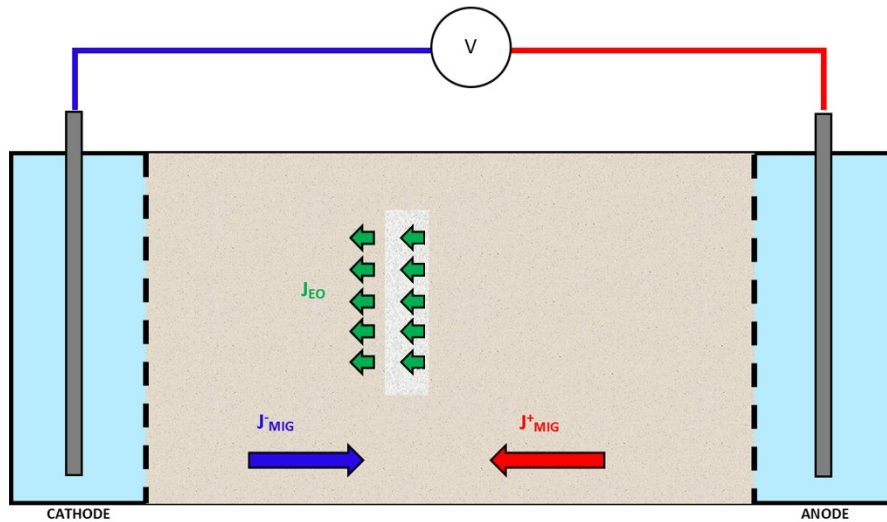
Figure 52) Electromigration flow components of electromigration and electroosmosis for solutes in a heterogeneous system with a clay inclusion (grey) in a sandy medium (beige)

It follows that the same electric filed streamlines focusing and defocusing apply to both the injected reactant and the low permeability inclusion; hence the choice of electrokinetic strategy is pivotal in determining the delivery efficacy and efficiency, thus reaching the remediation goals. The present study applies the same experimental approach presented in Chapter 3 to achieve the electrokinetic delivery of a spot injection of permanganate in a clay layer contained in a sandy porous medium. To this end, the knowledge gathered by the previous experiments was applied in defining the best system conditions, proving the importance of the results obtained so far; to benchmark the potential of EK the advective delivery is also explored and presented as a comparison.

4.3.2 Materials and methods

Experimental apparatus

The experiments were carried out in a 2D tank set-up with internal dimension equal to 600x210x11 mm, comprised of a plastic frame that supports two side panels; the frame is equipped with 16 injection ports on the sides which allow the connection to a multichannel peristaltic pump to create either the desired hydraulic flow for the advective case or for the buffer recirculation in EK experiments. The entire set-up was packed with the porous medium in the hydraulic delivery test,

while for the electrokinetic experiments, the set-up was divided in two electrode chambers and a central section (dimensions 500x210x11 mm), which is filled with the porous medium, similarly to the experiments discussed in Chapter 3. A removable top frame was created with specific slots for a consistent placing of the meshed bulkheads delimiting the electrode chambers, of injection well and electrodes (Figure 53 and Figure 54).
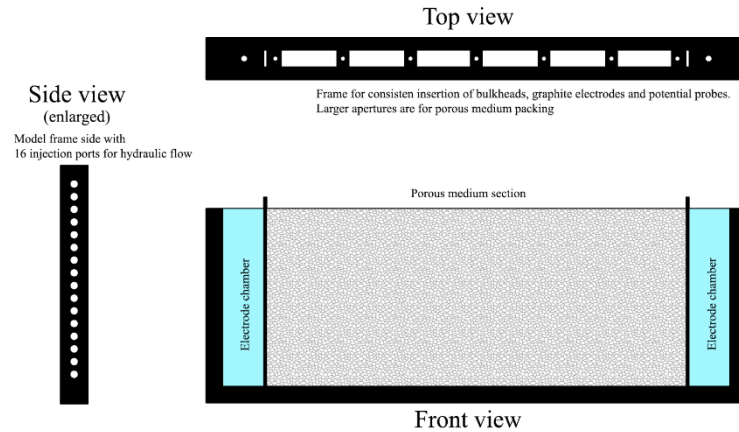
Figure 53) Additional details on the 2D set-up structure, displaying the injection ports on the sides and the top frame used for a consistent placing of the bulkheads and electrodes. See Figure 55 for comprehensive schematics.

The working electrodes (namely, the electrodes used to apply the DC current) are graphite rods sized ø=6 mm and L=300 mm. They were placed at a distance of 550 mm, submerged in the electrode chambers, which do not contain the porous medium but only the recirculating solution. Monitoring electrodes (wire electrodes, exposed tip 2mm, depth 120 mm) were placed abt.10 mm from the bulkheads to monitor the potential gradient in the porous medium (electrode distance 480mm), a second pair of electrodes was placed to measure the gradient across the clay inclusion (electrode distance 90 mm).
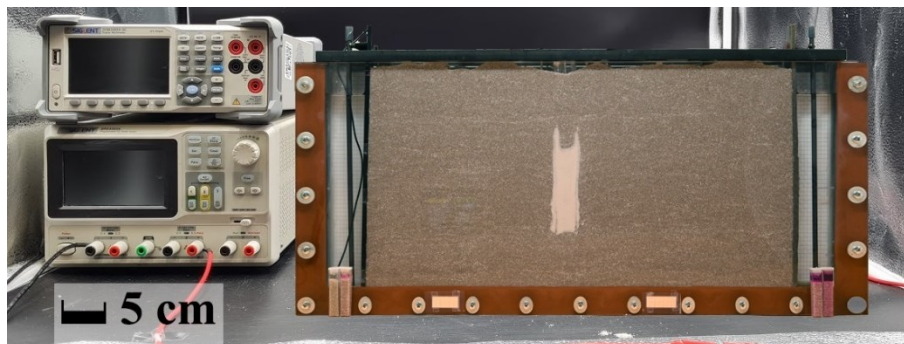
Figure 54) Photo of the experimental set-up for 2D tests, the recirculation system is behind the tank
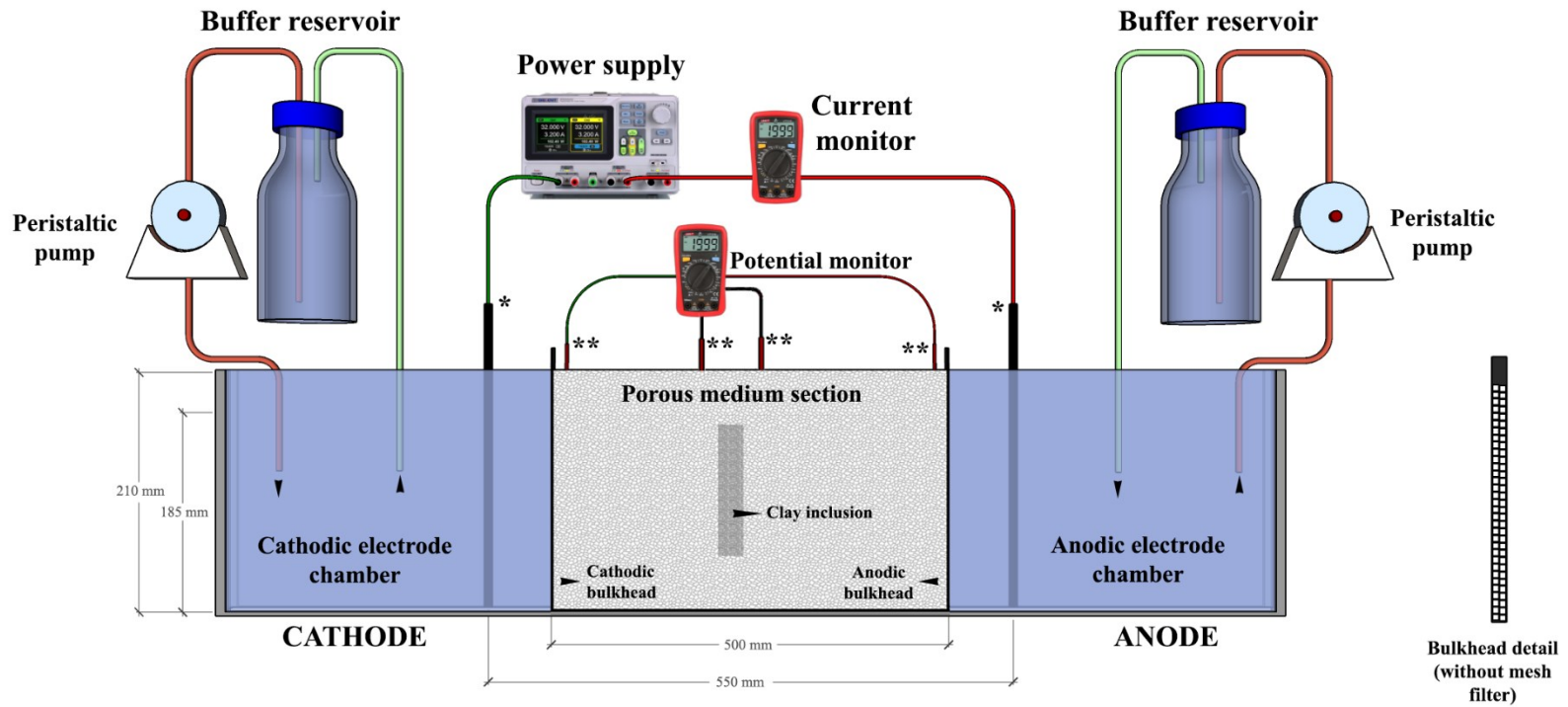
Figure 55) Schematics (not in scale to improve readability) of the 2D set-up used for the EK assisted delivery tests.

* Working electrodes - DC input
** Probing electrode - potential monitoring

Porous medium and solutions

The same sand (Dorsilit quartz sand) and clay (kaolin) used for the 1D experiments were employed (see Table 7 for their properties) and the same preparative and packing procedure applied. The background solution for the advection test was a carbonate/bicarbonate buffer, to provide a background density and prevent gravity sinking of permanganate; the buffer concentration was set to obtain a pH of 9 and a TDS concentration equal to 0.76 g L^{-1}. The electrokinetic delivery was performed saturating the porous medium with a synthetic water [187] to simulate a real groundwater composition, the concentration was increased with respect to common groundwater salinity to allow a higher permanganate concentration and a better quality of the photos used to follow the plume evolution; the synthetic water solution (SWS) composition is presented in Table 13. The specific background solution was also used to prepare the clay paste as previously described. The permanganate solution was prepared at a 0.948 g L^{-1}, corresponding to 6 mM, a 10 mL volume was injected using a syringe with a modified needle to reach the desired set-up depth, centered at the half-height of the clay layer. For the EK delivery, such concentration presents a conductivity equal to a third of the background solution, resulting in an 'EK high' scenario. Lastly, to neutralize electrolysis effects in the EK delivery, a carbonate buffer (pH 9) was recirculated in the electrode chambers, the same solution conductivity of the soil solution was adopted (Table 14).

Table 13) Composition and properties of the synthetic water solution

KH_2PO_4	(g L^{-1})	0.122
$NaHCO_3$	(g L^{-1})	0.084
$NaCl$	(g L^{-1})	1.075
NH_4Cl	(g L^{-1})	0.100
$CaCl_2$	(g L^{-1})	0.111
$MgSO_4$	(g L^{-1})	0.301
TDS	(g L^{-1})	1.640
pH	(units)	6.8
Conductivity	(μS cm^{-1})	2950
Ionic strength	(mM)	28.9

NaHCO$_3$	(g L^{-1})	2.462
Na$_2$CO$_3$	(g L^{-1})	0.170
TDS	(g L^{-1})	2.632
pH	(units)	8.9
Conductivity	(μS cm^{-1})	2900

Experimental procedure

A wet packing method was adopted to fill the set-up with the porous medium; previous to its use the sand was washed thoroughly to remove most of the colloids; the day before the experiments the sand was rinsed with distilled water and 2 pore volumes of the soil solution, while the day of the experiment the sand was further rinsed with 5 pore volumes of freshly prepared soil solution. The clay paste was again prepared to reach a 96%$_{V/W}$ water content ratio, mixing with a spatula until all lumps were eliminated; the paste was then transferred in the set-up at a 230 mm distance from the cathodic bulkhead with a size equal to 81x12.5 mm (HxL). A 25mm unsaturated top layer was created in all experiments after the packing procedure to avoid preferential flow or daylighting, the top of the clay layer does not fall in the desaturated porous medium.

For the advection-dispersion experiments the hydraulic flow was generated by a peristaltic pump connected to the lateral ports of the set-up; since the set-up is not confined the outlet flow was also created by a peristaltic pump in aspiration mode. The flow rate was regulated to obtain a seepage velocity of 1.25E-5 m s^{-1} (4.5 cm h^{-1}). The electrokinetic delivery was performed using an input potential of 64 Volts was applied in *constant voltage* mode with a DC Power supply, providing a potential gradient of abt. 1.15 V cm^{-1}. A second benchmark EK delivery was performed using a set-up fully saturated with the same carbonate buffer used in the advective delivery, in this case the 6 mM permanganate injection presents the same electrical conductivity of the background solution ("equal" scenario). In addition, in this experiments background solution and recirculating buffer have the same composition, thus reducing the system complexity and multicomponent effects.

All the experiments were monitored collecting images with a Nikon D500 camera equipped with a Nikkor 17-55mm DX lens; to ensure consistent exposure the camera was set to manual settings to provide a 0 EV exposure, in order to apply

the permanganate calibration previously obtained. No electric potential or current was monitored in this experiment. The potential gradient in the porous medium and the input current were measured using a multimeter equipped with a multiplexer card to allow a multichannel detection; data were collected every 5 minutes and a single scan of all channels takes 3 seconds.

4.3.3 Experimental results

From the collected images it was possible to follow the plume evolution for the advective and electrokinetic delivery:
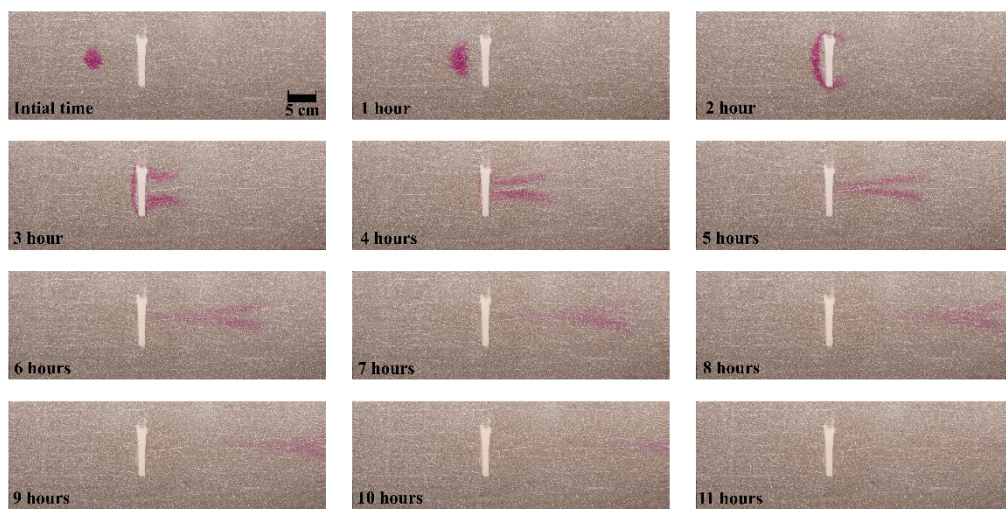
Figure 56) Plume evolution during advective delivery of permanganate
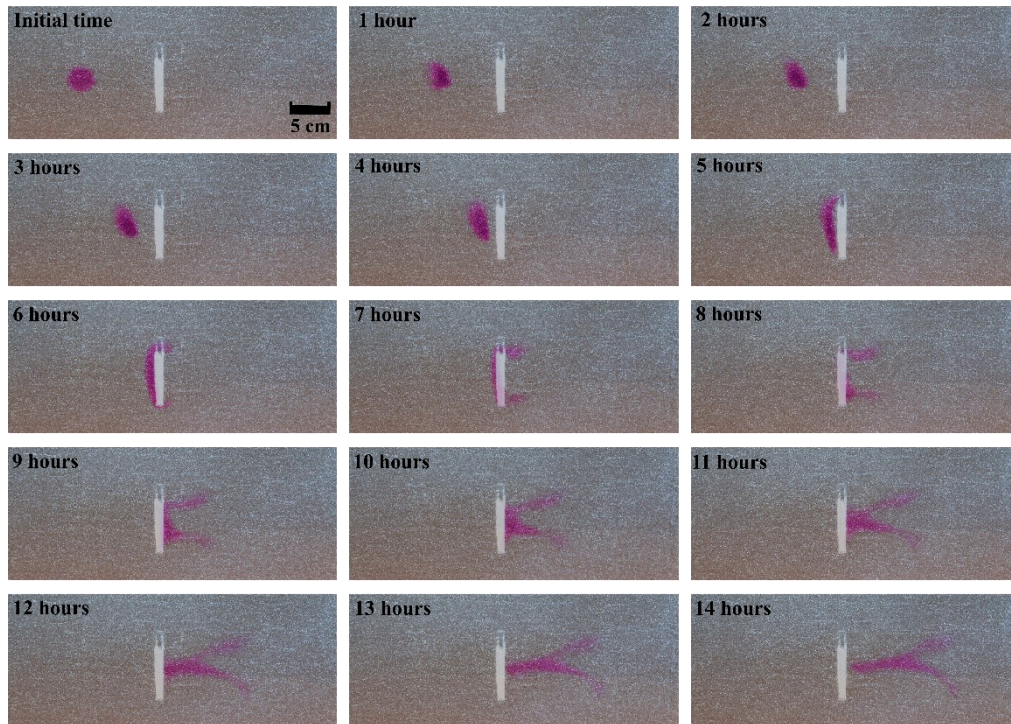
Figure 57) Plume evolution during electrokinetic delivery of permanganate in the "EK high" scenario

From the results presented in Figure 56 and Figure 57 major differences in the advective and electrokinetic delivery are evident. In the advective delivery, while approaching the clay layer the permanganate plume is subject to expansion and arching that lead to a bypass of the layer in its upper and lower boundary with the sandy medium. This effect not only results in a failed delivery in the low permeability layer, but also in the formation of a dead zone in the downstream sandy medium as appears from the 3- and 4-hours quadrants in Figure 57. On the other hand, despite the lower migration velocity in the EK delivery (due to the limited output of the power supply used) it is possible to notice that thanks to the plume contraction determined by the "EK high" scenario (which means, a focusing of the electric streamlines in the permanganate resulting from its conductivity lower than the background) a limited bypass around the clay layer and a noticeable pink color in the clay layer (Figure 57, 7-9 hour quadrants) are observed. As a consequence of the effective delivery of permanganate in the clay layer, the dead zone formed downstream the inclusion is greatly reduced compared to the advective experiment.

105

The different delivery efficiency can be better visualized using the enhanced color images reported in Figure 59 and Figure 72. Especially using the detail of the clay section presented in Figure 60 it is possible to notice a significant difference in the delivery mechanism. For the advective transport the blue color at the sand-clay boundary is constituted of MnO_2 particles resulting from permanganate reduction and is representative of the permanganate penetration, most likely attributable to diffusion as reported by previous studies [45, 152]. The evidence presented shows that despite the reduced thickness of the clay layer its bulk is inaccessible to the advective delivery of permanganate. As expected, the experiment clearly shows the limitation of advective transport for delivery of solutes in low permeability porous media and the resulting detrimental effect on the remediation of such areas. In the EK delivery application, permanganate is delivered in the entire clay layer, including its bulk. Consequently, the downstream sand medium directly in contact with the clay layer is also crossed by the majority of the injected permanganate. However, as the migration advances the plume assumes a 'V' shape that proceeds to the set-up outlet boundary. The direct consequence on a remediation application is to be evaluated considering the local permanganate concentration in the two forward branches and plume tail. More specifically, the 'V' shape can result in a positive effect, increasing the plume cross section and thus the interception of the downstream contaminant; on the other hand, if the shape modification leads to an excessive dilution index the reaction rates may decrease to a level that prevents the reaching of the remediation goals.
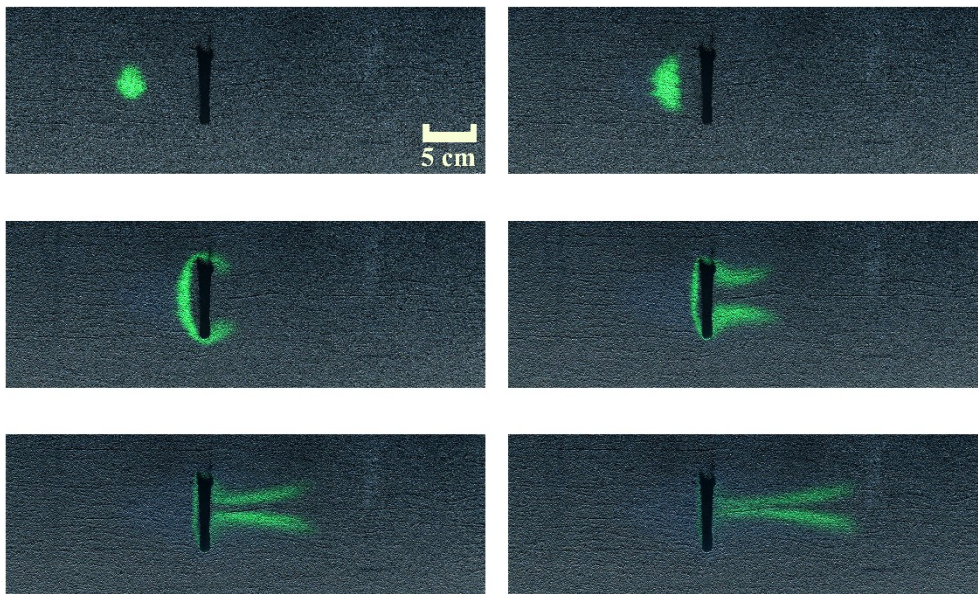
Figure 58) Enhanced color image for the advective delivery of permanganate, starting from 1 hour and progressing with 1 hour time step.
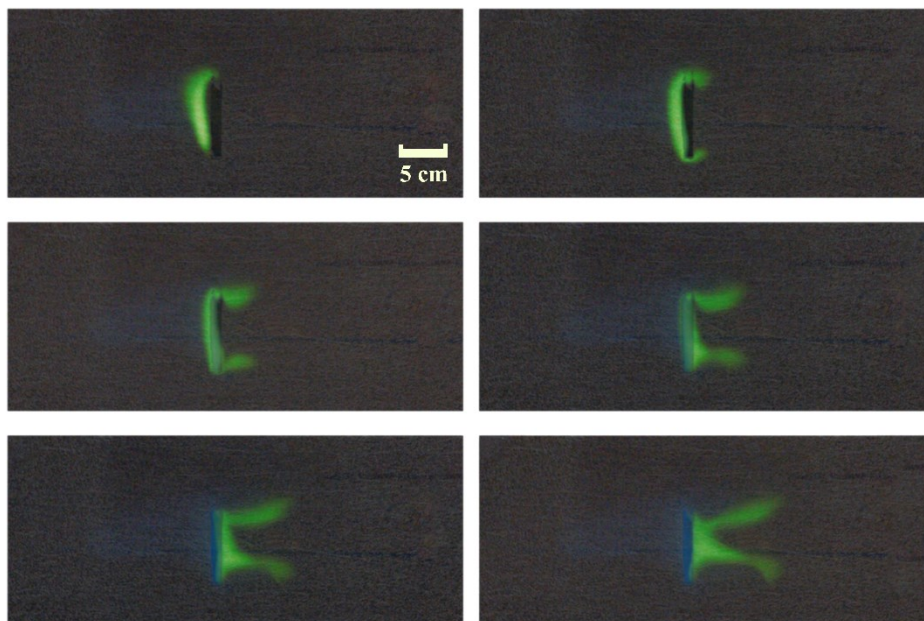
Figure 59) Enhanced color image of the EK delivery of permanganate, starting from 4 hours and progressing with 1 hour time step.

Advection-dispersion　　　**Electromigration**

5 cm
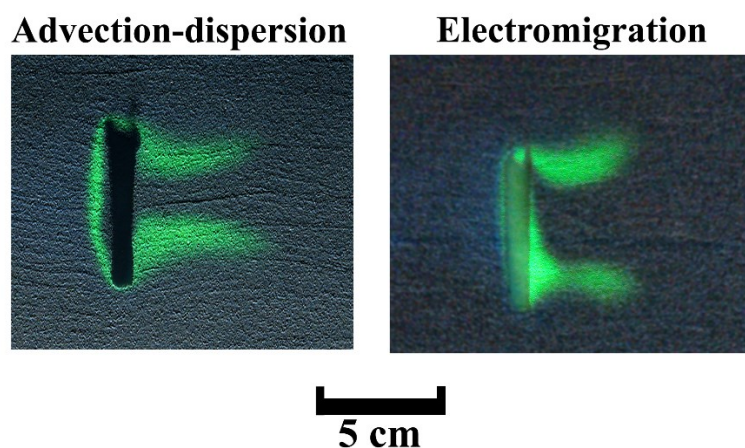
Figure 60) Detail of the clay inclusion for advective transport

The experiment performed using a carbonate solution and the injection of permanganate with an equal electrical conductivity also show important differences in the delivery efficiency. Using the enhanced color images in Figure 61 it is possible to notice a significant plume expansion when approaching the clay layer and a more significant bypass than the IPER scenario previously explored. Therefore, although the EK delivery still proved effective in delivering the

permanganate inside the low permeability inclusion, a strong influence of the amendment conductivity is observed.
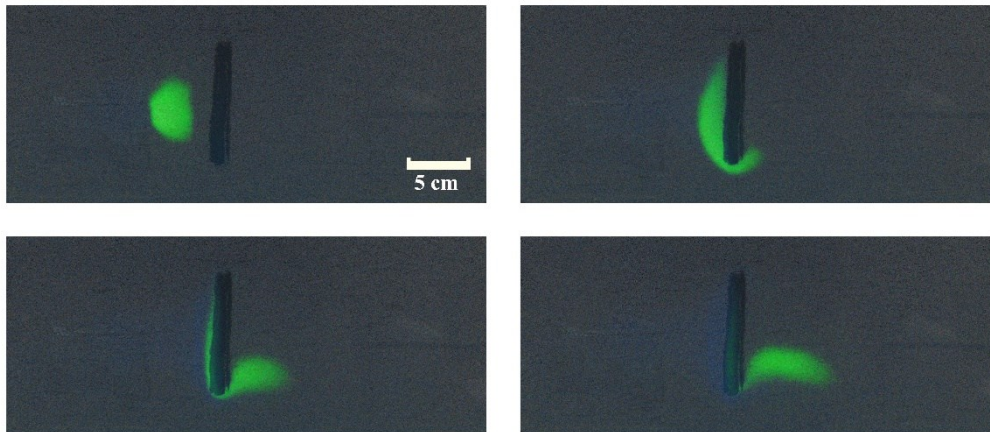
Figure 61) Enhanced colors images of the permanganate plume during EK transport in 'equal' conditions, time frame 4 hours, 8 hours, 11 hours, 14 hours

4.4 Discussion

The experiments performed in this study support the use of electrokinetics as a valid approach to deliver reactants for *in-situ* decontamination in low-permeability porous media, concurring with previous studies available in the scientific literature.

The delivery of permanganate in 1D geometry proved the ability of buffer recirculation in the electrode chambers to be effective in preventing the permanganate stalling caused by pH variations deriving from electrolysis. It follows that the electric field can be applied for extended time to achieve the desired delivery without significant impacts on the porous medium, and this includes pollutant mobilization following pH variations (especially for heavy metals). It was also possible to evidence that in the small-scale 1D system used, the electrical conductivity of the buffer with respect to the background solution has an impact on the migration velocities, which affect the time of contact with the porous medium and the length traveled over the same time. The possibility of tuning the migration velocity approaching and crossing the clay layer is extremely relevant: a complete crossing of the clay layer is optimal for contaminations extending in the downstream sandy medium, while a slower transport in the clay layer can increase the contact time with the pollutant in the low permeability medium increasing the

decontamination efficiency. The buffer conductivity also impacts the ohmic drop at the interface between the electrode well and the porous medium. It was observed that conductivity higher than the background solution (or, lower resistivity) results in higher currents and potential gradients in the porous medium with the same input voltage. It follows, the higher velocities observed are achieved with a lower power consumption than with an increased input potential gradient, and thus costs and environmental impact of the application are reduced.

The reactive experiments performed allowed to explore the delivery of oxidants and reductants in low permeability layers, focusing on their ability to promote reactions capable of removing an immobilized set-up contaminant. The adopted experimental condition was optimized by the previous step, and the study is the first to allow a direct visualization of the occurring reaction in the clay layer. In both cases, no mobilization of the methylene blue is observed in the first 30-70 minutes of experiment, therefore the decolorization can be entirely attributed to the reactions promoted by the injected amendments. Both permanganate and sulphur based reducing agent were effective in promoting the decolorization of methylene blue; in both oxidation and reduction, as a combined effect of reaction pathways and the delivered amendment about 25% of the contaminated clay was effectively decolorized. Notwithstanding the fact that such results were achieved with the delivery of one injection of permanganate and two injections of the reducing agent, one of the main evidence was the inability to deliver the second permanganate injection in the clay layer. Given the extent of the reaction, such effect can be explained with a modification of the porous medium caused by the deposited MnO_2 produced by the decontamination reaction; this modification also appears to evolve over time, since the entirety of the first injection is delivered in the clay layer. In the present scenario, the reductive decolorization appears to be the more versatile and appropriate for the treatment of the low-permeability layer, as it allows for sequential injections in case the remediations objectives are not met after the first delivery.

The delivery experiments in two-dimensional geometry confirmed the inability of the hydraulic flow to access the bulk of low-permeability inclusions, and only a partial delivery in the layer boundaries is achieved by diffusion. It was also possible to confirm the potential of electrokinetics to decouple the amendment delivery from the hydraulic permeability of the porous medium, accessing the low-permeability layer in its entirety more easily. It was also possible to demonstrate that a careful design of the EK delivery is required to obtain an effective and efficient delivery,

specifically as the plume dynamics resulting from conductivity gradients discussed in Chapter 3 play a fundamental role in the process. Regarding the delivery by hydraulic flow, being provided by gravity feed or pressure injection (including direct push) not only is an ineffective mean to deliver solutes in a low-permeability plug, but also results in a preferential pathway in the downstream sandy porous medium which can result in the formation of dead zones where the permanganate concentration is significantly lower than from the injection. In the framework of back diffusion, and the configuration of low permeability regions as secondary contamination sources, this implies that: i) the source itself is excluded from the remediation, ii) part of the permeable porous medium downstream these regions is subject to a significantly lower decontamination. These effects bear important consequences on the site management, requiring a careful planning of the remediation operation to ensure that the cleanup standards are met and maintained in time. The EK delivery, on the other hand, shows a delivery inside the clay medium in both 'high' and 'equal' scenario given the different transport mechanism, but the efficiency is subject to major variations determined by the different plume dynamics. Specifically, it was possible to identify the plume expansion caused by the presence of the clay layer as responsible for the bypass. The plume contraction introduced by the "high" scenario proved able to contrast such effects representing the optimal delivery strategy for the geometry under study. This introduces a limiting factor in the maximum concentration that can be delivered, defined by the soil solution concentration and composition; specifically, the general amendment concentration must result in an electrical conductivity lower than the background. Using literature data, a wide range of groundwater electrical conductivity is found, depending on the specific site conditions (lithology, geology, precipitation regime, etc.) spanning from 200 μS cm^{-1} to 5000 μS cm^{-1} [188-192] which indicates the necessity of a site characterization for the optimization of the delivery protocol. In cases with limited EC, and thus strong limitation on the maximum mass flux of the amendment, a soil flushing with a saline solution may be employed to provide a transient increase in conductivity. Injection of saline tracers is commonly applied in Electrical Resistance Tomography (ERT) [193] with very high concentrations and volumes; in the case of contaminated aquifers a careful evaluation is required to prevent the pollutant mobilization. Despite this complication, the mechanism elucidated by the experiments in 2D geometry shows the potential for EK-assisted delivery to limit the back diffusion of contaminants from low-permeability regions by allowing the amendment: i) to enter the clay section, ii) to cross the clay section and distributing in the downstream porous medium, tackling the back-diffusing contaminant.

In conclusion, thanks to the collected data, we were able to demonstrate the potential of electrokinetic as delivery strategy aimed to the remediation of low permeability layers or heterogenous aquifers. Thanks to the tests in 1D geometry and knowledge on plume dynamics gathered and discussed in Chapter 3, the conditions for an effective delivery in a low-permeability layer in 2D geometry were identified. The results also pointed out that further research is required to improve the delivery and possibly provide numerical tools to support the delivery design. Specifically, the effect of buffer concentration on the amendment migration velocity should be explored in 2D geometry on a larger scale than the 1D experiments, to assess whether the effect is maintained in a real case scenario. Also, delivery tests in 2D geometry with different low-permeability materials (bentonite, silts, etc.) and in a reactive scenario on different set-up pollutants dispersed and/or immobilized in the clay layer are required to provide evidence closer to a full-scale application.

Chapter 5

Final remarks

The electrokinetic delivery of soluble amendments represents a promising technology to overcome the limitation of hydraulic delivery of soluble amendments for groundwater remediation in both homogenous and heterogenous porous media. The electromigration mechanism results in a more efficient use of the reactants and is independent from the medium hydraulic conductivity, hence allowing the delivery in low-permeability media (clay, silts, etc.) otherwise excluded from the hydraulic flow. This points to the potential ability of EK-assisted delivery in treating the contaminant back diffusion and low-permeability regions acting as secondary sources. However, electrokinetic transport is a complex process that encompasses interrelated transport mechanism – electromigration, electroosmosis, and electrodispersion – acting simultaneously on the solutes and depending on many variables. The optimization of a delivery application requires an in-depth understanding of the different transport components and can benefit from numerical tools to predict and simulate the fate of the injected amendments in different conditions. This PhD project aims at adding to the current knowledge on EK delivery developing a series of experiments in 2D and 1D geometry exploring the aspects least studied by the available literature, to provide a support to the design process of the injection and delivery procedures.

In the first part of the study, the longitudinal and transversal distribution of an oxidant commonly used in ISCO remediation (permanganate) was explored in 2D geometry, in a configuration comparable to the horizontal section of an injection well in a full-scale site. Based on the collected results, important effects on the

transport and distribution of the amendments introduced by electrodispersion, determined by electrical conductivity gradients between the injected amendment and the background solution, were detected:

- the background solution introduces a limitation to the mass transfer of the injected amendment;
- conductivity gradients result in significant differences in the migration velocity, delivery area, and local concentration of the injected amendment;
- as a consequence of the previous points, reaction rates are strongly affected by conductivity gradients, as greater area of influence are associated to slower reaction rates and vice versa.

The observation on the different longitudinal and transversal distribution presents important implication for the design of the injection system, as the amendment can be delivered on a greater area with a reduced number of injection wells than for hydraulic delivery. At the same time, effects on the reaction kinetics and reactant consumption were evidenced by the second set of experiments, conducted in a reactive regime. It was possible to observe that in addition to the previous effect:

- the electrokinetic delivery results in a better mixing of the amendment with the contaminated groundwater than hydraulic delivery, hence providing higher reaction rates and removal efficiency;
- the plume dynamics created by conductivity gradients determines the local reactant concentration and consequently the reaction rate and reactant consumption. For example, when the plume expansion is achieved, a lower amendment consumption may lead to undesired interactions with superficial water bodies or safeguard areas.

It follows a careful case-specific evaluation is required, and in the present study this was allowed by the NP-PhreeqC-EK mathematical model, that was validated on the experimental data in both the conservative and reactive regime. The coupling with the Phreeqc-RM code also allows to include geochemical effects, thus allowing to tailor such conditions to the specific site under remediation, hence providing a valuable tool to support the delivery design and improve both efficiency and efficacy of the remediation.

The second part of the study was focused on the delivery of amendments in low-permeability inclusions, which is one of the most interesting and promising aspects of electrokinetics. One-dimensional experiments were performed to optimize the delivery procedures; it was possible to prove that buffer recirculation

effectively eliminates the stalling of the delivered amendment caused by pH variation promoted by electrolysis. Also, the effect of the electrical conductivity of the buffer used to stabilize the pH conditions in the electrode chamber was explored, evidencing relevant effects on the electrokinetic processes and delivery efficiency. In the small scale 1D system it was also possible to observe the ability of buffer conductivity to tune the migration velocity by modifying the current density without varying the input potential, which results in a lower power consumption. The experimental conditions adopted for the reactive tests allowed to visualize the degradation reaction promoted by the delivered amendments within the clay layer. Both the ISCO and reductants proved effective, but it was possible to collect significant data relative to the use of permanganate. Specifically, in the conditions explored it appears that consecutive injections of permanganate do not lead to an increase in the decontaminated volume of the clay, rather after the first injection permanganate is only partially delivered to the clay layer and does not show any visible reactivity. Lastly, the knowledge gathered from the previous experimentation was applied to a delivery of permanganate in a low-permeability layer in a 2D geometry. It was clearly demonstrated that the bulk of the clay layer is inaccessible to advective delivery due to its low hydraulic conductivity, while electromigration is successful in delivering the amendment. The study was able to prove that an effective delivery can be achieved only considering the plume dynamics evidenced in Chapter 3, supporting the importance of electrodispersion and multicomponent phenomena. In the specific case, the plume shrinking allowed to overcome the expansion caused by the clay layer and responsible for a significant bypass and a reduced delivery of permanganate. The gathered results represent a step forward in the understanding of EK delivery in heterogeneous porous medium and evidencing some of the possible limitations in their use for ISCO and ISCR. Further experimentation is required to extend the reactive delivery to 2D systems, as well improving the optimization of the delivery conditions (buffer concentration, saline solution flushing, multi-step injection of amendments).

We believe that results of the study represent an important step forward in the understanding of electrokinetic transport applied to the delivery of amendments for groundwater remediation.

References

[1] M.R.J. Wyllie, P.F. Southwick, An Experimental Investigation of the S.P. and Resistivity Phenomena in Dirty Sands, SPE-302-G 6(02) (1954) 44-57.

[2] W.M. Alley, Ground Water, in: G.E. Likens (Ed.), Encyclopedia of Inland Waters, Academic Press, Oxford, 2009, pp. 684-690.

[3] J. Margat, J. van der Gun, Groundwater around the World: A Geographic Synopsis, 2013.

[4] S. Zhang, G. Mao, J. Crittenden, X. Liu, H. Du, Groundwater remediation from the past to the future: A bibliometric analysis, Water Research 119 (2017) 114-125.

[5] R. Sethi, A. Di Molfetta, Groundwater engineering : a technical approach to hydrogeology, contaminant transport and groundwater remediation, Springer, Cham, 2019.

[6] N.C. Mueller, J. Braun, J. Bruns, M. Černík, P. Rissing, D. Rickerby, B. Nowack, Application of nanoscale zero valent iron (NZVI) for groundwater remediation in Europe, Environmental Science and Pollution Research 19(2) (2012) 550-558.

[7] K.R. Reddy, Technical Challenges to In-situ Remediation of Polluted Sites, Geotechnical and Geological Engineering 28(3) (2010) 211-221.

[8] F.I. Khan, T. Husain, R. Hejazi, An overview and analysis of site remediation technologies, Journal of Environmental Management 71(2) (2004) 95-122.

[9] H. Gomes, C. Dias-Ferreira, A. Ribeiro, Overview of in Situ and ex Situ Remediation Technologies for PCB-contaminated Soils and Sediments and Obstacles for Full-scale Application, The Science of the total environment 445-446C (2013) 237-260.

[10] R. Baciocchi, L. D'Aprile, I. Innocenti, F. Massetti, I. Verginelli, Development of technical guidelines for the application of in-situ chemical oxidation to groundwater remediation, Journal of Cleaner Production 77 (2014) 47-55.

[11] A.I.A. Chowdhury, Hydraulic and Electrokinetic Delivery of Remediants for In-situ Remediation, Civil and Environmental Engineering, The University of Western Ontario, Electronic Thesis and Dissertation Repository, 2016.

[12] W. Dott, D. Feidieker, M. Steiof, P.M. Becker, P. Kämpfer, Comparison of ex situ and in situ techniques for bioremediation of hydrocarbon-polluted soils, International Biodeterioration & Biodegradation 35(1) (1995) 301-316.

[13] K.A. Muller, C.D. Johnson, C.E. Bagwell, V.L. Freedman, Review of Amendment Delivery and Distribution Methods, and Relevance to Potential In Situ Source Area Treatment at the Hanford Site, United States, 2019.

[14] S. Kuppusamy, T. Palanisami, M. Megharaj, K. Venkateswarlu, R. Naidu, Ex-Situ Remediation Technologies for Environmental Pollutants: A Critical Perspective, in: P. de Voogt (Ed.), Reviews of Environmental Contamination and Toxicology Volume 236, Springer International Publishing, Cham, 2016, pp. 117-192.

[15] P.G. Tratnyek, R.L. Johnson, Nanotechnologies for environmental cleanup, Nano Today 1(2) (2006) 44-48.

[16] S. Rosansky, W. Condit, R. Sirabian, Best Practices for Injection and Distribution of Amendments, NavFac Technical Report (2013).

[17] T.I.T.R.C.S.C.O. Team, Technical and Regulatory Guidance for In Situ Chemical Oxidation ofContaminated Soil and Groundwater - Second edition, (2005).

[18] J. Bear, Dynamics of Fluids in Porous Media, Dover1988.

[19] B.M. Das, Advanced soil mechanics, 2019.

[20] R.L. Siegrist, M. Crimi, T.J. Simpkin, R.C. Borden, In situ chemical oxidation for groundwater remediation, (2011).

[21] K.D. Greer, J.W. Molson, J.F. Barker, N.R. Thomson, C.R. Donaldson, High-pressure injection of dissolved oxygen for hydrocarbon remediation in a fractured dolostone aquifer, Journal of Contaminant Hydrology 118(1) (2010) 13-26.

[22] K. Mundle, D.A. Reynolds, M.R. West, B.H. Kueper, Concentration rebound following in situ chemical oxidation in fractured clay, Ground Water 45(6) (2007) 692-702.

[23] B.H. Kueper, H.F. Stroo, C.M. Vogel, C.H. Ward, M.D. Annable, Chlorinated solvent source zone remediation, 2014.

[24] T.J. Pac, J. Baldock, B. Brodie, J. Byrd, B. Gil, K.A. Morris, D. Nelson, J. Parikh, P. Santos, M. Singer, A. Thomas, In situ chemical oxidation: Lessons learned at multiple sites, Remediation Journal 29(2) (2019) 75-91.

[25] C.J.C. Biscombe, The Discovery of Electrokinetic Phenomena: Setting the Record Straight, Angewandte Chemie International Edition 56(29) (2017) 8338-8340.

[26] S. Wall, The history of electrokinetic phenomena, Current Opinion in Colloid & Interface Science 15(3) (2010) 119-124.

[27] N. Mosavat, E. Oh, G. Chai, A Review of Electrokinetic Treatment Technique for Improving the Engineering Characteristics of Low Permeable Problematic Soils, International Journal of GEOMATE 2 (2012) 266-272.

[28] Z. Jian, T. Yanli, L. Cunyi, G. Xiaonan, Experimental Study of Electro-Kinetic Dewatering of Silt Based on the Electro-Osmotic Coefficient, Environmental Engineering Science 36(6) (2019) 739-748.

[29] A. Persat, M. Suss, J. Santiago, Basic principles of electrolyte chemistry for microfluidic electrokinetics. Part II: Coupling between ion mobility, electrolysis, and acid-base equilibria, Lab on a chip 9 (2009) 2454-69.

[30] R. Peng, Electrokinetic Transport Phenomena in Nanochannels and Applications of Nanochannel-based Devices in Nanoparticle Detection and Molecule Sensing, UWSpace, 2018.

[31] A.N. Alshawabkeh, Y.B. Acar, Removal of contaminants from soils by electrokinetics: A theoretical treatise, Journal of Environmental Science and Health . Part A: Environmental Science and Engineering and Toxicology 27(7) (1992) 1835-1861.

[32] Y.B. Acar, R.J. Gale, A.N. Alshawabkeh, R.E. Marks, S. Puppala, M. Bricka, R. Parker, Electrokinetic remediation: Basics and technology status, Journal of Hazardous Materials 40(2) (1995) 117-137.

[33] M. Malekzadeh, J. Lovisa, N. Sivakugan, An Overview of Electrokinetic Consolidation of Soils, Geotechnical and Geological Engineering 34 (2016).

[34] J. Feijoo, L.M. Ottosen, X.R. Nóvoa, T. Rivas, I. de Rosario, An improved electrokinetic method to consolidate porous materials, Materials and Structures 50(3) (2017) 186.

[35] G.R. Kozan, W.B. Fenwick, Summary Reviews of Soil Stabilization Processes. Report 7. Electrical Stabilization of Fine-Grained Soils, ARMY ENGINEER WATERWAYS EXPERIMENT STATION (1961).

[36] T. Paillat, E. Moreau, P.O. Grimaud, G. Touchard, Electrokinetic phenomena in porous media applied to soil decontamination, Dielectrics and Electrical Insulation, IEEE Transactions on 7 (2000) 693-704.

[37] Y.B. Acar, A.N. Alshawabkeh, Principles of electrokinetic remediation, Environmental Science & Technology 27(13) (1993) 2638-2647.

[38] A. Ribeiro, C. Vilarinho, J. Araújo, J. Carvalho, Electrokinetic Remediation of Contaminated Soils With Chromium, ASME 2018 International Mechanical Engineering Congress and Exposition, 2018.

[39] L.M. Ottosen, T.H. Larsen, P.E. Jensen, G.M. Kirkelund, H. Kerrn-Jespersen, N. Tuxen, B.H. Hyldegaard, Electrokinetics applied in remediation of subsurface soil contaminated with chlorinated ethenes – A review, Chemosphere 235 (2019) 113-125.

[40] S.O. Kim, J.J. Kim, K.W. Kim, S.T. Yun, Models and Experiments on Electrokinetic Removal of Pb(II) from Kaolinite Clay, Separation Science and Technology 39(8) (2005) 1927-1951.

[41] S.M. Ponder, J.G. Darab, T.E. Mallouk, Remediation of Cr(VI) and Pb(II) Aqueous Solutions Using Supported, Nanoscale Zero-valent Iron, Environmental Science & Technology 34(12) (2000) 2564-2569.

[42] N. Alshawabkeh Akram, T. Yeung Albert, R. Bricka Mark, Practical Aspects of In-Situ Electrokinetic Extraction, Journal of Environmental Engineering 125(1) (1999) 27-35.

[43] G. Fan, L. Cang, H.I. Gomes, D. Zhou, Electrokinetic delivery of persulfate to remediate PCBs polluted soils: Effect of different activation methods, Chemosphere 144 (2016) 138-147.

[44] J. Nosek, M. Cernik, Influence of the electric field on migration of the iron nanoparticles, NanoCon2011, Brno, Czech Republic, 2011, p. 5.

[45] A.I.A. Chowdhury, J.I. Gerhard, D. Reynolds, B.E. Sleep, D.M. O'Carroll, Electrokinetic-enhanced permanganate delivery and remediation of contaminated low permeability porous media, Water Research 113 (2017) 215-222.

[46] B. Buszewski, E. Dziubakiewicz, Electromigration Techniques, in: B. Buszewski, E. Dziubakiewicz, M. Szumski (Eds.), Electromigration Techniques - Theory and Practice, Springer-Verlag Berlin Heidelberg, Berlin, 2013, p. 357.

[47] V.G. Babskii, M.Y. Zhukov, A.I. Yudovich, Mathematical Theory of Electrophoresis, Springer US1989.

[48] A. Asadi, B. Huat, H. Nahazanan, H. Abdeh Keykha, Theory of Electroosmosis in Soil, International Journal of Electrochemical Science 8 (2013) 1016-1025.

[49] R. Sprocati, J. Flyvbjerg, N. Tuxen, M. Rolle, Process-based modeling of electrokinetic-enhanced bioremediation of chlorinated ethenes, Journal of Hazardous Materials 397 (2020) 122787.

[50] R.T. Gill, M.J. Harbottle, J.W.N. Smith, S.F. Thornton, Electrokinetic-enhanced bioremediation of organic contaminants: A review of processes and environmental applications, Chemosphere 107 (2014) 31-42.

[51] J.H. Park, D. Lamb, P. Paneerselvam, G. Choppala, N. Bolan, J.-W. Chung, Role of organic amendments on enhanced bioremediation of heavy metal(loid) contaminated soils, Journal of Hazardous Materials 185(2) (2011) 549-574.

[52] T.-M. Oh, G.-C. Cho, Correlation between hydraulic conductivity and electrical conductivity for porous media, International Journal of Geo-Engineering 5 (2013) 17-24.

[53] A. Revil, A. Coperey, Z. Shao, N. Florsch, I.L. Fabricius, Y. Deng, J.R. Delsman, P.S. Pauw, M. Karaoulis, P.G.B. de Louw, E.S. van Baaren, W. Dabekaussen, A. Menkovic, J.L. Gunnink, Complex conductivity of soils, Water Resources Research 53(8) (2017) 7121-7147.

[54] A.N. Alshawabkeh, Electrokinetic Soil Remediation: Challenges and Opportunities, Separation Science and Technology 44(10) (2009) 2171-2187.

[55] H.-C. Yeh, M. Wang, C.-C. Chang, R.-J. Yang, Fundamentals and Modeling of Electrokinetic Transport in Nanochannels, Israel Journal of Chemistry 54(11‐12) (2014) 1533-1555.

[56] Electrokinetics Across Disciplines and Continents, Springer International Publishing2016.

[57] R. Kuhn, S. Hofstetter-Kuhn, Capillary electrophoresis : principles and practice, 1 ed., Springer-Verlag Berlin and Heidelberg1993.

[58] T. Isbir, D. Kirac, B. Demircan, B. Dalan, Gel Electrophoresis, in: S. Maloy, K. Hughes (Eds.), Brenner's Encyclopedia of Genetics (Second Edition), Academic Press, San Diego, 2013, pp. 165-167.

[59] J. Lyklema, Electrokinetics after Smoluchowski, Colloids and Surfaces A: Physicochemical and Engineering Aspects 222(1) (2003) 5-14.

[60] M.I. Esrig, S. Majtenyi, A new equation for electroosmotic flow and its implications for porous media, Highway Res. Board 11 (1965) 31-45.

[61] M. Villen-Guzman, B. Arhoun, J.M. Paz-Garcia, C. Vereda-Alonso, C. Gomez-Lahoz, J.M. Rodriguez-Maroto, Electrokinetic Remediation Procedure Applied to Polluted Soils in Southern Spain, Journal of Hazardous, Toxic, and Radioactive Waste 23(4) (2019) 04019017.

[62] A.A. Suied, S.A. Ahmad Tajudin, M.N. Zakaria, A. Madun, Potential Electrokinetic Remediation Technologies of Laboratory Scale into Field Application- Methodology Overview, Journal of Physics: Conference Series 995 (2018) 012083.

[63] M. Masi, A. Ceccarini, R. Iannelli, Multispecies reactive transport modelling of electrokinetic remediation of harbour sediments, Journal of Hazardous Materials 326 (2017) 187-196.

[64] H.I. Gomes, C. Dias-Ferreira, A.B. Ribeiro, S. Pamukcu, Influence of electrolyte and voltage on the direct current enhanced transport of iron nanoparticles in clay, Chemosphere 99 (2014) 171-179.

[65] R. Sprocati, A. Gallo, R. Sethi, M. Rolle, Electrokinetic Delivery of Reactants: Pore Water Chemistry Controls Transport, Mixing, and Degradation, Environmental Science & Technology (2020).

[66] N. Roach, Electrokinetic delivery of permanganate into low-permeability soils, Int. J. Environment and Waste Management Int. J. Environment and Waste Management 1 (2006) 4-19.

[67] D. Hodges, A. Fourie, D. Thomas, D. Reynolds, Overcoming Permanganate Stalling during Electromigration, Journal of Environmental Engineering 139(5) (2013) 677-684.

[68] D. Hodges, A. Fourie, D. Reynolds, D. Thomas, Development of an Apparatus for pH-Isolated Electrokinetic In Situ Chemical Oxidation, Journal of Environmental Engineering 137(9) (2011) 809-816.

[69] S. Dwivedi, Solid oxide fuel cell: Materials for anode, cathode and electrolyte, International Journal of Hydrogen Energy (2020).

[70] K.B. Lipkowitz, R. Larter, T.R. Dundari, D.B. Boyd, Reviews in computational chemistry., 19 (2003).

[71] P. Atkins, T. Overton, Shriver and Atkins' Inorganic Chemistry, OUP Oxford2010.

[72] J. Garche, C.K. Dyer, Encyclopedia of electrochemical power sources, (2009).

[73] J. Doe, R. Miles, R. Roe, C. Santa, Electroosmotic Flow (DC).

[74] A.E. Bussian, Electrical conductance in a porous medium, GEOPHYSICS 48(9) (1983) 1258-1268.

[75] J. Cai, W. Wei, X. Hu, D.A. Wood, Electrical conductivity models in saturated porous media: A review, Earth-Science Reviews 171 (2017) 419-433.
[76] M.C. Sauer, P.F. Southwick, K.S. Spiegler, M.R.J. Wyllie, Electrical Conductance of Porous Plugs - Ion Exchange Resin-Solution Systems, Industrial & Engineering Chemistry 47(10) (1955) 2187-2193.
[77] M.H. Waxman, L.J.M. Smits, Electrical Conductivities in Oil-Bearing Shaly Sands, SPE-1863-A 8(02) (1968) 107-122.
[78] S.F.Y. Li, Capillary Electrophoresis: Principles, Practice and Applications, Elsevier Science1992.
[79] U.S.E.P. Agency, RESOURCE GUIDE FOR ELECTROKINETICS LABORATORY ANDFIELD PROCESSES APPLICABLE TO RADIOACTIVE ANDHAZARDOUS MIXED WASTES IN SOIL AND GROUNDWATER FROM1992 TO 1997, (1997).
[80] N.J. Cherepy, D. Wildenschild, Electrolyte Management for Effective Long-Term Electro-Osmotic Transport in Low-Permeability Soils, Environmental Science & Technology 37(13) (2003) 3024-3030.
[81] C.A.J. Appelo, D. Postma, Geochemistry, groundwater and pollution, CRC Press, Boca Raton, 2013.
[82] H.-J. Butt, K. Graf, M. Kappl, Physics and chemistry of interfaces, WILEY-VCH, Weinheim, 2011.
[83] P. Koorevaar, G. Menelik, C. Dirksen, Elements of Soil Physics, (1987).
[84] J.K. Mitchell, K. Soga, Fundamentals of soil behavior, John Wiley & Sons, Hoboken, NJ, 2013.
[85] J. Alves Júnior, J. Baldo, The Behavior of Zeta Potential of Silica Suspensions, New Journal of Glass and Ceramics 04 (2014) 29-37.
[86] H.B. Oakley, The Origin of the Charge on Colloidal Particles, The Journal of Physical Chemistry 30(7) (1926) 902-916.
[87] N. Abd Rahman, F. Ibrahim, B. Yafouz, Dielectrophoresis for Biomedical Sciences Applications: A Review, Sensors (Basel) 17(3) (2017) 449.
[88] A.E. Scheidegger, The physics of flow through porous media, (2018).
[89] D. Dutta, Electrokinetic Transport of Charged Samples through Rectangular Channels with Small Zeta Potentials, Analytical Chemistry 80(12) (2008) 4723-4730.
[90] C. Felix, A. Yaroshchuk, S. Pasupathi, B.G. Pollet, M.P. Bondarenko, V.I. Kovalchuk, E.K. Zholkovskiy, Electrophoresis and stability of nano-colloids: History, theory and experimental examples, Advances in Colloid and Interface Science 211 (2014) 77-92.
[91] A. Adams, Transport of Nanoscale Zero Valent Iron Using Electrokinetic Phenomena, University of Western Australia, AUS, 2006.
[92] J.H. Masliyah, S. Bhattacharjee, Electrokinetic and colloid transport phenomena, (2011).
[93] L. Zhang, M. Wang, Modeling of electrokinetic reactive transport in micropore using a coupled lattice Boltzmann method, Journal of Geophysical Research: Solid Earth 120(5) (2015) 2877-2890.

[94] C. Shackelford, D. Daniel, Diffusion in Saturated Soil. I: Background, Journal of Geotechnical Engineering 117 (1991).

[95] N. Epstein, On tortuosity and the tortuosity factor in flow and diffusion through porous media, Chemical Engineering Science 44(3) (1989) 777-779.

[96] B. Ghanbarian, A. Hunt, R. Ewing, M. Sahimi, Tortuosity in Porous Media: A Critical Review, Soil Science Society of America Journal 77 (2013) 1461.

[97] F.L. Tye, Tortuosity, Journal of Power Sources 9(2) (1983) 89-100.

[98] M. Matyka, Z. Koza, How to Calculate Tortuosity Easily?, AIP Conference Proceedings 1453 (2012) 17-22.

[99] R. Gillham, M. Robin, D. Dytynyshyn, H. Johnston, Diffusion of nonreactive and reactive solutes through fine-grained barrier materials, Canadian Geotechnical Journal 21 (2011) 541-550.

[100] G.E. Archie, The Electrical Resistivity Log as an Aid in Determining Some Reservoir Characteristics, SPE-942054-G 146(01) (1942) 54-62.

[101] J. Newman, K.E. Thomas-Alyea, Electrochemical Systems, (2012).

[102] D. Jougnot, D. Roubinet, L. Guarracino, A. Maineult, Modeling Streaming Potential in Porous and Fractured Media, Description and Benefits of the Effective Excess Charge Density Approach, 2020, pp. 61-96.

[103] W.-L. Hsu, D.J.E. Harvie, M.R. Davidson, D.E. Dunstan, J. Hwang, H. Daiguji, Viscoelectric Effects in Nanochannel Electrokinetics, The Journal of Physical Chemistry C 121(37) (2017) 20517-20523.

[104] L.M. Vane, G.M. Zang, Effect of aqueous phase properties on clay particle zeta potential and electro-osmotic permeability: Implications for electro-kinetic soil remediation processes, Journal of Hazardous Materials 55(1) (1997) 1-22.

[105] G.S. Parkinson, Iron oxide surfaces, Surface Science Reports 71(1) (2016) 272-365.

[106] M. Jackson, E. Leinov, On the Validity of the "Thin" and "Thick" Double-Layer Assumptions When Calculating Streaming Currents in Porous Media, International Journal of Geophysics 2012 (2012).

[107] J. Lyklema, J.T.G. Overbeek, On the interpretation of electrokinetic potentials, Journal of Colloid Science 16(5) (1961) 501-512.

[108] K. Mahanta, G. Mishra, M. Kansal, Estimation of the electric double layer thickness in the presence of two types of ions in soil water, Applied Clay Science 87 (2013).

[109] J.M. Paz-Garcia, B. Johannesson, L.M. Ottosen, A.B. Ribeiro, J.M. Rodriguez-Maroto, Modeling of Electric Double-Layers Including Chemical Reaction Effects, Electrochimica Acta 150 (2014) 263-268.

[110] S.S. Dukhin, B.V. Deryaguin, Fundamentals of interface and colloid science, in: A.S. Dukhin, P.J. Goetz (Eds.), Studies in Interface Science, Elsevier2002, pp. 17-73.

[111] A.V. Delgado, F. González-Caballero, R.J. Hunter, L.K. Koopal, J. Lyklema, Measurement and interpretation of electrokinetic phenomena, Journal of Colloid and Interface Science 309(2) (2007) 194-224.

[112] F.V. Molina, Soil Colloids: Properties and Ion Binding, CRC Press2016.

[113] P. Erlandsson, Electroosmotic pumps with electrochemically active electrodes, Linköping University Electronic Press2018.

[114] K.W. Oh, 6 - Lab-on-chip (LOC) devices and microfluidics for biomedical applications, in: S. Bhansali, A. Vasudev (Eds.), MEMS for Biomedical Applications, Woodhead Publishing2012, pp. 150-171.

[115] F. Liu, A. Klaassen, C. Zhao, F. Mugele, D. Van den Ende, Electroviscous Dissipation in Aqueous Electrolyte Films with Overlapping Electric Double Layers, The Journal of Physical Chemistry B 122 (2017).

[116] M.J. Mitchell, R. Qiao, N.R. Aluru, Meshless analysis of steady-state electro-osmotic transport, Journal of Microelectromechanical Systems 9(4) (2000) 435-449.

[117] M. Hajnos, J. Cieśla, Electrokinetic (Zeta) Potential of Soils, in: J. Gliński, J. Horabik, J. Lipiec (Eds.), Encyclopedia of Agrophysics, Springer Netherlands, Dordrecht, 2011, pp. 264-267.

[118] D. Hillel, Introduction to environmental soil physics, (2007).

[119] G. Schmid, Zur Elektrochemie feinporiger Kapillarsysteme I. Übersicht, Zeitschrift für Elektrochemie und angewandte physikalische Chemie 54(6) (1950) 424-430.

[120] M.M.I. Abaza, C.G. Clyde, Evaluation of the rate of flow through porous media using electrokinetic phenomena, Water Resources Research 5(2) (1969) 470-483.

[121] A.B. Ribeiro, E.P. Mateus, N. Couto, Electrokinetics Across Disciplines and Continents New Strategies for Sustainable Development, Springer International Publishing2016.

[122] M.A. Karim, Electrokinetics and soil decontamination: concepts and overview (Review), Journal of Electrochemical Science and Engineering - jESE 4 (2014) 293-313.

[123] P.R.C. Gascoyne, J. Vykoukal, Particle separation by dielectrophoresis, ELECTROPHORESIS 23(13) (2002) 1973-1983.

[124] J.F. Lemp Jr., E.D. Asbury, E.O. Ridenour, Electrophoresis of colloidal biological particles, Biotechnology and Bioengineering 13(1) (1971) 17-47.

[125] M. Rolle, R. Sprocati, M. Masi, B. Jin, M. Muniruzzaman, Nernst-Planck-based Description of Transport, Coulombic Interactions, and Geochemical Reactions in Porous Media: Modeling Approach and Benchmark Experiments, Water Resources Research 54(4) (2018) 3176-3195.

[126] R. Sprocati, M. Masi, M. Muniruzzaman, M. Rolle, Modeling electrokinetic transport and biogeochemical reactions in porous media: A multidimensional Nernst–Planck–Poisson approach with PHREEQC coupling, Advances in Water Resources 127 (2019) 134-147.

[127] T. Hanai, Theory of the dielectric dispersion due to the interfacial polarization and its application to emulsions, Kolloid-Zeitschrift 171(1) (1960) 23-31.

[128] M. Masi, G. Losito, Spectral induced polarization for monitoring electrokinetic remediation processes, Journal of Applied Geophysics 123 (2015) 284-294.

[129] A.H. Elsayed-Ali, T. Abdel-Fattah, H.E. Elsayed-Ali, Laboratory Experiment on Electrokinetic Remediation of Soil, Journal of Chemical Education 88(8) (2011) 1126-1129.

[130] S.P. Friedman, Soil properties influencing apparent electrical conductivity: a review, Computers and Electronics in Agriculture 46(1) (2005) 45-70.

[131] D.A.G. Bruggeman, Berechnung verschiedener physikalischer Konstanten von heterogenen Substanzen. I. Dielektrizitätskonstanten und Leitfähigkeiten der Mischkörper aus isotropen Substanzen, Annalen der Physik 416(7) (1935) 636-664.

[132] A. Kriaa, M. Hajji, F. Jamoussi, A.H. Hamzaoui, Electrical conductivity of 1 : 1 and 2 : 1 clay minerals, Surface Engineering and Applied Electrochemistry 50(1) (2014) 84-94.

[133] A. Revil, L. Cathles, S. Losh, J.A. Nunn, Electrical conductivity in shaly sands with geophysical applications, Journal of Geophysical Research 103 (1998) 23925-23936.

[134] A. Revil, P. Glover, Theory of ionic-surface electrical conduction in porous media, Physical Review B 55 (1997) 1757-1773.

[135] Y.B. Acar, R.J. Gale, J. Hamed, G. Putnam, Geotechnical engineering 1990, National Research Council, États-Unis, 1990.

[136] J.M. Paz-Garcia, Physicochemical and numerical modeling of electrokinetics in inhomogenous matrices, Technical University of Denmark, Kgs. Lyngby, 2012.

[137] A.H. Jalil, U. Pyell, Quantification of Zeta-Potential and Electrokinetic Surface Charge Density for Colloidal Silica Nanoparticles Dependent on Type and Concentration of the Counterion: Probing the Outer Helmholtz Plane, The Journal of Physical Chemistry C 122(8) (2018) 4437-4453.

[138] G. Sposito, N.T. Skipper, R. Sutton, S.-h. Park, A.K. Soper, J.A. Greathouse, Surface geochemistry of the clay minerals, Proceedings of the National Academy of Sciences 96(7) (1999) 3358-3364.

[139] E. Dickinson, J.G. Petersen, R. Compton, The electroneutrality approximation in electrochemistry, Journal of Solid State Electrochemistry 15 (2011) 1335-1345.

[140] H.-H. Lee, J.-W. Yang, A new method to control electrolytes pH by circulation system in electrokinetic soil remediation, Journal of Hazardous Materials 77(1) (2000) 227-240.

[141] W.C. Yang, Handbook of Fluidization and Fluid-Particle Systems, Taylor & Francis2003.

[142] S.A. Ahmad Tajudin, I. Jefferson, A. Madun, M.H.Z. Abidin, M.F.T. Baharuddin, M.A. Mohammad Razi, Monitoring of Electric Current during Electrokinetic Stabilisation Test for Soft Clay Using EKG Electrode, Applied Mechanics and Materials 773-774 (2015) 1560-1564.

[143] H. Gomes, Coupling electrokinetics and iron nanoparticles for the remediation of contaminated soils, 2014.

[144] A. Revil, N. Linde, A. Cerepi, D. Jougnot, S. Matthäi, S. Finsterle, Electrokinetic coupling in unsaturated porous media, Journal of Colloid and Interface Science 313(1) (2007) 315-327.

[145] K. Krabbenhøft, J. Krabbenhøft, Application of the Poisson–Nernst–Planck equations to the migration test, Cement and Concrete Research 38(1) (2008) 77-88.

[146] A. Revil, P. Leroy, Constitutive equations for ionic transport in porous shales, Journal of Geophysical Research: Solid Earth 109(B3) (2004).

[147] S. Pennathur, J.G. Santiago, Electrokinetic Transport in Nanochannels. 1. Theory, Analytical Chemistry 77(21) (2005) 6772-6781.

[148] R. Sprocati, M. Rolle, M. Masi, M. Muniruzzaman, NP-Phreeqc-EK: a Multidimensional Multiphysics Simulator for Electrokinetic Transport and Biogeochemical Reactions in Porous Media, CMWR 2020 - Computational Methods in Water Resources XXIII, 2020.

[149] D. Parkhurst, Description of input and examples for PHREEQC Version 3--A computer program for speciation, batch-reaction, one-dimensional transport, and inverse geochemical calculations, 2013.

[150] D.L. Parkhurst, L. Wissmeier, PhreeqcRM: A reaction module for transport simulators based on the geochemical model PHREEQC, Advances in Water Resources 83 (2015) 176-189.

[151] J. Virkutyte, M. Sillanpää, P. Latostenmaa, Electrokinetic soil remediation — critical overview, Science of The Total Environment 289(1) (2002) 97-121.

[152] D.A. Reynolds, E.H. Jones, M. Gillen, I. Yusoff, D.G. Thomas, Electrokinetic migration of permanganate through low-permeability media, Ground Water 46(4) (2008) 629-37.

[153] Y. Yukselen-Aksoy, Electrokinetic Delivery and Activation of Persulfate for Oxidation of PCBs in Clayey Soils, Journal of Geotechnical and Geoenvironmental Engineering 139 (2012) 175-184.

[154] J.S.H. Wong, R.E. Hicks, R.F. Probstein, EDTA-enhanced electroremediation of metal-contaminated soils, Journal of Hazardous Materials 55(1) (1997) 61-79.

[155] H. Gomes, J. Rodríguez-Maroto, A. Ribeiro, S. Pamukcu, C. Dias-Ferreira, Electrokinetics and Zero Valent Iron Nanoparticles: Experimental and Modeling of the Transport in Different Porous Media, 2015, pp. 279-294.

[156] H.I. Gomes, C. Dias-Ferreira, L.M. Ottosen, A.B. Ribeiro, Electroremediation of PCB contaminated soil combined with iron nanoparticles: Effect of the soil type, Chemosphere 131 (2015) 157-163.

[157] H.I. Gomes, J.M. Rodríguez-Maroto, A.B. Ribeiro, S. Pamukcu, C. Dias-Ferreira, Numerical prediction of diffusion and electric field-induced iron nanoparticle transport, Electrochimica Acta 181 (2015) 5-12.

[158] M. Masi, J.M. Paz-Garcia, C. Gomez-Lahoz, M. Villen-Guzman, A. Ceccarini, R. Iannelli, Modeling of electrokinetic remediation combining local

chemical equilibrium and chemical reaction kinetics, Journal of Hazardous Materials 371 (2019) 728-733.

[159] B.H. Hyldegaard, R. Jakobsen, E.B. Weeth, N.D. Overheu, D.B. Gent, L.M. Ottosen, Challenges in electrochemical remediation of chlorinated solvents in natural groundwater aquifer settings, Journal of Hazardous Materials 368 (2019) 680-688.

[160] Y. Ye, G. Chiogna, O. Cirpka, P. Grathwohl, M. Rolle, Experimental investigation of compound-specific dilution of solute plumes in saturated porous media: 2-D vs. 3-D flow-through systems, Journal of Contaminant Hydrology 172 (2015) 33-47.

[161] M. Rolle, T. Le Borgne, Mixing and Reactive Fronts in the Subsurface, Reviews in Mineralogy and Geochemistry 85(1) (2019) 111-142.

[162] M. Muniruzzaman, M. Rolle, Multicomponent ionic transport modeling in physically and electrostatically heterogeneous porous media with PhreeqcRM coupling for geochemical reactions, 2019.

[163] Y.B. Acar, M.F. Rabbi, E.E. Ozsu, Electrokinetic Injection of Ammonium and Sulfate Ions into Sand and Kaolinite Beds, Journal of Geotechnical and Geoenvironmental Engineering 123(3) (1997) 239-249.

[164] A. Abiko, J.C. Roberts, T. Takemasa, S. Masamune, KMnO4 revisited: Oxidation of aldehydes to carboxylic acids in the tert-butyl alcohol - aqueous NaH2PO4 system, Tetrahedron Letters 27(38) (1986) 4537-4540.

[165] J. Clayden, N. Greeves, S. Warren, P. Wothers, Organic chemistry, Oxford University Press, New York, NY, 2001.

[166] E.J. Witzemann, THE ROLE OF ATMOSPHERIC OXYGEN IN THE OXIDATION OF GLUCOSE WITH POTASSIUM PERMANGANATE IN THE PRESENCE OF VARYING AMOUNTS OF ALKALI. THE PRODUCTS OF OXIDATION, Journal of the American Chemical Society 38(1) (1916) 150-161.

[167] W.L. Evans, C.W. Holl, THE MECHANISM OF CARBOHYDRATE OXIDATION. III. THE OXIDATION OF THE HEXITOLS d-MANNITOL, d-SORBITOL AND DULCITOL, Journal of the American Chemical Society 47(12) (1925) 3102-3105.

[168] W.L. Evans, C.A. Buehler, C.D. Looker, R.A. Crawford, C.W. Holl, THE MECHANISM OF CARBOHYDRATE OXIDATION. I. d-GLUCOSE, d-MANNOSE, d-FRUCTOSE, d- AND l-ARABINOSE AND dl-GLYCERIC ALDEHYDE, Journal of the American Chemical Society 47(12) (1925) 3085-3098.

[169] C.T. Rueden, J. Schindelin, M.C. Hiner, B.E. DeZonia, A.E. Walter, E.T. Arena, K.W. Eliceiri, ImageJ2: ImageJ for the next generation of scientific image data, BMC Bioinformatics 18(1) (2017) 529.

[170] Y. Takashimizu, M. Iiyoshi, New parameter of roundness R: circularity corrected by aspect ratio, Progress in Earth and Planetary Science 3(1) (2016) 2.

[171] J. Bear, Dynamics of Fluids in Porous Media, (2013).

[172] P.K. Kitanidis, The concept of the Dilution Index, Water Resources Research 30(7) (1994) 2011-2026.

[173] P.G. Tratnyek, R.L. Johnson, G.V. Lowry, R.A. Brown, IN SITU Chemical Reduction For Source Remediation, in: B.H. Kueper, H.F. Stroo, C.M. Vogel, C.H. Ward (Eds.), Chlorinated Solvent Source Zone Remediation, Springer New York, New York, NY, 2014, pp. 307-351.

[174] R.D. Ludwig, C. Su, T.R. Lee, R.T. Wilkin, S.D. Acree, R.R. Ross, A. Keeley, In Situ Chemical Reduction of Cr(VI) in Groundwater Using a Combination of Ferrous Sulfate and Sodium Dithionite: A Field Investigation, Environmental Science & Technology 41(15) (2007) 5299-5305.

[175] R. Rodrigues, S. Betelu, S. Colombano, T. Tzedakis, G. Masselot, I. Ignatiadis, In Situ Chemical Reduction of Chlorinated Organic Compounds, in: E.D. van Hullebusch, D. Huguenot, Y. Pechaud, M.-O. Simonnot, S. Colombano (Eds.), Environmental Soil Remediation and Rehabilitation: Existing and Innovative Solutions, Springer International Publishing, Cham, 2020, pp. 283-398.

[176] J. Dolfing, M. van Eekert, A. Seech, J. Vogan, J. Mueller, In Situ Chemical Reduction (ISCR) Technologies: Significance of Low Eh Reactions, Soil and Sediment Contamination: An International Journal 17(1) (2007) 63-74.

[177] C. Christiansen, I. Damgaard, M. Broholm, T. Kessler, K. Klint, B. Nilsson, P. Bjerg, Comparison of Delivery Methods for Enhanced In Situ Remediation in Clay Till, Ground Water Monitoring & Remediation 30 (2010) 107-122.

[178] F. Mondino, A. Piscitello, C. Bianco, A. Gallo, A. de Folly D'Auris, T. Tosco, M. Tagliabue, R. Sethi, Injection of Zerovalent Iron Gels for Aquifer Nanoremediation: Lab Experiments and Modeling, Water 12(3) (2020) 826.

[179] A. Tiraferri, R. Sethi, Enhanced transport of zerovalent iron nanoparticles in saturated porous media by guar gum, Journal of Nanoparticle Research 11(3) (2008) 635.

[180] V. Gingine, R. Cardoso, Soil Structure Influence on Electrokinetic Dewatering Process, in: A.B. Ribeiro, E.P. Mateus, N. Couto (Eds.), Electrokinetics Across Disciplines and Continents: New Strategies for Sustainable Development, Springer International Publishing, Cham, 2016, pp. 19-42.

[181] R.C. Wrixon, G.A. Cooper, Theoretical and Practical Application Guidelines for Using Electrokinetics to Improve Casing Support in Soft Marine Sediments, IADC/SPE Drilling Conference, Society of Petroleum Engineers, Dallas, Texas, 1998, p. 7.

[182] B. Acar Yalçin, N. Alshawabkeh Akram, Electrokinetic Remediation. I: Pilot-Scale Tests with Lead-Spiked Kaolinite, Journal of Geotechnical Engineering 122(3) (1996) 173-185.

[183] C.-n. Hsu, A. Yeung, R. Menon, Electrokinetic extraction of lead from kaolinites: II. Experimental investigation, The Environmentalist 31 (2011) 33-38.

[184] H.I. Gomes, C. Dias-Ferreira, L.M. Ottosen, A.B. Ribeiro, Electrodialytic remediation of polychlorinated biphenyls contaminated soil with iron nanoparticles and two different surfactants, Journal of Colloid and Interface Science 433 (2014) 189-195.

[185] N. Alshawabkeh Akram, B. Acar Yalçin, Electrokinetic Remediation. II: Theoretical Model, Journal of Geotechnical Engineering 122(3) (1996) 186-196.

[186] H.I. Gomes, C. Dias-Ferreira, A.B. Ribeiro, S. Pamukcu, Enhanced Transport and Transformation of Zerovalent Nanoiron in Clay Using Direct Electric Current, Water, Air, & Soil Pollution 224(12) (2013) 1710.

[187] M. Minella, N. De Bellis, A. Gallo, M. Giagnorio, C. Minero, S. Bertinetti, R. Sethi, A. Tiraferri, D. Vione, Coupling of Nanofiltration and Thermal Fenton Reaction for the Abatement of Carbamazepine in Wastewater, ACS Omega 3(8) (2018) 9407-9418.

[188] N. Chandrasekar, S. Selvakumar, S. Yasala, J. Wilson, T. Peter, Hydrogeochemical assessment of groundwater quality along the coastal aquifers of southern Tamil Nadu, India, Environmental earth sciences 71 (2013).

[189] V. Post, Electrical Conductivity as a Proxy for Groundwater Density in Coastal Aquifers, Ground water 50 (2011) 785-92.

[190] M. Rodríguez-Rodríguez, A. Fernández-Ayuso, M. Hayashi, F. Moral Martos, Using Water Temperature, Electrical Conductivity, and pH to Characterize Surface–Groundwater Relations in a Shallow Ponds System (Doñana National Park, SW Spain), Water 10 (2018) 1406.

[191] S. Uddin, Analysis of Electrical conductivity of Ground water at different locations of Dildar Nagar of U.P, India, Advances in Applied Science Research vol 6 (2015).

[192] P.A. White, Measurement of Ground-Water Parameters Using Salt-Water Injection and Surface Resistivity, Groundwater 26(2) (1988) 179-186.

[193] J. Doetsch, N. Linde, T. Vogt, A. Binley, A. Green, Imaging and Quantifying Salt-Tracer Transport in a Riparian Groundwater System by Means of 3D ERT Monitoring, Geophysics 77 (2012) B207-B218.

[194] F. Septi Irwansyah, I. Susilawati, I. Fitriyati, I. Ch, B. Nuryadin, M. Ramdhani, An approach to determine the concentration of coloured solution using android smartphones, IOP Conference Series: Materials Science and Engineering 434 (2018) 012088.

[195] S. Šafranko, P. Živković, A. Stanković, M. Medvidović-Kosanović, A. Széchenyi, S. Jokić, Designing ColorX, Image Processing Software for Colorimetric Determination of Concentration, To Facilitate Students' Investigation of Analytical Chemistry Concepts Using Digital Imaging Technology, Journal of Chemical Education 96(9) (2019) 1928-1937.

[196] T.S. Kuntzleman, E.C. Jacobson, Teaching Beer's Law and Absorption Spectrophotometry with a Smart Phone: A Substantially Simplified Protocol, Journal of Chemical Education 93(7) (2016) 1249-1252.

[197] J.C. del Valle, A. Gallardo-López, M.L. Buide, J.B. Whittall, E. Narbona, Digital photography provides a fast, reliable, and noninvasive method to estimate anthocyanin pigment concentration in reproductive and vegetative plant tissues, Ecology and Evolution 8(6) (2018) 3064-3076.

[198] M. Persson, Accurate Dye Tracer Concentration Estimations Using Image Analysis, Soil Science Society of America Journal - SSSAJ 69 (2005).

[199] I. Forrer, A. Papritz, R. Kasteel, H. Flühler, D. Luca, Quantifying dye tracers in soil profiles by image processing, European Journal of Soil Science 51(2) (2000) 313-322.

[200] A. M., M. R., C. S., S. M., Proposal for a Standard Default Color Space for the Internet: sRGB, in: R. Buckley (Ed.), Recent progress in color management and communications, Society for Imaging Science and Technology, Springfield, Va, 1998, pp. 198-205.

[201] J.R.F. Carvalho, J. Delgado, Overall map and correlation of dispersion data for flow through granular packed beds, Chemical Engineering Science 60 (2005) 365-375.

[202] M. Rolle, D. Hochstetler, G. Chiogna, P.K. Kitanidis, P. Grathwohl, Experimental Investigation and Pore-Scale Modeling Interpretation of Compound-Specific Transverse Dispersion in Porous Media, Transport in Porous Media 93(3) (2012) 347-362.

[203] T. Appelo, Solute transport solved with the Nernst-Planck equation for concrete pores with 'free' water and a double layer, Cement and Concrete Research 101 (2017).

[204] P. Glover, Petrophysics MSc course notes, University of Leeds, UK (2000).

[205] I. Gueven, S. Frijters, J. Harting, S. Luding, H. Steeb, Hydraulic properties of porous sintered glass bead systems, Granular Matter 19 (2017).

[206] E.E. Saka, C. Güler, The effects of electrolyte concentration, ion species and pH on the zeta potential and electrokinetic charge density of montmorillonite, Clay Minerals 41(4) (2006) 853-861.

[207] M. Chorom, P. Rengasamy, Dispersion and zeta potential of pure clays as related to net particle charge under varying pH, electrolyte concentration and cation type, European Journal of Soil Science 46 (2005) 657-665.

[208] Y. Yukselen, A. Kaya, Zeta Potential of Kaolinite in the Presence of Alkali, Alkaline Earth and Hydrolyzable Metal Ions, Water, Air, and Soil Pollution 145(1) (2003) 155-168.

APPENDIX

Appendix to Chapter 3

Electrical equivalence for the 2D system

To better depict the difference between 1D and 2D systems an electric analogy can be used; mono-dimensional systems, despite their heterogeneity will behave as a series of resistors, where each resistor corresponds to a section of porous medium in different physic-chemical conditions [92, 101]. It follows, the current flow is forcedly equal in all sections, as it is in the equivalent electrical circuit; differences in electrical conductivity still affects transport only on the longitudinal direction, as discussed in the theoretical section (Chapter 2). A two-dimensional system equates, in electrical term, to a circuit with parallel resistors components: homogeneous sections behave as single resistors, whereas heterogeneous areas behave as parallel resistors. To provide a practical example, a 2D EK system comprised by electrode chambers, the porous medium and an injected amendment (potassium permanganate, $KMnO_4$) is depicted in Figure 62.

The 'Anode' and 'Cathode' resistors include the contribution of the solid-liquid interfaces, electrolyte, and the interface with the porous medium; the first and last 'Sand' resistors refers to the volume of porous medium upstream and downstream the injected amendment whereas the parallel resistor block depicts the porous medium sections were the injection occurred. The latter is defined by the longitudinal and transversal extension of the injection, and in a 2D system comprises a portion of sand which is unaffected and presents the same resistivity of the first and last section. The switch on the $KMnO_4$ branch signifies the permanganate injection, specifically the switch closes once the injection occurred. It follows that until that time the system behaves as a series of resistors, while after the injection the parallel resistor component is added [92, 101]. When the DC power supply operates in *constant voltage mode*, the current density circulating in the system is defined by the total resistance, hence by the system conductivity. Before the permanganate injection, as a series of resistors, the current density is distributed homogenously, whereas when the parallel resistor component is present a higher current flow occurs in the branch with the higher resistance, hence the lower conductance.
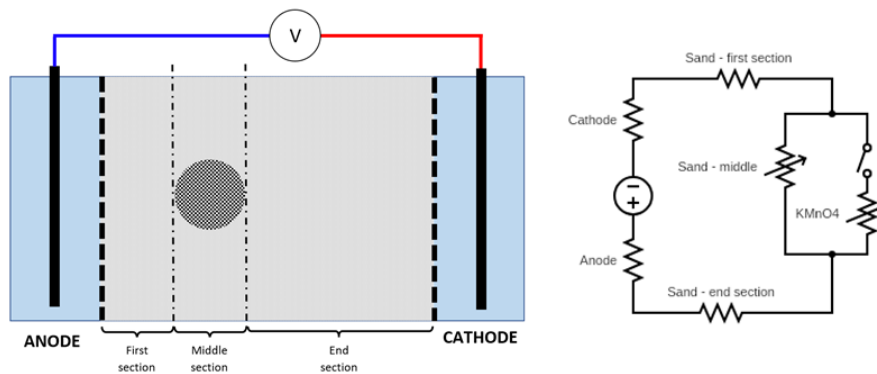
Figure 62) On the left: scheme of a 2D system, with electrodes placed in chambers isolated from the porous medium by bulkheads (dotted lines); an amendment injection is represented by the circle in the porous medium section. On the right: schematic representation in electrical terms of the 2D system; the Cathode and Anode resistance includes the buffering solution, the electrode material, and the bulkhead-sand interface effects.

Photographic detection and quantification of permanganate

The qualitative evolution of the injected permanganate can be observed easily by photographic detection in terms of shape and area (hence volume, assuming a symmetry across the set-up width). This allows to obtain important information on the effect of the background conductivity on the EK transport in the longitudinal and transversal direction. However, to fulfill the objective of the study a quantification of the permanganate is also required in multiple time-steps of the experiment, along the longitudinal and transversal direction. Since the porous medium used is translucent (note: not transparent) it is possible to correlate the light intensity to the permanganate concentration. Different work in literature shows the possibility to obtain good linear correlation between color intensity and concentration [194, 195], in specific conditions the Lambert-Beer law at the base of spectrophotometric analysis can be applied [196]. However, such studies are limited to transparent solutions and require a very controlled set-up. More complex approaches can be found on biological samples [197] but more importantly on tracer analysis on soil samples [198, 199]. From these studies, strong interferences from soil roughness, reflexes, light scattering, light intensity variations showed to significantly affect the calibration outcome and requires complex procedures to be eliminated. In all cases, no linear correlation can be obtained between concentration and color intensity, but evidences suggest a correlation between the concentration logarithm and a second order polynomial of the separate Red, Green and Blue intensities [198, 199]. A calibration procedure was developed using the same experimental set-up and wet-packing procedure, this time injecting multiple permanganate plumes at different concentration and collecting images with the

same illumination and camera settings. Each photo comprises three permanganate spots, two calibration spots at the same concentration to obtain a standard deviation of data, and a reference value to account for intensity fluctuations; the latter is a 3 mM permanganate spot. A background value, namely the color intensity of the glass beads saturated by the soil solution, can be obtained from any area of the set-up unaffected by the permanganate injection. Calibration was performed in the 0-10 mM range; image elaboration was performed by a MATLAB script; the following steps are applied:

i) the absolute sRGB color space (0-255) is converted to a normalized grayscale [200];

ii) the reference and the two calibration intensities were collected as average on a 50-pixel area crossing the center of the spots to account for the scattering caused by the porous medium;

iii) the background intensity is obtained from an area 550 pixels below the injected spots; from the preliminary tests this area is not interested by permanganate transport;

iv) the calibration and the reference intensities are depurated from the background intensity; then the corrected calibration intensity is normalized by the corrected reference;

At the end of the process, the resulting corrected and normalized intensities are interpolated with a polynomial function to minimize the standard deviations, the best fitting is provided by a 6th grade polynomial. The same intensity processing was applied to the images collected during the experiments to obtain the permanganate and the background intensity values. The lower detection limit (LOD) allowed by the technique depends partly on the camera setting and is also bound to change in different porous materials (clay, sand, etc.); in the present case the LOD is 0.04 mM. The confidence intervals for the longitudinal concentration profile were chosen as twice the standard deviation obtained from the calibration; the same elaboration can also be used for a pixel-by-pixel image elaboration to obtain concentration maps (Figure 63).

Image analysis

Thanks to the intense purple color of permanganate and the light uniform background we can use color threshold to identify the plume and apply image analysis to obtain velocity and trajectory of the plume barycenter and shape alterations (namely, area and roundness). The initial image pool was firstly reduced selecting images captured every 10'; images were processed using ImageJ software

131

[169] according the following protocol: firstly a Gaussian Blur filter was applied to eliminate the light refraction from the glass beads, which complicates the following steps, then the green color channel was selected since it presents the highest contrast between permanganate and background. A threshold filter was applied to the image to obtain a black and white image, where the permanganate plume is pure black and the background pure white. Lastly, a Particle Analyzer plugin allowed the spot identification for each frame, computing area, roundness, and the position of its centroid (Figure 64).

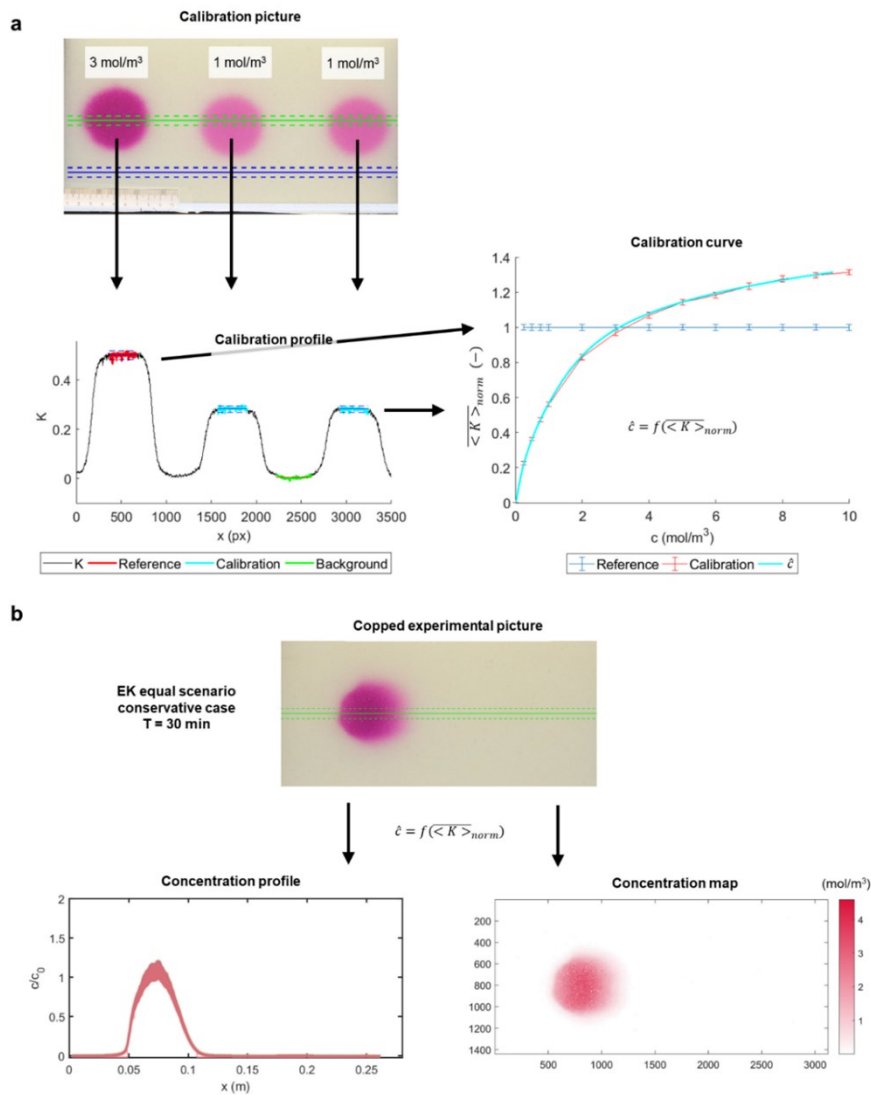**Figure 63) Schematic illustration of the calibration steps and their implementation on a photogram (time 30 minutes) in the "EK equal" experiment to retrieve the concentration profile and 2D concentration map. Adapted from Sprocati, et al. [65]**
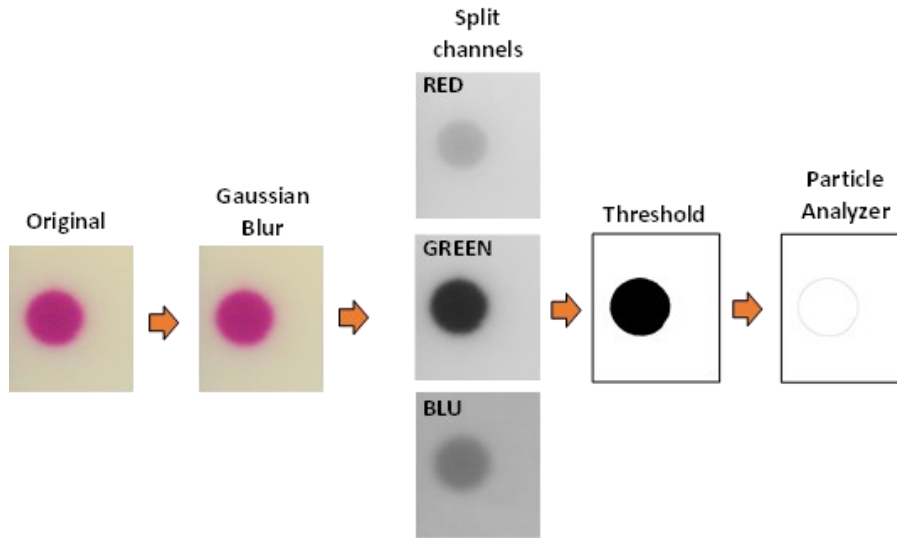
Figure 64) Schematic representation of the image processing in ImageJ [169] on the permanganate plume (initial time for the advective transport)

Plume shape and trajectories

The shape descriptors obtained from the experimental data were computed by the ImageJ software following the plume identification previously described (Figure 64). In this case, for each time frame (namely, each photo) the boundary of the permanganate plume was identified using the color contrast with the glass beads background; the software is able to trace the pixels composing the plume perimeters and perform multiple calculations yielding different informations.

- Center of mass (or barycenter): it is computed based in the color intensity of the entire plume, hence not only from geometrical parameters. This coordinated were used to perform the particle tracking and computing the migrational velocity.
- Roundness: roundness was selected as shape description to provide information on the plume distortion. Circularity (CR) is defined from area (A) and perimeter (P) ($CR = 4\pi \cdot A/P^2$), hence it is preferred in those cases where particles present very different shapes (needles, plates, etc.). Roundness (R) is a way to account for aspect ration in the definition of roundness, which is apt for the case at hand where the plume perimeter remains smooth but ovalisation occurs. Roundness is computed as $R = 4 \cdot A/(\pi \cdot X^2)$, where 'X' is the plume major axis [170].

133

- Area: the software uses the pixel counts and the scale defined by the user to compute the plume area. The scale was obtained adding a metric scale in the lightbox during the experiments, which was then within the image framed by the camera. Normalization was performed on the initial plume area (before the electric field was applied).

The image analysis allowed also to trace the plume barycenter during the experiments, the obtained velocities and trajectories. Known the time step between images and the pixel/cm scale (the same used for computing the plume area), the Tracking function of ImageJ allow the manual definition of the plume position, which was performed using the center of mass for each photo. The software outputs are the velocity and the particle trajectory.
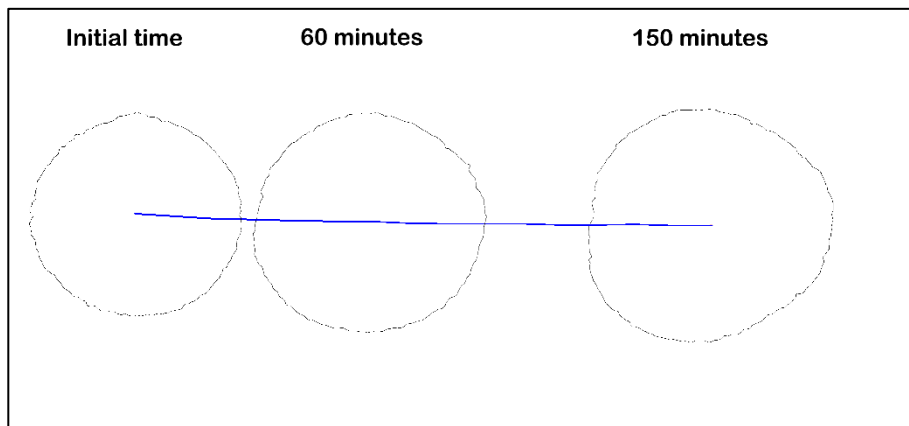
Figure 65) Permanganate plume tracking for the conservative advective experiment; detail of initial time, 1 hour and 150 minutes of transport
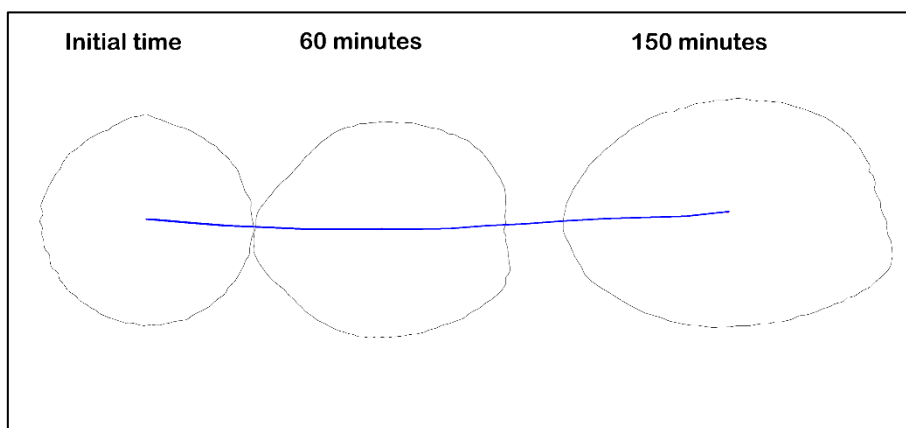
Figure 66) Permanganate plume tracking for the conservative electromigration experiment with "EK equal" conditions; detail of initial time, 1 hour and 150 minutes of transport
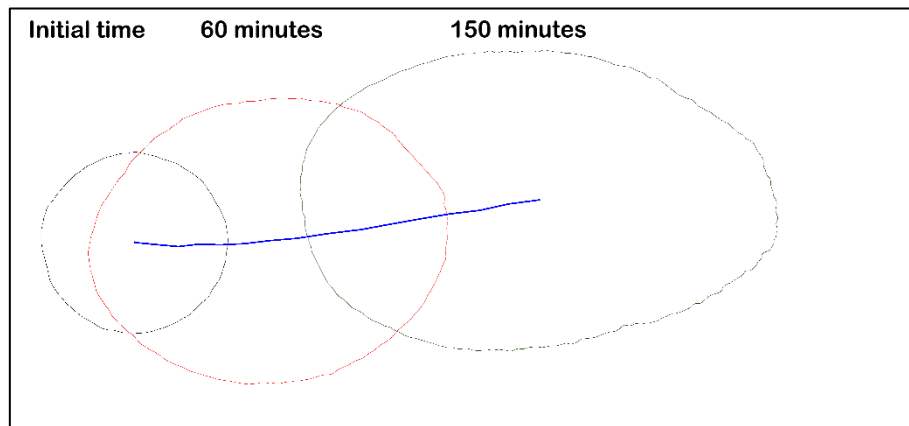
Figure 67) Permanganate plume tracking for the conservative electromigration experiment with "EK low" conditions; detail of initial time, 1 hour and 150 minutes of transport
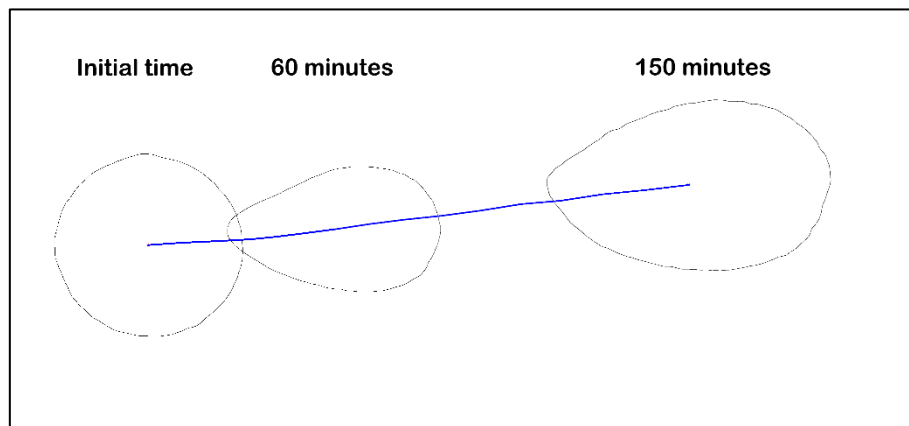
Figure 68) Permanganate plume tracking for the conservative electromigration experiment with "EK high" conditions; detail of initial time, 1 hour and 150 minutes of transport

Both ADV and "EK equal" delivery shows linear trajectories, parallel to the water table level, whereas "EK low" and high shows upward trajectories. Considering that the experiments were performed separately on different glass beads, packed in two separate moments, and using different solutions for both permanganate and buffering electrolyte this evidence suggests an influence of the ionic concentration gradient on electromigration. Density effects are unlikely responsible, as for the ADV, "equal" and "low" case the permanganate presents a slightly higher density (+ 0.12-0.14 Kg m^{-3}) while density is slightly lower (- 0.48 Kg m^{-3}) in the "high" scenario.

Plume spatial moments

It is possible to approach these plume dynamics using quantitative metrics of spreading, dilution and mixing based on spatial moments. The zeroth order moment characterize the total mass of solute for the i-th specie in a 2D system of area Ω:

$$M_{0,i}(t) = \int_{\Omega} c_i(x,t)\, d\Omega \quad ;$$

<div align="right">Equation 54</div>

while the second order central moment is used to quantify the centroid displacement in the longitudinal (m) and transversal (n) direction of the 2D set-up:

$$M_{i,2,mn}(t) = \int_{\Omega} c_i(x,t)\left(x_m - \bar{x}_{i,m}(t)\right)\left(x_n - \bar{x}_{i,n}(t)\right) d\Omega \ ,$$

<div align="right">Equation 55</div>

where $\bar{x}_{i,m}(t)$ indicates the plume centroid position, defined by ratio of the first order moment in the m-th direction and the total mass as:

$$x_{i,m}(t) = \frac{1}{M_{0,i}(t)} \int_{\Omega} c_i(x,t) \cdot x_m \cdot d\Omega \ .$$

<div align="right">Equation 56</div>

The variation in time of the zeroth and second order moment can be used to quantify the spreading of the permanganate plume and its dispersion. The resulting dilution index (Equation 57) quantifies the plume volume expansion and thus the distribution of the injected species in the set-up [172], also the point concentration can be defined using the zeroth order moment (Equation 58).

$$Dil = -\int_{\Omega} p_i(x,t) \cdot \ln\!\left(p_i(x,t)\right) d\Omega \ ,$$

<div align="right">Equation 57</div>

$$p_i(x,t) = \frac{c_i(x,t)}{M_{0,i}(t)} \ .$$

<div align="right">Equation 58</div>

To provide metric for the different reaction kinetics, a mixing area A_{mix} can be defined as the domain area where, in any time step, the reaction rate is greater than

an arbitrary threshold value. In this case the reaction rate threshold was set equal to r_{lim}=2E-5 mol m^{-3} s^{-1} and is defined by the Heaviside step function:

$$A_{mix} = \int_{\Omega} H\big(r_{MnO_4(x,t)} - r_{lim}\big)d\Omega \ .$$

Additional discussion on transport mechanism

The effect of different ionic concentrations on migration can be explained firstly considering the definition of conductivity for a soil solution, which can be computed using the Nernst-Einstein equation [92, 101]:

$$\sigma_T = \frac{F^2}{R \cdot T} \cdot \sum_i c_i \cdot z_i^2 \cdot D_i \ ;$$

where F is the Faraday constant (96485 s A mol^{-1}), R the perfect gas constant (8.314 J K^{-1} mol^{-1}), T is the absolute temperature (K); the *i-th* term of the summation is each ionic specie present in solution, c is its molar concentration, z its valence and D its diffusion coefficient (m^2/s) [57, 92, 101]. It must be pointed out that the value of σ thus obtained is valid only for free solutions, while in the case of solutions saturating a porous medium the effective diffusivity D* should be used including the medium tortuosity [94, 95]. Although many authors observed a contribution of the porous medium itself to conductivity, and different set-up at different complexity have been suggested in the present work the simplest approach, the use of Nernst-Einstein equation with the effective diffusion coefficient was applied. Recalling the Nernst-Einstein-Townsend equation, the complex dependency of current from the diffusion coefficient of the single species implies that different ion fluxes would be present at the same time in the set-up, failing the charge conservation law.

$$I = \frac{F^2}{RT} \cdot \sum_{i=1}^{N} z_i^2 \cdot (n \cdot D_i^*) \cdot c_i \cdot \nabla E \ ,$$

A second effect is the multicomponent transport and the single species transference numbers, which describes the ability of the ionic specie to transport current density [101, 136, 145], for a cation of a binary specie A^+B^- [101]:

$$t_{i+} = \frac{z_+ k_+^{EM}}{z_+ k_+^{EM} - z_- k_-^{EM}}$$

As a single current must be present in the system, it follows that a limiting effect is imposed by the specie with the lowest ionic mobility; in the simplest case of a single electrolyte the comprehensive diffusion coefficient is defined as [92, 101]:

$$D = \frac{z_+ k_+^{EM} D_- - z_- k_-^{EM} D_+}{z_+ D_+ - z_- D_-}$$

The low transference number ions slow down the migration of high transference number ions, which in turns speed up the former [92, 101]; in a process very similar to the multicomponent transport in the advection-dispersion regime [161, 162]. In the experiments performed, the scenario is more complex than a binary electrolyte: the background ions from the electrolyte buffer are homogenously distributed in the system, but the permanganate injection displaces the background solution creating a volume where their concentration is null. It follows, when the electric field is applied permanganate ions move towards the anode replacing bicarbonate ions (HCO_3^-); as the bicarbonate diffusion coefficient is lower than the one of permanganate (1.09E-9 m^2 s^{-1} and 1.5E-9 respectively) the latter is slowed down in the sense that only a fraction of the injected concentration is able to migrate at its nominal velocity [65, 92, 101]. Cations also play an important role in the effective migration velocity, as their concentration defines the amount of anions required to abide electroneutrality and charge conservation, therefore their concentration and diffusivity must also be considered. The final electromigration velocity is then resulting from a complex balance of different parameters, among which concentration is a variable: it is expected then to observe modification in the plume concentration and of the background solution, the latter only locally on the plume trajectory [65, 126].

Structure of the mathematical model [65]

The mathematical model used to describe the delivery is based in the Nernst-Plank-Poisson equation modified for porous media, which includes the porosity terms 'n'; the flux of the *i-th* specie is defined as:

$$J_i^{Tot} = -nD_i^* \nabla c_i - nD_i^* \frac{z_i F}{RT} c_i \nabla E + nuc_i$$

Where the first term describes chemical diffusion, the second electromigration and the third advection. The diffusion coefficient D_i^* is the effective diffusion coefficient, to account for tortuosity, ∇c_i indicates the concentration gradient, z_i the ion charge, F is the Faraday constant, R the gas constant, T the temperature and u the seepage velocity. In the case of the advective-dispersive case the middle terms equals zero ($\nabla\Phi=0$), and the dispersion coefficient (Longitudinal and Transversal) are described as follows [201, 202]:

$$D_i^L = D_i + 0.5 \, ud$$

$$D_i^T = D_i + D_i^{aq} \left(\frac{Pe_i^2}{Pe_i + 2 + 4\delta^2}\right)^\beta$$

Where d indicated the average grain size and Pe_i the Péclet number ($Pe_i = ud/D_i^{aq}$); δ indicates the ratio between the length of a pore channel and its hydraulic radius, and β is an empirical exponent accounting for the effect of incomplete mixing in the pore channels. Both δ and β values are empirical and based on previous studies [202]. Lastly, the material balance in the presence of a source/sink term (r_i) is defined as:

$$\frac{\partial(nc_i)}{\partial t} + \nabla \cdot \boldsymbol{J}_i^{Tot} = r_i$$

The modeling of electrokinetic transport using the NPP equation is based in the relation between the solution charge density (ρ_e) and the applied electric field [92, 101]:

$$\nabla^2 \Phi = -\frac{F}{\varepsilon} \sum_{i=1}^{N} z_i c_i = -\frac{\rho_e}{\varepsilon}$$

where ε is the dielectric constant of the porous medium and N is the number of charged species in solution. As discussed in the theoretical section, the electric conduction in porous medium is exclusively carried out by ions. Hence the current density can be expressed from the total ionic flux [92, 101]:

$$\boldsymbol{I} = F \sum_{i=1}^{N} z_i \boldsymbol{J}_i^{Tot} = -F \sum_{i=1}^{N} z_i n D_i \nabla c_i - \left(F^2 \sum_{i=1}^{N} z_i^2 \frac{n D_i}{RT} c_i \right) \nabla \Phi + F n \boldsymbol{v_{eo}} \sum_{i=1}^{N} z_i c_i$$

Which combined to the material balance yields [92, 101]:

$$F \sum_{i=1}^{N} z_i \frac{\partial (n c_i)}{\partial t} + \nabla \cdot \left(F \sum_{i=1}^{N} z_i \boldsymbol{J}_i^{Tot} \right) = F \sum_{i=1}^{N} z_i r_i$$

The system comprised of Equation 64 and Equation 67-Equation 69 constitute the Nernst-Plank-Poisson equation, which defines the transport of charged species including reactive terms. For the present case, the latter is referred to the permanganate consumption by glucose oxidation [65]:

$$r_{MnO_4^-} = k_{r,MnO_4^-} \, c_{MnO_4^-} \, c_{C_6H_{12}O_6}$$

where k_{r,MnO_4^-} is the empirical kinetic rate constant.

The mathematical model was developed coupling the PhreeqcRM code [126, 149, 203] and COMSOL Multiphysics to obtain the correct chemical speciation for the system from the initial concentration. The COMSOL software was used to compute the system conductivity and the resulting current distribution, using the data to solve the NPP equation through the NP-Phreeqc-EK code [65, 126].

Operatively, the initial composition of the background solution (experimental data) was analyzed by the Phreeqc code, which computed the equilibrium concentration based on tabulated geochemical equilibrium reaction constant. The aqueous composition was then used by COMSOL to solve the NPP system for the first time step, determining the migration and concentration parameters for every ionic specie; these data were again processed by Phreeqc to obtain the equilibrium composition starting a cycle for each time-step.

The experimental domain, namely the section of the model filled with the porous medium, was divided in a triangular mesh with 13400 elements, thanks to the injection strategy of permanganate the injection zone could be defined with a circle of 21.5 mm of radius for all the tests; a finer mesh was used on the boundaries of the model and of the permanganate plume to better describe the system. For the concentration at the model boundaries, Dirichlet conditions were applied using the experimental background concentration for each scenario; boundary electric potential was set using the measured values during the experiments; this is possible thanks to the recirculation chambers which provide a regeneration of the background solution. Electrolysis and electrode reactions were considered negligible and not included in the model thanks to the recirculation system ability to maintain pH in the alkaline-neutral range; temperature, required for a correct evaluation of the diffusion coefficient, was also defined at 22°C from the experimental measures [65]. The porosity value was set at 0.4 which is consistent with the values obtained both experimentally and through theoretical calculation for a perfectly packed porous medium with spherical grains and narrow size distribution [204, 205]. The only parameter fitted by the simulations were the medium tortuosity, which resulted to vary in the 0.5-0.6, and the kinetic constant for the glucose oxidation by permanganate. Lastly, a constraint on the permanganate concentration was applied discarding concentrations lower than 4 mM (0.04 mol m^{-3}) to account for the photographic quantification lower limit of detection.

In conclusion, all the initial model inputs (concentration, current density, potential gradient, or hydraulic flow, reported in Table 15 and Table 16) were obtained from experimental measures during the tests. The mathematical code allowed to solve the fundamental equations describing the system (see paragraphs above and theoretical section) for each of the time-steps considered and each solute present in the domain.
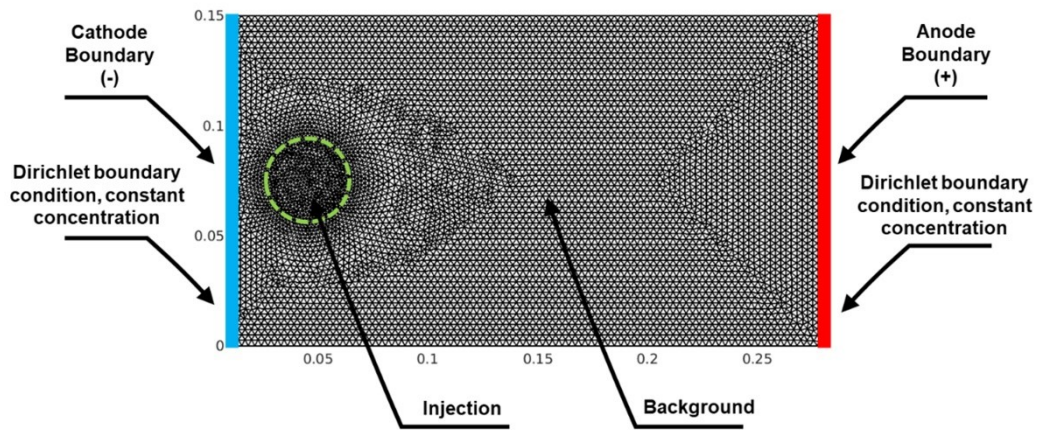
Figure 69) Schematic representation of the mathematical model domain and boundary conditions

Table 15) Values for the mathematical model input parameters, adapted from Sprocati, et al. [65]

INPUT PARAMETER	Conservative								Reactive							
	ADV	EK			ADV	EK		
		equal	low	high		equal	low	high
Porosity	0.40	0.40	0.40	0.40	0.40	0.40	0.40	0.40
Tortuosity	0.61	0.61	0.51	0.56	0.61	0.61	0.51	0.56
Electric potential at the anode (V)								
0 h	-	146	148.7	143.8	-	146.5	130	143.1
1 h	-	138.4	131.6	131.4	-	139.6	122.9	132.4
2 h	-	136.3	127.2	127.5	-	136.7	122.3	127.6
3 h	-	136.2	123.7	132.8	-	135.1	122.1	131.1
Seepage velocity (cm/h)	6.5	0	0	0	6.5	0	0	0
Kinetic rate constant (k_{r,MnO_4^-}) (m³/s/mol)	0	0	0	0	8×10^{-6}	8×10^{-6}	8×10^{-6}	8×10^{-6}

Table 16) Initial concentration values for the solutions used in the experiment and, aqueous diffusion coefficient s at 22°C.

	Units	ADV and EK equal	EK low	EK high	Aqueous diffusion coefficient 22°C (m²/s)
Temperature	°C	22	22	22	-
pH	-	9.01	9.00	8.96	-
Alkalinity	eq/L	3.01×10^{-3}	1.00×10^{-3}	9.09×10^{-3}	-
OH⁻	mol/m³	8.86×10^{-6}	8.44×10^{-6}	8.14×10^{-6}	4.86×10^{-9}
H⁺	mol/m³	1.02×10^{-9}	1.02×10^{-9}	1.19×10^{-9}	8.59×10^{-9}
HCO₃⁻	mol/m³	2.69×10^{-3}	9.04×10^{-4}	8.09×10^{-3}	1.09×10^{-9}
CO₃²⁻	mol/m³	1.47×10^{-4}	4.49×10^{-5}	4.36×10^{-4}	8.82×10^{-10}
NaCO₃⁻	mol/m³	5.57×10^{-6}	6.24×10^{-7}	4.27×10^{-5}	1.11×10^{-9}
NaHCO₃	mol/m³	4.10×10^{-6}	4.83×10^{-7}	3.42×10^{-5}	6.21×10^{-10}
Na⁺	mol/m³	3.00×10^{-3}	1.00×10^{-3}	9.01×10^{-3}	1.23×10^{-9}
MnO₄⁻	mol/m³	3.00×10^{-3}	3.00×10^{-3}	3.00×10^{-3}	1.50×10^{-9}
K⁺	mol/m³	3.00×10^{-3}	3.00×10^{-3}	3.00×10^{-3}	1.81×10^{-9}

Appendix to Chapter 4

Clay Zeta potential

In addition to the supplied information, the clay Zeta Potential (ζ) was evaluated at different ionic strengths and pH values using Electrophoretic Light Scattering (ELS); it must be pointed out that such value is only qualitative for the case under study as the ELS technique operates on colloidal suspensions and not bulk material, where complex pore-solution interactions can modify the ζ value [111]. Nonetheless, the Zeta Potential contributes to determining the magnitude of EOF, hence it is important to understand its trend in different conditions. The measures were performed with a Malvern Zetasizer Nano on 0.5 mg mL^{-1} solutions, placed for 5 minutes in a sonicating bath prior the measure.
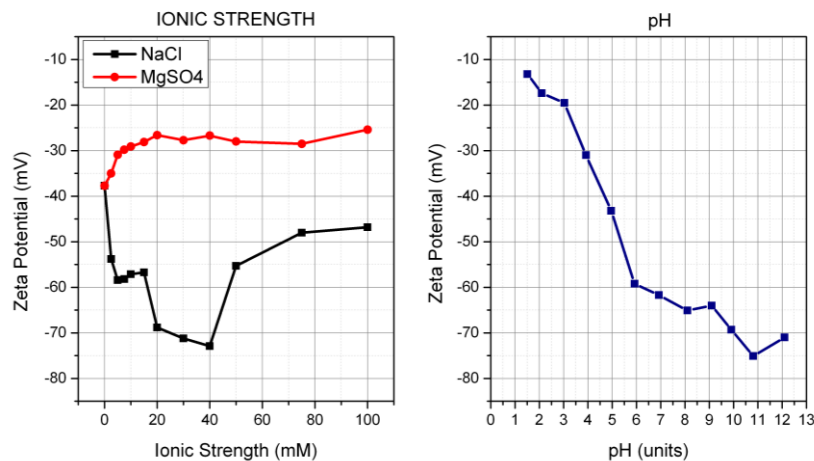

Figure 70) Kaolin zeta potential at different ionic strength and different ions (left) and at different pH value (right)

The ζ trend with the pH variation is common for kaolin clays [104]and derives from the protonation/de-protonation of the silanol groups [83, 84], of greater interest is the response to the ionic strength and the ionic specie in solution. While MgSO4 causes a stabilization of the colloidal clay (ζ values closer to a zero-charge), NaCl causes a significant decrease in potential for ionic strength in the 10-40 mM range: in these conditions the electroosmotic flow is significantly increased, and the migration of anions further opposed. The effect of dissolved cations species has proved to affect the zeta potential in previous studies [206, 207] and the complexity of the Electric Double Layer theory from the clay physico-chemical properties and sample preparation amply discussed [111, 208].

Experimental set-up

Additional information on the experimental set-up is provided in this section, schematics refer to the 2D experiments but are equivalent for the 1D tests, with the exception a column was used instead of a 2D tank. All tests were performed with the main system (tank, reservoirs, and pumps) inserted in a photographic lightbox (60x60x86 cm), which was equipped with an LED light capable of providing uniform illumination. In addition, a second LED light (with same color temperature) was placed behind the camera and used to improve the illumination of the front of the tank. This was important to increase the contrast between sand and permanganate, and to eliminate reflections; a diffusor was installed on this light to eliminate reflections on the tank panels (especially in the porous medium section). The placement of the reservoirs in the lightbox was essential to eliminate temperature gradients with the electrode chambers, as the internal LED light raised the temperature of 1-2°C from the room temperature. The camera distance was determined by the placement of the tank (or column) in order to provide a correct framing with a focal length equal to 50mm, to reduce perspective distortion as it would complicate the image analysis. For the image analysis, a metric scale was added in all the pictures; for the data elaboration the images were cropped to frame the porous medium only. To further improve image quality the camera sensor was aligned parallel to the tank and centered with the porous medium section. A matte-white backdrop was placed on the table surface, under the entire set-up to provide uniform color and hide cables used for the power supply and multimeters, which would have caused reflections on the tank panels. These instruments were placed under the table.

Figure 71) Schematics of the entire the experimental set-up, lamp and light images does not correspond to the actual equipment and only represents their placement.

Migration velocity upstream the clay inclusion (2D tests)

The image analysis performed using ImageJ [169] allowed to obtain the plume barycenter velocity for the transport toward the clay layer in the 2D delivery experiment; from the data presented in Figure 72 it is possible to observe a lower reduction in velocity for the 'EK high delivery when approaching the clay layer.
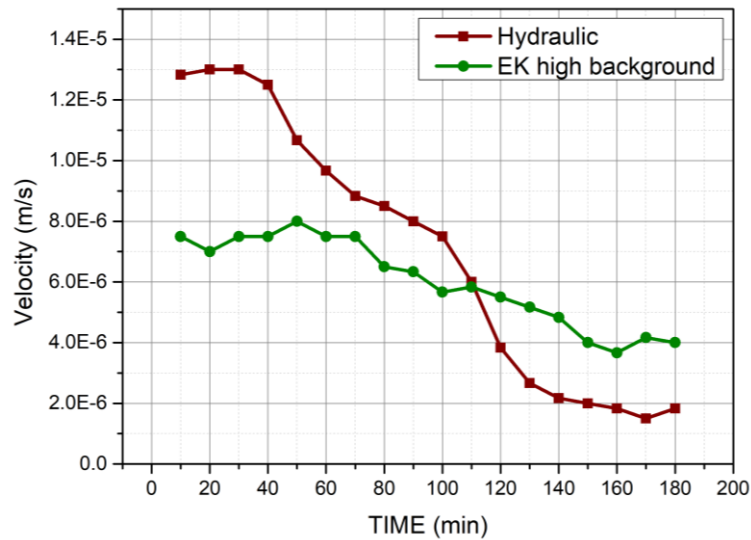

Figure 72) Plume velocity for the hydraulic and electrokinetic delivery of permanganate

Potential gradient and current in the 2D-"EK high" delivery test

The potential applied across the electrodes is equal to abt. 1.15 V cm^{-1} and the potential measured across the porous medium equals 1.16 V cm^{-1} and shows a constant value over the entire experiment. the potential across the clay layer resents of the conductivity modification caused by the permanganate plume arrival and possibly effects of the clay layer (namely, ions and colloids release). The current variation is expected from the constant voltage mode set on the power supply, and it successfully maintains a constant voltage gradient despite a complex system evolution which involves the migration of the buffer ions into the system and of the synthetic water ions into the electrode chambers.
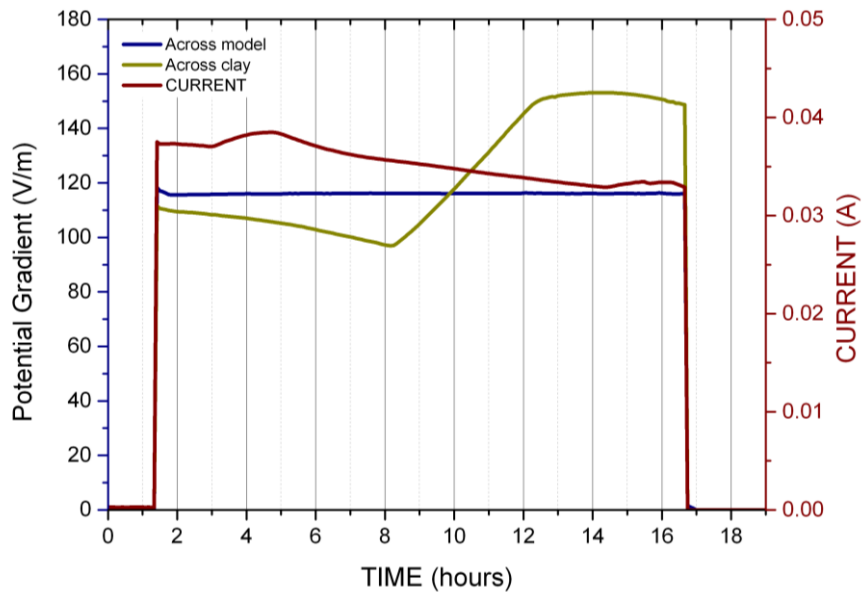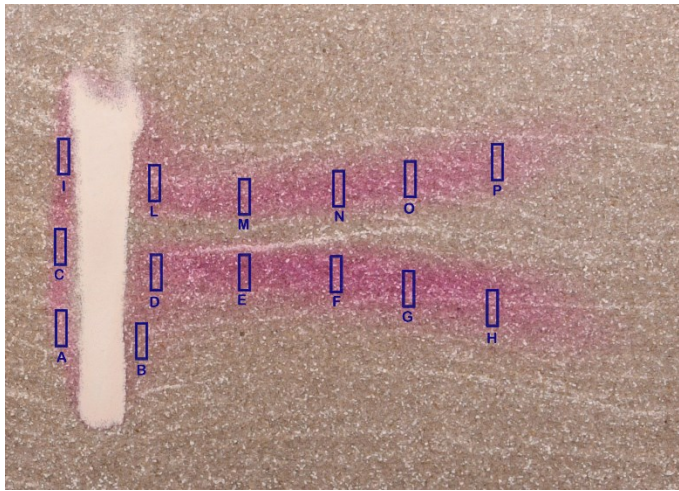
Figure 73) Potential gradient measured across the entire porous medium and across the clay layer and circulating current during the experiment.

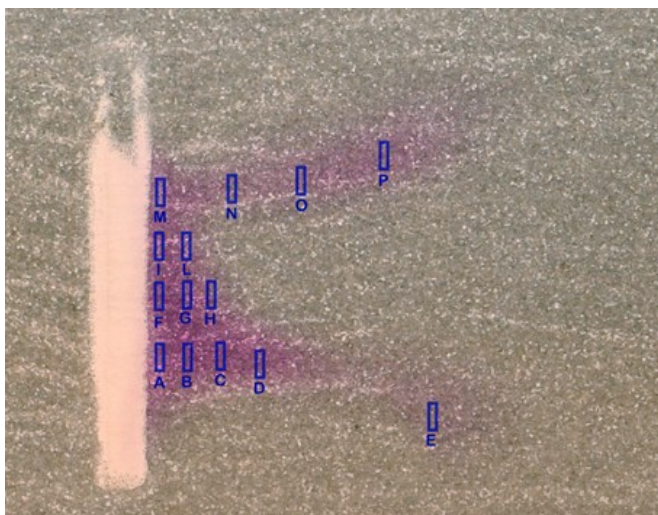## Permanganate concentration distribution during the 2D delivery

Given the medium complexity (especially the presence of a white colloidal component in the sand, which was not eliminated by the washing) obtaining the concentration profile for permanganate during the bypass of the clay layer is complicate, however it was possible to obtain local concentration in different area of the plume; for the 4 hours plume results are presented in Figure 74; The dead zone downstream the clay layer, where no permanganate is delivered due to the bypass, is evident.

PLUME SPOT	MnO$_4^-$ (mM)
A	0.82
B	0.80
C	0.91
D	1.01
E	1.64
F	1.38
G	1.35
H	1.01
I	0.81
L	0.82
M	1.09
N	0.90
O	0.78
P	0.75

Figure 74) Plume profile after 4 hours of advection

It is possible to observe a difference in the plume dynamics when exiting the clay layer for the electrokinetic delivery, due to the greater penetration in the inclusion. Specifically, while in the advective case the downstream permanganate plume results mostly from the upper and lower bypass of the layer, with a gap between the two resulting plumes. In the EK delivery approach it is evident that the downstream permanganate flows through the clay layer and thus migrates more homogeneously in the downstream sand medium. Applying the calibration to the image collected after 9 hours of application of the electric field it is possible to compute the plume concentration exiting the clay layer:

PLUME SPOT	MnO$_4^-$ (mM)
A	2.74
B	3.48
C	3.29
D	2.35
E	1.71
F	3.14
G	2.76
H	1.90
I	2.30
L	1.74
M	1.78
N	1.47
O	1.61
P	1.75

Figure 75) Concentration distribution in the permanganate plume exiting the clay layer for the "EK high" delivery.